91602
new 82-10 LEGAL NOTICE

This report was prepared by Ontario Hydro and, while effort has been made to assure the accuracy and applicability of the material contained herein, neither Ontario Hydro nor any person acting on its behalf:

(a) makes any warranty, express or implied with respect to the use of any information, apparatus, method or process disclosed in this report or that such use may not infringe privately owned rights; or

(b) assumes any liabilities with respect to the use of, or for damages resulting from the use of, any information, apparatus, method or process disclosed in this report.

COMPLIMENTARY COPY
Please Credit Ontario Hydro Research If Reproduced in Whole or in Part

ontario hydro
research division

EMBEDDED FIBER OPTIC STRAIN SENSORS FOR REINFORCED PLASTICS AND ELASTOMERIC MATERIALS

Report No: 91-247-K

R.J. Lewak, Engineer
Materials Chemistry Section
Chemical Research Department

ABSTRACT

As reinforced plastics and elastomers are used in critical components of the negative pressure containment safety systems of Ontario Hydro's CANDU nuclear generating stations, a method of monitoring the response of these materials to operational and extraordinary loads and thereby determining the deterioration of these materials with time would be highly advantageous. Such a method which has received wide application in the aerospace industry is embedded fiber optic strain sensors. In this study two types of fiber optic strain sensors, interferometric based and attenuation based, were studied as fiber optic strain sensors in two extreme types of materials, a rigid material such as fiberglass reinforced plastic (FRP), and a flexible material such as polyester fabric reinforced silicone rubber. For the interferometric sensors a Mach-Zehnder interferometric technique was used. Specimens of FRP and silicone rubber were made with interferometric sensors embedded. The procedure for making the specimens is described in detail. The response of the sensors to tensile loads was then measured. An electronic fringe counter was required for the interferometric sensors and the design and construction of a fringe counter is described in detail.

job	file	date	report no.
32-514-052	835.91	November 8, 1991	91-247-K

Attenuation based fiber optic sensors were made using an axial displacement technique and embedded in the same materials. Following tensile tests performed on these specimens it was concluded that the interferometric sensors, being much more sensitive than the attenuation sensors, were more suited to the flexible rubber materials, while the attenuation sensors were suited to the rigid materials. It was recommended that the specimens containing the sensors be artificially aged in order to determine if fiber optic strain sensors could detect deterioration of the materials with time.

91602
new 82-10

ontario hydro
research division

EXECUTIVE SUMMARY

EMBEDDED FIBER OPTIC STRAIN SENSORS FOR REINFORCED PLASTICS AND ELASTOMERIC MATERIALS

R.J. Lewak

Reinforced plastics and elastomers are used in certain critical components in the negative pressure containment safety systems of Ontario Hydro's CANDU nuclear generating stations. Because of the critical nature of the uses of these materials, concern has been raised by the licensing authority regarding the condition of these materials as they deteriorate with age. Studies attempting to duplicate the conditions in which the materials operate and then measure the deterioration characteristics, or, studies which artificially age the materials and then measure the deterioration are being performed at present. Investigation and inspection of the actual materials may only be accomplished during outages scheduled once a decade but no measurements of deterioration are made while the material is operational.

The methods of construction of both reinforced plastic and elastomeric materials usually consist of forming the material in layers. The possibility exists of embedding a sensor into the core of the material during the stages of formation of the component. Fiber optic sensors are small enough so that their presence would not affect material performance. In addition fiber optic sensors are all dielectric, perform over a wide range of temperatures, have high ruggedness, have variable sensitivity, and are compatible with electronic and optical multiplexing. For these reasons fiber optic sensors were studied as embedded strain sensors for reinforced plastics and elastomers. Two types of materials were studied, one extremely flexible, polyester reinforced silicone rubber used as seals in pressure relief ducts and vacuum buildings, and one extremely rigid, fiberglass reinforced plastic (FRP) used in piping in dousing systems. These two materials are representative of the extremes in reinforced elastomers and plastics. Two types of intrinsic sensor techniques were studied with both materials, attenuation based sensing of strain and interference based sensing of strain.

job	file	date	report no.
31-514-052	835.91	November 8, 1991	91-247-K

Optical fibers are composed of two components, the core and cladding. They operate by the mechanism of total internal reflection in which a beam of light sent through the core is reflected back into the core by the cladding. There are two basic types of optical fibers, single mode and multimode. Single mode fiber has a core diameter close to the wavelength of light and in some cases single mode fibers are also polarization preserving. Single mode fiber is required for interference sensors but due to their low losses are not suitable for attenuation sensors which use multimode fiber.

The literature on embedded fiber optic sensors used to measure a large number of physical and chemical phenomena is wide and varied. This report details literature on fiber optic sensors for measurements of radiation dose, force, vibration, pressure and temperature. In the field of optical fiber strain sensors, the literature is focussed on four basic techniques: phase modulation (interferometry), polarization modulation, attenuation, and time domain reflectometry. In addition the literature review lists a number of review articles on the entire subject of optical fiber sensors.

Work on interferometric fiber optic sensors first consisted of the creation of a fiber optic Mach-Zehnder interferometer using a 4 mW He-Ne laser as a light source. The bringing together of both beams from each arm of the interferometer, the reference fiber arm and the measurement fiber arm, formed an interference fringe pattern. If the measurement fiber was strained the fringe pattern would move depending on the amount of strain. Trials were made on different lengths of fiber as well as fibers with and without jacket and cladding to determine if these factors lead to differences in measurement characteristics. No significant difference was observed which is important because the manufacture of the material would involve curing at high temperature which would damage any polymer jacket or cladding on the fibers. Specimens of FRP were made with embedded sensors from sheets of preimpregnated Ciba Geigy Vicotex M9 Glass/Epoxy. As this procedure is important to the success of the fiber optic strain sensor, it is described in detail. Specimens of polyester reinforced silicone rubber were made from the material supplied by Freudenberg-NOK used in the PRD seals at Pickering NGS in 1990. The technique used to embed the sensor was that used to make splices in this material. Because it was observed that the fringe pattern changed extremely rapidly when the sensor is strained, an electronic fringe counter was designed and constructed. Tensile tests on the FRP specimens showed that the optical fiber sensors gave good, repeatable linear results and

were able to read strains as small as 0.5 μstrain. Tensile tests on the rubber specimens showed much the same results although with much higher strain values for the same load applied.

Work on attenuation based optical fiber sensors began with determining which type of sensor configuration was to be used. Multimode optical fiber was required to be used for this type of sensor and microbend sensor configurations were attempted using braided fibers and induced microbends. These were unsuccessful due to the low loss characteristics of the of the fiber. Misalignment attenuation sensors were next considered and an axial displacement sensor made from two separate fibers displaced a small amount in the axial, or strain direction was chosen for embedding into specimens. The manufacture of both FRP and polyester reinforced rubber with embedded axial displacement sensors was performed similarly to that for the interference sensors. Since the theoretical correlation between strain and attenuation is extremely complex and depends on immeasurable values and since no two attenuation sensors were alike in their response, tensile tests on specimens were performed measuring the attenuation of a 4 mW He-Ne laser beam versus the load applied. Results showed good sensitivity, repeatability, and range for the attenuation based sensors.

It is recommended that this work be continued by submitting the specimens to accelerated aging conditions and then determining if the sensors are able to detect changes in the characteristics of the materials due to aging effects. In addition, it is recommended that the attenuation based sensor be used exclusively for flexible, weak materials which have large strains while the interference based sensor be used on the smaller strain in rigid, strong materials.

TABLE OF CONTENTS

		PAGE
1.0	INTRODUCTION	1
2.0	OPTICAL FIBER STRUCTURE AND OPERATION	3
3.0	LITERATURE REVIEW	4
4.0	INTERFEROMETRIC FIBER OPTIC STRAIN SENSOR	6
	4.1 Interferometric Trials	8
	4.2 Preparation of Test Specimens	10
	4.2.1 Fiberglass Reinforced Plastic Specimens	10
	4.2.2 Fabric Reinforced Rubber Specimens	11
	4.3 Electronic Fringe Counter	12
	4.3.1 Photodiodes and Mounting Assembly	12
	4.3.2 Amplifier Circuit	12
	4.3.3 Direction Discriminator	13
	4.3.4 Counter/Display Circuit	14
	4.3.5 Signal Generator	14
	4.3.6 Tests of Electronic Fringe Counter	15
	4.4 Tensile Tests Using Interferometric Optical Fiber Sensor	15
5.0	ATTENUATION FIBER OPTIC STRAIN SENSOR	16
	5.1 Types of Fiber Optic Attenuation Sensors	17
	5.1.1 Microbend Sensors	17
	5.1.2 Misalignment Sensors	17
	5.2 Experimental Development of Attenuation Based Embedded Fiber Optic Strain Sensor	18
	5.2.1 Axial Displacement Induced Attenuation Sensor	20
6.0	CONCLUSIONS AND RECOMMENDATIONS	22
	6.1 Interferometric Fiber Optic Strain Sensor	22
	6.2 Attenuation Fiber Optic Strain Sensor	23
7.0	ACKNOWLEDGEMENTS	24
8.0	REFERENCES	25
FIGURES		30
DISTRIBUTION		last page

ontario hydro
research division

To Dr. D. Mills
Director of Research

EMBEDDED FIBER OPTIC STRAIN SENSORS FOR REINFORCED PLASTICS AND ELASTOMERIC MATERIALS

1.0 INTRODUCTION

Reinforced plastics and elastomers are the materials used in certain critical components in the negative pressure containment safety systems of Ontario Hydro's CANDU nuclear generating stations. In particular, reinforced elastomers are used in components which form part of the containment envelope including airlock door inflatable seals, pressure relief duct expansion/contraction joint seals, vacuum building roof seal, and pressure relief valve diaphragms. Reinforced plastics are used in forming key portions of the dousing system including the spray headers, risers and downcomers.

Because of the critical nature of the uses of these materials, concern has been raised by the Atomic Energy Control Board regarding the condition of these materials as they deteriorate with age. At the present time, studies are being performed regarding the aging characteristics of both fabric reinforced silicone rubber which is used as pressure relief duct seals and vacuum building roof seals and fiberglass reinforced plastic used as piping for the dousing system. These studies either attempt to duplicate the conditions encountered by the material over its lifetime in a real time frame and then measure the deterioration or alternatively, age the material artificially in an accelerated manner substituting elevated temperature for a short time for operating temperatures over a real time frame. The material deterioration is then measured following the accelerated aging. Both types of studies have the disadvantage of attempting to duplicate conditions rather than using the actual conditions. Since these studies rely on models of the actual conditions, the possibility exists that errors may arise in the artificial aging of the components.

During the scheduled vacuum building outage which occurs once a decade, these components are inspected, tested and repaired or replaced as required. Inspection, however, is only of the surface and of surface features such as measurement of hardness.

Certain tests performed during the outages such as pressurization tests on the pressure relief duct and full douse tests in which the emergency water storage tank is emptied through the dousing system, allow for the opportunity of instrumenting certain components such as the FRP piping of the dousing system and measuring the material's response to the test conditions. By comparison with the previous test ten years before, an estimation may then be made as to the deterioration of the material over the decade. The key liability of this procedure is that no measurement of the deterioration of components is made while the component is in the station operative condition. Since the lead time for the replacement of components is often as much as one year, and since spare parts for each and every system are not kept in storage, if a defective component is detected during outage tests it may not be possible to replace it within the short outage time period. Therefore, a permanent sensor which would be able to monitor the deterioration of the component while in service would be advantageous in both cost and safety considerations.

The methods of construction of both reinforced plastic and elastomeric materials usually consist of forming the material in layers or laminae. The possibility exists with these types of materials of embedding a sensor into the core of the material during the stages of formation of the component. The sensor would be required to be small enough so that its presence would not affect material performance. Fiber optic sensors have the advantages of being all dielectric, light weight and small size, immune from electrical interference, able to perform over a wide range of temperatures, able to have a large bandwidth, able to have a high degree of ruggedness, able to have variable sensitivities depending upon the parameter measured, compatible with electrical and optical multiplexing, and being able to have relatively low component costs which are driven by the large communications market. Therefore, fiber optic sensors would seem ideal for performing as embedded strain sensors in the reinforced plastics and elastomers used in the components of the negative pressure containment system.

In this study the methods, techniques and performance of embedded fiber optic sensors were investigated for two types of reinforced laminated materials which represent the extremes of flexibility. The first is a glass fiber reinforced polyester resin which is a hard brittle material and the second is a polyester fabric reinforced silicone rubber which is extremely flexible. Two types of techniques were studied for both materials. The first used interference of coherent light to measure strain and the second used attenuation of coherent light for the same measurement. Because the two techniques are vastly different in

terms of fiber type, measurement resolution and fabrication technique, the study was divided into two sections, one considering interference and the second considering attenuation. The common elements in both sections are that both employed reinforced rubber and reinforced plastic as materials of investigation.

2.0 OPTICAL FIBER STRUCTURE AND OPERATION

There are two basic types of fiber optic sensors. One type, called extrinsic sensor, relies on the optical fiber to relay information to and from an additional measurement system which may be a gas cell, a cantilever, mirrors, or any one of dozens of other mechanisms which may generate, modulate or transform a light beam. The second type, the intrinsic sensor, relies on the properties of the optical fiber itself to convert environmental action into a modulation of either the intensity, phase, or polarization of a light beam passing through it. This study focuses on intrinsic sensors exclusively because they consist only of the optical fiber itself and thus present less of an invasion of the material than extrinsic sensors.

Optical fibers are constructed of two components, the core and the cladding. The cladding will have a lower index of refraction than the core. Optical fibers operate by total internal reflection. That is, a beam of light directed along the axis of the fiber will be reflected continuously by the lower index material, the cladding, back into the core of the fiber so that little, if any, of the light is lost through the walls of the optical fiber. There are two basic types of optical fibers, multimode fibers and single mode fibers. In the multimode fiber the core diameter is a large multiple of the propagating wavelength of light. The single mode fiber has a core diameter which is close to the wavelength of the propagating light. The cutoff condition, where only one mode is allowed to propagate down the fiber is given by the modal volume, V, [1]:

$$V < 2.405 \quad \text{where}$$

$$V = \frac{2\pi\, an}{\lambda} (2\Delta)^{\frac{1}{2}}$$

$$\text{and} \quad \Delta = \frac{n^2 - m^2}{2n^2}$$

where n is the index of the core, m is the index of the cladding, a is the radius of the core and λ is the wavelength of the propagating light.

In addition, some single mode fibers are also polarization preserving. This is accomplished by using an elliptical core of extremely small dimensions so that the light can only propagate with the polarization direction in the direction of the major ellipse axis. This type of fiber has the disadvantage of coupling difficulties because of the small dimensions. Another method of polarization preservation is to use fibers with a built in stress birefringence which causes an index of refraction difference along a major and a minor axis of the fibers. A third method is that using a fiber with high losses except in the polarization direction.

3.0 LITERATURE REVIEW

Optical fiber sensors have developed over the last fifteen years into a new field of study having a wide range of published literature. What had begun as an offshoot of the major optical fiber technological application, telecommunications, had, when combined with technologies having a parallel development, namely signal and optical processing and analysis generated a torrent of new and valuable work in this field. As part of this study a literature review of this subject was performed. This review does not attempt to cover the entire range of literature on this subject. Instead, this review attempts to present a number of the more valuable pieces of literature over the last ten to twelve years with particular application to fiber optic strain sensors.

Work has been done to use embedded optical fiber sensors to measure a large number of physical and chemical phenomena. These include radiation dosimetry [2], force [3], vibration [4], pressure [5,9], and temperature [6,7,8,9]. In addition work has been done for embedded fiber optic sensors in composite materials which are able to detect both microfractural damage to the material [10] and fatigue damage [11]. In terms of embedded fiber optic strain measurement, four basic techniques are used, polarization modulation, phase modulation (interferometry), attenuation, and time domain reflectometry. Polarization sensors using interferometry used as strain gauges have been described in [12] and [13]. A twin core polarization interferometer sensor to measure strain and temperature is presented in [14]. Conversely, a polarization based fiber optic sensor which is immune from temperature effects and uses a dual fiber coil is presented in [15]. A single fiber polarization sensor has been used for both the detection of strain and damage in composite materials [16] and a prototype single fiber polarimetric fiber optic strain gauge for embedment in composite materials is described in [17].

In addition, fiber optic sensor development has also described sensors using combined polarimetric and Michelson interferometer systems for measurement of physical pheneomena [18] and combined polarimetric and Fabry-Perot interferometer systems for strain measurement [19].

Attenuation based embedded fiber optic sensors for measurement of structural distortion have been described as early as 1982 [20]. Structural integrity monitoring using attenuation based fiber optic strain measurement is described in [21]. A number of different techniques to produce the microbends in an optical fiber required for an attenuation based strain sensor are described in [22] and an attenuation based strain sensor employing twisted optical fibers is presented in [23]. In [24], an attenuation fiber optic strain sensor in which permanent microbends are fabricated into the optical fiber before embedment is described.

Interferometric based embedded fiber optic strain sensors have been described as early as 1978 using Mach-Zehnder interferometer arrangement [25] which could measure strains of less than 0.4 μ-strain. A similar type of gauge is described for the measurement of dynamic strains [26]. A more complex system which consists of multiplexing a dynamic strain gauge network is described in [27]. In [28] there is described an interferometric optical fiber sensor which could simultaneously measure strain and temperature. An overview of Mach-Zehnder interferometric optical fiber sensors is given in [29] which discusses theoretical and practical performance and also demodulation techniques for different sensing applications. The embedment of an interferometric optical fiber strain sensor in a graphite epoxy laminate presented in [30] and an embedded interferometric fiber optic strain sensor and fringe counter is presented in [31].

Optical time domain reflectometry (OTDR) is a technique in which an optical pulse is launched down an optical fiber embedded in the material and the reflected signal is measured and analysed to determine strain in the material and other physical phenomena. This technique was used for measurement of strain in fiber optics communications conductors [32] using the conductors as sensors. The technique has been used for embedded three dimensional strain sensors in graphite epoxy composite materials [33]. A multiplexed distributed system employing OTDR, polarization optical time domain reflectometry (POTDR) and frequency domain reflectometry (OFDR) techniques is presented in [34].

Fiber optic sensor technology also includes studies on the modulation and demodulation of fiber optic signals in order to permit easier and more accurate measurement. A pseudoheterodyne method for a polarimetric fiber optic sensor is described in [35]. Other techniques for demodulation for interferometric fiber optic sensors are presented in [36,37,38,39,40].

Lastly in this literature review, a number of applications and review articles on fiber optic sensors have been published. These include applications for embedment of fiber optic sensors in reinforced concrete buildings and structures [41], and embedded optical fiber sensors for materials evaluation including cure monitoring for polymers and composites [42]. Other review articles on a wide range of fiber optic sensors and applications are presented in [43,44,45,46,47,48].

4.0 INTERFEROMETRIC FIBER OPTIC STRAIN SENSOR

The basis of operation of the interferometric fiber optic strain sensor is the interference of two coherent light beams to produce a pattern of light and dark fringes. This fringe pattern may then be related to the difference in light path length between the two light beams by considering the phase change of one of the beams with respect to the other. By passing both light beams through optical fibers to form both arms of a Mach-Zehnder interferometer and then deforming one of the optical fiber arms from its original configuration to one with a different path length, the change in original fringe pattern may be related to the path length change. If one or both of the optical fiber arms are embedded in a material and the path length change is due to material strain, then the material strain may be related to the change in original fringe pattern.

The phase change due to fiber elongation can be derived as follows [25]:

$$\Delta\phi = \beta\Delta L + L\Delta\beta \qquad (1)$$

where $\Delta\phi$ is the phase change, β is the propagation constant of the mode in the fiber, and L is the fiber length. The term $\beta\Delta L$ represents the physical change of length produced by the strain and $\beta\Delta L = \beta\epsilon L$ where ϵ is strain $\Delta L/L$. The second term, the change in ϕ due to a change in β can come from a strain-optics effect where the strain changes the refractive index of the fiber and a waveguide mode dispersion effect due to change in fiber diameter D so that:

$$L\Delta\beta = L\frac{d\beta}{dn}\Delta n + L\frac{d\beta}{dD}\Delta D$$

where n is the refractive index of the fiber core. Since the core and cladding indices typically differ by only 1%, $\beta = nk_o$, where k_o is the free space propagation contant of the light mode. Therefore:

$$\frac{d\beta}{dn} = k_o = \frac{\beta}{n}$$

From a tensor strain analysis of the fiber, the strain-optic effect Δn is:

$$\Delta n = -\tfrac{1}{2}\, n^3[\epsilon(1-\mu)p_{12} - \mu\epsilon p_{11}]$$

where ϵ = strain = $\Delta L/L$
μ = Poisson's ratio of the fiber = 0.17 for fused silica
p_{12}= strain optic tensor element = 0.27 for fused silica
p_{11}= strain optic tensor element = 0.121 for fused silica

Substituting these expressions into equation (1) :

$$\Delta\phi = \beta\Delta L + L\frac{\beta}{n}\{-\tfrac{1}{2}n^3[\epsilon(1-\mu)p_{12} - \mu\epsilon p_{11}]\}$$

$$= \beta\Delta L + L\frac{\beta}{n}\epsilon\{-\tfrac{1}{2}n^3[(1-\mu)p_{12} - \mu p_{11}]\}$$

$$\frac{\Delta\phi}{\Delta L} = \beta - \tfrac{1}{2}\beta n^2[(1-\mu)p_{12} - \mu p_{11}]$$

The value β, the propagation constant for the mode in the fiber, is equal to :

$$\beta = \frac{2\pi n}{\lambda}$$

For fused silica and using the wavelength of helium-neon laser light:

$$n = 1.456 \text{ and } \lambda = 632.8\text{nm}$$

$$\beta = 1.446 \times 10^7\ \text{m}^{-1}$$

and $$\frac{\Delta\phi}{\Delta L} = 1.134 \times 10^7 \text{ radians/meter}$$

since 2π radians equals a phase shift of 1 fringe:

$$\frac{\Delta\phi}{2\pi\Delta L} = 1.805 \times 10^6 \text{ fringes/m} = 1.805 \text{ fringes}/\mu\text{m}$$

$$\Delta L = 0.554\ \mu\text{m/fringe} = (0.554 \times \text{number of fringes})\mu\text{m}$$

and strain $\epsilon = \frac{(0.554 \times \text{number of fringes})}{\text{length of the fiber}}\ \mu\text{-strain}$

This is then the theoretical relationship between a change in fringe number and a change in strain in the sensing fiber. This analysis assumes that only the sensing fiber arm of the interferometer is strained and that the reference fiber is unperturbed. In practice, this assumption implies a non-imbedded reference fiber which would be difficult to maintain. An alternative to a loose reference fiber would be to embed the reference fiber in the laminated material in a circular configuration as described in [31]. This would allow for the determination of the difference in phase shift between the two arms and relation to a strain value. According to [31], the relationship between strain of the material and phase shift is:

$$\epsilon = k\lambda/\{(C+n)[31+2\pi^2(1-\mu)(a-R)]\} \text{ where } k = 1,2,3,...$$

$$C = \frac{n^3}{2}[\mu(p_{12} - p_{11}) - p_{12}]$$

R is the radius of the circular reference fiber and a is the radius of the measurement fiber if it is arranged in an S shape.

4.1 Interferometric Trials

The purpose of the interferometric trials was to determine the performance of the interferometric fiber sensor not embedded in any material in order to compare it with the theoretical values. In this case, an interferometric setup was constructed on an optical table as shown in Figures 1 to 5. The coherent polarized light beam from a Uniphase 4 mW He-Ne laser is focussed by a coupler which focuses the light onto a single mode optical fiber using a microscope objective. This first single mode fiber is actually a biconical fiber splitter which splits the beam into two equal arms. Each arm is then coupled from the biconical beam splitter to a single mode sensor fiber and a single mode reference fiber using GRIN (GRaded INdex) lens couplers as shown in Figure 4. The sensor fibers are Newport F-SPV-10 single mode fibers having three components, core, cladding, and a polymer jacket. These trials involved sensors with the jackets stripped

off or unstripped, and the cladding either etched off or unetched. The sensor and reference arms are of equal length. The beams are then recombined using a beam splitter cube as shown in Figure *5* to form a fringe pattern. In Figure *6* both beams are shown separately. The secondary fringes are from mismatch of the cleavage planes between the GRIN lenses and the fibers. Figure *7* shows better cleavage and match. By bringing them together as in Figure *8* and adjusting the relative positions of each beam with produce the fringe pattern as in Figure *9*. Stretching on arm of the interferometer will cause the fringes to move either into the center of the fringe pattern or towards the outer edge of the pattern. The sensor fiber was stretched in the middle by adhering one end to a fixed aluminum tower and the other end to a moveable linear positioner as shown in Figure *1* with an epoxy adhesive. A total of six separate trials were made, with the fringe count being tallied manually and the fiber elongation being measured by a digital dial gauge as shown in Figure *2*. The results of the six trials are as follows:

TRIAL	SENSOR TYPE	FRINGES/μm
1	epoxied portion of fibers stripped, 15 cm	1.73
2	unstripped, 15 cm	1.69
3	unstripped, 15 cm	1.64
4	stripped and etched, 15 cm	1.76
5	stripped and etched, 15 cm	1.77
6	unstripped, 3cm, epoxy cured at 125 ^{o}C	1.79

The fringe count versus fiber extension curves for each test are graphically presented in Figures *10* to *15*. These results are close to the theoretically calculated value of 0.554 μm/fringe or 1.80 fringes/μm.

From the tests and results a number of conclusions may be drawn. The first is that the sensor response is not affected by the sensor length. Both the 3 cm long sensor and the 15 cm long sensor exhibit the same fringe sensitivity. The second is that sensor output was linear up to at least an elongation of 400 μm over a 15 cm sensor. This elongation corresponds to a strain of 0.33%. The third conclusion is that stripping and etching the cladding from the fiber improves the strain measurement to a small extent. A similar effect can be achieved by curing the epoxy at a high temperature. This effect is significant because the manufacture of both the fabric reinforced rubber and fiber

reinforced plastic require curing at high temperature. Lastly, the above values were taken as an average of 1.73 fringes/μm or 0.578 μm/fringe for use in further tests.

4.2 Preparation of Test Specimens

4.2.1 Fiberglass Reinforced Plastic Specimens

The fiber reinforced plastic (FRP) specimens were made from Ciba Geigy Canada Vicotex M9 Glass/Epoxy Prepreg which is a balanced glass fabric, 834 g/m^2, impregnated by an Araldite epoxy resin at 43% by weight. The manufacture of a fiberglass specimen containing an optical fiber sensor proceeds as follows

1. As shown in Figure *16*, two layers of prepreg FRP trimmed to the correct specimen size are laid up, each having half the number of plies of the final specimen. This is done by peeling the blue and green protective sheets from each ply and bonding them together. One of the layers is placed on a mould release coated layer of mylar plastic.

2. As seen with difficulty in Figure *17*, the optical fiber is carefully placed onto the surface of the prepreg layer so that it sticks to the epoxy surface.

3. The second layer is then placed over the fiber as seen in Figure *18*, and the protective blue plastic removed from the top layer as seen in Figure *19*.

4. It is then determined where on the specimen the optical fiber leads should exit. A sheet of mylar plastic is then masked at these positions as seen in Figure *20*. The mylar is then sprayed with mould release agent, the masks are removed and holes made in the masked mylar, area which are without release agent, to receive the ends of the optical fiber.

5. The sheet of mylar is then pressed mould release down onto the specimen and the fiber ends are threaded through the holes as seen in Figure *21*. The entire specimen is then covered with another layer of mylar sheet.

6. The specimen or specimens are then placed in a heated press as shown in Figure *22* at a pressure of 300 kPa (43.5 psi) and a temperature of 125 ^{o}C for a period of one hour, which is the curing pressure, temperature and time for this epoxy. Figure *23* shows specimens after curing is completed. At this point cover the fiber where it meets the specimen with a

large drop of RTV (room temperature vulcanized) rubber. The RTV prevents high bending stresses and fiber fracture at this critical junction.

7. The mylar is then cut around the fibers in the shape of the mask and the mylar coverings are removed from the specimen.

8. The specimen is then trimmed of excess epoxy resin using a Dremel MotoTool. Figure *24* shows the finished specimen and Figure *25* shows the fiber/FRP junction.

4.2.2 Fabric Reinforced Rubber Specimens

The material chosen for these specimens was polyester fabric reinforced silicone rubber. This material is the same as that used in the expansion/contraction joint seals in the Pickering NGS pressure relief duct and the vacuum building roof seal in the Pickering NGS vacuum building. The material was made by Freudenberg-NOK, Tillsonburg, Ontario by first laying up a layer of semi-cured silicone rubber, laying a layer of polyester fabric down and applying pressure and temperature in a press, then applying a second layer of silicone rubber and applying pressure and temperature in a press. The material is then cured in an oven at 160 ^{o}C for three hours. Ideally, fiber optic sensors would be introduced to the center of this material next to the polyester layer during the step before the final layer of silicone rubber is applied. This, however, was not possible as the material was delivered in its finished form and was taken from the lot used to make the Pickering NGS PRD seals. To introduce a fiber optic sensor into the center of this material a technique was employed by which splices of this material are made. The manufacture of specimens of this material was as follows:

1. As seen in Figure *26*, two pieces of reinforced silicone rubber have had the rubber layer removed from one side using a knife and described in detail in [49]. Figure *27* shows a close-up of the surface texture required.

2. As shown in Figures *28* to *30*, a thin bead of room temperature vulcanized rubber (RTV) is then spread over the entire fabric surface of both pieces of rubber.

3. The fiber sensor is then placed on one piece and embedded in the RTV as shown in Figure *31*.

4. The two pieces are then placed together with the RTV sides together and stapled together at the corners to prevent relative motion as shown in Figure 32.

5. The specimen is then placed in an unheated press at 300 kPa and the RTV is allowed to cure for 24 hours. The specimen is shown in Figure 33. To finish the process, any exposed edges are sealed with RTV and a small bead of RTV is placed at the specimen fiber junction to relieve any bending stresses.

4.3 Electronic Fringe Counter

The first six trials using the nonembedded sensors relied on manually counting the fringe movement as the sensor was strained. Manual counting methods proved extremely difficult because even at low strain rates fringes moved extremely quickly. The fastest strain rate was in the order of 1 μ-m/sec. In addition, room vibration caused high frequency fringe oscillation which frustrated counting and the uniform appearance of each fringe was confusing and could lead to error. Attempts were made to videotape fringe movement, then replay in slow motion, and this technique proved effective but extremely time consuming. Therefore, an electronic fringe counter was designed and constructed to perform this task.

The principle of operation of the fringe counter is based on a counter described in [31]. Two photodiodes are placed facing the source of the interference fringes to be counted, with one diode spatially advanced slightly with respect to the other along an axis perpendicular to the fringes. If the fringes move in one direction, the advanced diode will detect a higher light level before the other, and vice-versa. By coupling the diodes to an amplifier circuit, appropriate logic and a counter, a system for counting fringes can be developed.

4.3.1 Photodiodes and Mounting Assembly

Figure 34 shows the two photodiodes (Motorola MRD 500) mounted in a phenolic resin assembly. The assembly is designed to sit on the edge of a table, and allows the user to separate the two diodes horizontally by loosening the two thumbscrews and moving the slider. The diodes connect to the circuits through BNC coaxial cables.

4.3.2 Amplifier Circuit

The amplifier circuit is shown in Figure 35. There are two channels, one for each diode, each of which has three stages.

A LF356 JFET transimpedance amplifier which is a very high impedance voltage follower which converts the voltage signal from the diodes into a current signal for the remainder of the circuit. A 50K pot is used to adjust the input offset of the signal, and the capacitors are designed to filter unwanted noise. The second stage is an LM324 Op Amp and adjustment of the 50K pot allows the gain of this stage to be set between unity and one hundred. The third stage is the LM339 Voltage Comparator Stage which converts the analog output of the diodes into a digital 0-5 step signal, based on the comparison voltage which can be adjusted using the 1K pot. This circuit has a hysteresis of 75 mV to avoid problems with electromagnetic noise picked up by the circuit. If the comparison voltage is set at 0.500V, the circuit output will be zero until the output from stage two reaches 0.500V when it will jump to 5V. It will remain at 5V until the stage 2 output reaches 0.425V.

4.3.3 Direction Discriminator

The direction discriminator is shown in Figure *36*. This circuit consists of two identical subcircuits, an upcounter and a downcounter. Each circuit consists of two NOT gates (74LS04), two J-K flip flops (74LS73) which are cross linked to two monostable multivibrators (74LS221), and a final monostable multivibrator which optimizes the output pulse. Both subcircuits are connected to both diodes, but the connections are in opposition. The basic subcircuit can be understood be referring to the logic diagram in Figure *37* and Figure *38* which shows the relevant signals in the circuit when an up-count event plays across the diodes:

Diode #1 and Diode #2: These are the actual signals coming from the voltage comparator on the amplifier board. Diode #1 signal is slightly advanced.

Signal at J(A) and Clock(A): Signals seen at the inputs of the upper J-K flip flop, after passing through the NOT gate.

Signal at J(B) and Clock(B): Signals seen at the inputs of the lower J-K flip flop after passing through the NOT gate.

With this circuit, the J-K flip flops 'read' a signal at J continuously, but only transfer this signal to the output (Q) when the clock experience a negative going transition. The multivibrators output a high signal until they experience a positive going transition, which sets the output low for a fixed duration. Following the events in Figure *37*:

1) Diode #1 goes high: no result since the clock inputs are connected to diode #2

2) Diode #2 goes high: this causes a negative going transition of clock (B), so the high J(B)(due to diode #1) input is transferred to the output Q(B).

3) Q(B) going high triggers multivibrator B, whose normally high output goes low for 70 μ-sec. This is connected to CLR(A), so that the output Q(A) is clamped low for this duration. Q(A) was at a random level before this event, but it will not change now until its clock gets a negative transition.

4) Diode #1 goes low: no result

5) Diode #2 goes low: this triggers clock(A), so the high at J(A) (due to diode #1 being low) is transferred to Q(B). This signals a complete fringe count cycle.

6) Q(B) going high triggers multivibrator A, which in turn clamps Q(B) to ground for 70 μ-sec and causes the final multivibrator to output a short (7 μs) negative going pulse which will be counted by the counter/display circuit. The circuit is now ready to count again.

To summarize, the circuit output only changes when diode #2 undergoes a transition only if diode #1 previously experienced this transition. No signal other than that matching a complete upcount will trigger the circuit. A schematic diagram of the direction discriminator is shown in Figure 39.

4.3.4 Counter/Display Circuit

Figure 40 shows the counter/display circuit which is shown in schematic in Figure 41. The LED display circuit consists of 5 cascading decade counters linked one to one to 5 display/driver chips and 5 seven segment LEDs. Upcount signals from the direction discriminator are applied at pin 12 of the rightmost counter and downcount signals at pin 13. The band of counters maintains a running count of the fringes and feeds signals to the drivers above, which drive the LED displays.

4.3.5 Signal Generator

Figure 42 shows the signal generator which is shown in Figure 43 in schematic. The signal generator generates the staggered signals necessary to cause the fringe counter to count. The

LM777 clock circuit generates a stable squarewave signal. The 74LS161 4-bit binary counter converts this signal into 4 longer wavelength signals, one of which (Q2) is fed into a 74LS174 delay flip flop to delay it by one clock pulse. Taking the output of Q2 and the delay flip flop gives the signals required.

4.3.6 Tests of Electronic Fringe Counter

A number of tests were performed on the bare sensor using the same interferometric system as before. Under good conditions the counter was able to count in excess of 100 fringes per second. Figure *44* shows a plot of the agreement between a manual count from a videotape and a fringe counter count of the same experiment. In all cases the error is less than or equal to one fringe. Five trials were performed using the dial gauge as a correlation of the fringe counter. The results were as follows:

Test	Fiber Elongation (μm)	Error
1	0 - 250	.000
2	0 - 450	.000
3	0 - 250	-.010
4	0 - 500	-.010
5	0 - 300	.000

Therefore, the fringe counter is an accurate method of fringe counting but with a great deal more advantages in time and effort required.

4.4 Tensile Tests Using Interferometric Optical Fiber Sensor

Tensile tests were performed on both polyester fabric reinforced silicone rubber specimens and FRP specimens with embedded optical fiber sensors using the interferometric technique and the electronic fringe counter. A tensile testing machine, JJ Lloyd T5K, was used for these tests. Figures *45* and *46* show the results for two specimens of the polyester fabric reinforced silicone rubber. The strain was calculated from the electronic fringe counter readings as described in 4.0. The results show strain versus load rather than the conventional vice-versa because in these tests the strain is the variable in question. Although there is no independent confirmation of strain, due to the fact that the extensiometer on the tensile machine did not have a fine enough resolution, both curves are exactly the same. This would indicate that both fiber optic sensors are operating correctly.

Since the extensiometer of the tensile machine could not resolve the specimen extension to a sufficient degree, an electrical resistance strain gauge was employed. Unfortunately, the strain gauge could not be bonded to the rubber specimens satisfactorily. It could, however, be bonded to the FRP specimens. A strain gauge was bonded to one of the FRP specimens and it was tensile loaded in the tensile machine for five trials and strain was measured as described previously. The results of these trials are shown in Figure *47*. An average load and a standard deviation was calculated for each strain reading and plotted in Figure *48* with an error band of two standard deviations. A total of five FRP samples with embedded optical fiber sensors were tested in the tensile machine and the results are given in Figures *49*, *50*, *51*, *52*, and *53* with the results of the resistive gauge shown for comparison. It was hoped that the FRP samples would be uniform enough that the fiber sensor results would fall within the error bounds of the resistive gauge. This was not true for the most part, and the resistive gauge can only be used as a rough guide that the fiber sensors are reading correctly. However, the fiber sensors give good, linear results and were able to read strains on the order of 0.5 μ-strain.

5.0 ATTENUATION FIBER OPTIC STRAIN SENSOR

As the name implies, attenuation based fiber optic sensors measure the quantity of interest by correlating it to the amount of light which is attenuated during its passage through the fiber sensor. As such, this type of sensor is an *intrinsic* sensor. A light source such as a laser, laser diode or arc lamp is coupled into one end of the optical fiber. The quantity of interest is applied to the material containing the fiber optic sensor then acts on the material in such a manner as to alter the transmission characteristics of the optical fiber. The transmitted light is then measured with an optical power meter or other sutitable detector, depending on the application. The main advantage of attenuation based sensors is their simplicity, both in construction and operation. As seen previously, the technique of interferometry is considerably more difficult to implement as is the technique of polarimetry. The major disadvantage is the difficulty in ensuring that the measurand of interest is the only factor which contributes to the attenuation. For example, longitudinal strain may be the quantity being measured, but lateral strain may also cause attenuation to a lesser or greater extent. A second disadvantage is in producing multiple sensors with consistent responses. Generally, the response curve varies for each sensor. Depending on application, lack of sensitivity may be a problem. The best attenuation base strain sensors have a resolution in the order of 1 microstrain, which is considerably larger than the resolution of interferometric sensors.

5.1 Types of Fiber Optic Attenuation Sensors

5.1.1 Microbend Sensors

The majority of attenuation based fiber optic sensors operate on the principle that light propagating along the core of an optical fiber can be made to 'leak' out if the curvature of the fiber exceeds some value at any given point. These curves are known as microbends. Since optical fibers operate on total internal reflection, a change in the angle at which the light strikes the interface between the core and cladding, as shown in Figure 54, which is produced by a microbend, will lead to loss of light from the core to the cladding. Telecommunication is the dominant application of optical fibers and sets the standards for optical fiber production which has resulted in fiber technology advanced to the point where losses are minimal. Therefore, to induce attenuation in a controlled fashion into optical fiber, artificial microbends in the shape of an undulating sinusoid are induced mechanically.

For the measurement of strain, a number of different techniques for the introduction of microbends have been attempted. One technique has been to thread the sensor between the links of a small chain [22]. As the chain is strained, the links realign and in the process bend the optical fiber. Another technique has been to braid two optical fibers together [23]. This imposes curves of known radius of the fibers. When tension is applied along the length of the fiber braid, it stretches, reducing the radius of curvature of the twists and reducing light losses. If the optical fiber is made from polymers rather than silica, permanent microbends may be introduced by heating the fiber in a press with a corrugated mould [24]. As the strain sensor extends, the microbends decrease in radius allowing for less attenuation of the light.

5.1.2 Misalignment Sensors

Misalignment sensors involve an entirely different means of attenuation than the microbend sensors. If a splice is to be made between two separate optical fibers, great care must be taken for accurate alignment between both fibers in order to minimize transmission loss. Three types of misalignment are common, lateral and angular misalignment and axial displacement. Lateral misalignment occurs when the axis of one fiber is not colinear with the other. Angular misalignment occurs when the fibers do not run in similar directions. Axial displacement losses occur when the two ends of accurately aligned fibers move apart in the direction of their common axis. Light losses are

sensitive to both lateral misalignment and axial displacement much more than to axial misalignment. However, since the axial displacement losses depend upon the relative movement between two fibers along their length, this effect may be used to sense strain, since, as stress is applied to both fibers embedded in a material, the ends will move apart decreasing the transmission of light.

To calculate the theoretical loss between two fibers and referring to Figure 55, where d is the distance between the fiber ends, r is the radius of the fibers, θ is the half angle of the cone of emitted light and R is the radius of the cone at distance d from the source fiber. If P_s is the power output from the source fiber and P_r is the power entering the receiving fiber:

$$R = r + d \tan\theta$$

$$P_r = P_s * \frac{\pi r^2}{\pi R^2}$$

$$= P_s r^2/(r^2 + 2rd*\tan\theta + d^2*\tan^2\theta)$$

Therefore, the light power received by the optical fiber is inversely proportional to the square of the distance between the source and receiving fibers.

5.2 Experimental Development of Attenuation Based Embedded Fiber Optic Strain Sensor

Since a number of techniques were available for an attenuation based fiber optic strain sensor, an experimental program was carried out to determine the difficulties in manufacturing the two materials, FRP and fabric reinforced rubber, with each type of sensor, and the ease of use and quality of each type of sensor. Unlike the interferometric sensor which required an optical fiber having low loss characteristics, the exact opposite holds true for the attenuation based sensor. It is necessary that losses occur in the optical fiber due to bending. For that reason, different types of optical fiber were used for the attenuation based sensors. Both single mode and multimode fibers were considered. The fiber cores were both silica based and polymer based. Since the manufacture of both types of materials require curing under pressure and heat, it was first necessary to determine if the cure process would affect the fiber transmission characteristics.

To determine the thermal response, a length of fiber was cleaved at both ends and the maximum light transmission was measured

using a 4 mW He-Ne laser and a radiometric power meter. It was then heated to 130 ^{o}C for one hour under no pressure. Upon inspection following the heating, it was noticed that plastic outer jacket of the fiber had melted. The core and cladding of the fiber, however, appeared intact. The fiber's transmission was unchanged. Since the jacket is only used to protect the bare fiber and since the sensor would be embedded, the jacket is not required for this application. To determine the response of the fiber to pressure, a length of fiber was cleaved at both ends and the light transmission measured. It was then position in the center of four plies of FRP and the sample was then cured in a press at 300 kPa (43.5 psi). Since the FRP is semi-transparent it was possible to see the fiber within the cured FRP sample. The fiber deviated significantly from its original straight path along the sample in that the plies had undergone a relative sliding before the epoxy cured. The transmission had dropped to 94% of its original value.

The shifting of the position of the fiber withing the FRP was a significant problem as the attenuating techniques require that the fiber maintain a specific geometry in order that it attenuate light in a predictable manner. It is also required that transmission and loss versus strain be correlated both before and after embedment of the sensor. It was found that shifting and sliding occurred for different numbers of plies and even reducing the pressure did not eliminate this effect. Eventually it was discovered that if the pressure was increased incrementally at intervals of several minutes once the curing temperature was achieved, the plies would not slide when the maximum pressure was applied.

A number of the different attenuating mechnisms were tried. Some, such as the chain mechanism were rejected outright as impractical due to size causing a perturbation in the material when embedded and the fact that the adhesive bonding between plies would also bond the links of the chain and prevent it from producing regular bends in the fiber. Several attempts were made to produce cables of twisted fibers that would respond to strain directed along their lengths. These met with no success. Both multimode and single mode fibers were employed but absolutely no increase in transmission was observed when the sensors were stressed. An attempt was made to induce permanent microbends in Newport F-MLD multimode fibers which possess a silica core. After several trials in which the fiber was placed between two corrugated plates with wavelength of 0.75 cm and then heated in a press it was found that the high temperature heating required to induce permanent bends in the silica core melted the polymer jacket and did nothing to produce permanent bends in the fiber. The fiber was then pressed and heated at a low 80 ^{o}C

temperature which produced a partial success. The polymer jacket had permanently bent. However, the wavelength was not that of the corrugations and was longer than recommended. In addition repeatability of results was not possible and only random fluctuations in the tranmission characteristics were observed when the sensor was strained. Other, mechanical methods, such as staples, pins, and tacks, were tried in order to hold the fiber in a microbent position during layup and curing of the laminates. However, either the mechanical devices would seriously affect the strength of the laminates or if they were external to the material the devices did not produce the required microbent sensor. It became evident that there was no apparent method of holding the fiber in an adequately microben position during curing process and so the microbend sensor technique was abandoned.

5.2.1 Axial Displacement Induced Attenuation Sensor

In order to test this concept two separate lengths of optical fiber were cleaved at both ends. A 4 mW He-Ne laser was coupled into one fiber, the other end being secured on a mount. The second fiber was placed in a fiber positioner, mounted on a micrometer stage and manoeuvered into position, aligned along the axis of the first fiber. The end of the moveable fiber was fed into an optical power meter. The fiber ends were brought together until they just touched and their relative lateral positions adjusted until the light transmission was maximized. Using the micrometer stage, the fiber ends were separated in increments of 0.05 mm and the corresponding drop in transmission recorded. These results are presented in Figure *56*. The results show a high sensitivity to displacement. Furthermore, assuming consistent fiber cleaving methods, achieving fairly consistent sensor response should not be a problem. The geometry is simple and should not pose any problem when embedded within the materials.

The major obstacle to the axial displacement sensor was preventing the fiber ends from misaligning during the curing process of the laminated materials. A customized aligning mechanism was developed which consisted of a slip of Mylar plastic of 1.5 x 2.5 cm x 0.1 mm thick in which a straight groove was etched using a knife. The groove was made as deep as possible without piercing the Mylar. The optical fiber, when stripped of its jacket, fit snugly within this groove. One of the fiber ends was threaded along this groove until it reached the midpoint of the strip. Tape was then placed over the top leaving only the tip of the fiber exposed. The other fiber end was threaded from the other side of the groove until it just touched the first fiber. The fiber junction was then covered with

tape to prevent the epoxy or RTV used in the composite materials from intervening between the two fiber tips. A diagram of the sensor is shown in Figure 57. When the 4 mW He-Ne laser was coupled into one fiber and measured at the output of the other transmitted optical power in excess of 1 mW was obtained. Since there is always an appreciable loss when coupling light into a fiber, this aligning mechanism was precise enough for the intended purpose.

5.2.1.1 Specimen Fabrication and Testing

The FRP specimens were constructed as reported previously. These specimens consisted of 8 plies and measured 20 x 6 cm. The sensors were embedded between the fourth and fifth plies, parallel to the lengths of the specimens. The fibers exited the specimens 5 cm from their ends to prevent the jaws of the tensile testing machine from damaging the sensors. The first specimen was tested using the tensile testing machine at an extension rate of 1 mm/min. and the results shown in Figure 58. The resolution of the extensiometer of the testing machine was only 1 mm so that a correlation between extension and optical power loss was not possible. In addition, the response curve of the sensor may not remain unchanged both before and after specimen curing. Since all attenuation based sensors are sensitive to the geometry of the fibers, it would be possible that small movements during the cure process could alter the response curve some unknown degee. Because the sensor geometry could not be authenticated after curing, essentially no correlation could be made between sensor response and specimen extension. As mentioned previously, however, the final application for these sensors would be in the detection of aging characteristics of composite materials of these types. Therefore, the absolute measurement of the strain quantity correlation with the optical power attenuation is not as important as the comparative measurements of the optical power attenuation at different aging periods during the component's life for the same load conditions.

The measurement also presented a number of difficulties which were required to be overcome. The first is that there appears to be an initial range of low sensitivity in the sensors at low strains. This may be explained by 'slack' being taken up either in the material or in the fibers until a correspondence is reached between the fiber dislocation and the material strain. The second is that noise will exist in the measuring system. The solution to this is a long warm-up time for the electronic instruments, especially the laser.

A total of thirteen FRP specimens were constructed with embedded sensors. Of these, five of the specimens were deemed suitable to

undergo aging and further testing. There were several reasons for the large proportion of unsuitable specimens. Several suffered from damaged fiber leads which did not allow proper coupling with the laser. In other cases, the transmission of light through the sample was too low to be of value. This only occurred in the first few specimens made until more experience was gained in securely aligning and cleaving fiber ends. In many cases with the FRP specimens there was a lack of response to the applied load. It was noticed that there was slippage in the jaws of the tensile testing machine at loads greater than 1500 newtons. It appeared that this load was not great enough to strain the specimen to a significant amount. To counteract this effect the cross sectional area was reduced by reducing the number of plies in a specimen from eight to four. In addition the width in the measured portion of the specimen containing the sensor was narrowed to two centimeters. In order to improve the jaw grip, pin loading was introduced. Baseline tests were performed on the modified specimens and the results are shown in Figures *58* through *62*.

Polyester fabric reinforced silicone rubber specimens were made as previously containing an embedded attentuation fiber optic sensor. Because these specimens were much weaker than the FRP specimens many of the problems involved with the FRP specimens such as jaw grip and not enough load to produce response were not encountered. Four of these specimens were made and tested. The results are shown in Figures *63* to *66*.

6.0 CONCLUSIONS AND RECOMMENDATIONS

6.1 Interferometric Fiber Optic Strain Sensor

From the work which has been performed on the development of an interferometric fiber optic strain sensor for use with both FRP and fabric reinforced rubber a number of conclusions and recommendations may be made. The first is that, although the results of tests on the interferometric fiber optic strain sensor could not be verified via conventional techniques, the results are very promising in that they are linear, precise, and repeatable.

The second conclusion is that the manufacture of an embedded fiber optic sensor in materials such as reinforced rubber or FRP is a skilled process. The level of skill required is on the order of that of a skilled fiber composite layup machinist or one who makes splices in reinforced rubber. There was no damage to the core or cladding of the optical fiber from the curing process itself from either the rubber or the FRP. Damage occurred

primarily at the material/fiber interface where great care must be taken. It is concluded that if the procedures annotated previously for fiber embedment are followed, an operational sensor will be achieved.

A fourth conclusion is that it is necessary to use some type of fringe counter with interferometric sensors. In this study, a direction discriminator electronic fringe counter was designed and built. This electronic fringe counter had its own set of problems including dependence on the absolute intensity of laser light, calibration requirement, and no data logging capability. It is therefore recommended that a heterodyne phase detector be designed and constructed for further work with interferometric sensors.

Lastly, it is recommended that accelerated aging techniques be applied to the specimens having embedded interferometric sensors in order to determine if the sensors could detect changes in material characteristics due to aging.

6.2 Attenuation Fiber Optic Strain Sensor

From the work on the attenuation fiber optic strain sensor it may be concluded that attenuation based fiber optic strain sensor must be constructed exclusively from multimode fibers rather then single mode and that of the attenuation sensors which have been investigated, the most reliable and accurate has been the axial displacement sensor. The axial displacement sensor provided adequate sensitivity, range, repeatablility and ease of construction. Secondly, unlike interferometric sensors and telecommunications applications, attenuation based fiber optic sensors require optical fiber in which the losses are significant over a short range. The loss in single mode fibers is much too low for attenuation based applications. Because multimode fibers have a much larger diameter than single mode fibers, problems may arise in which the fiber affects the material due to its size. However, this disadvantage is balanced by the increased durability of multimode fibers. Secondly, multimode polymer fibers are not applicable for applications such as FRP and reinforced rubber in which high curing temperatures are required. In order to survive the high curing temperature, glass fibers must be used.

Because attenuation based sensors are not as sensitive to strain as are the interferometric sensors, it is recommended that the attenuation sensor not be used in applications where strains are expected to be small. This is particularly apparent in FRP applications where there was difficulty in consistently producing responsive specimens. No problems were encountered in the

reinforced rubber specimens, however, in that the strains in the rubber were quite large. Since large strains produce a large number of fringes in the interferometric sensor, it is recommended that attenuation sensors be used in applications in which the strains are expected to be large such as reinforced rubber and other flexible materials, and that interferometric sensors be used in more rigid, unyielding materials such as FRP, exclusively. Lastly, like interferometric sensors, it is recommended that accelerated aging processes be applied to specimens having attenuation based sensors embedded in them, in order to determine if the sensors detect any change in characteristics of material due to aging effects.

7.0 ACKNOWLEDGEMENTS

This study would not have been possible without the skill and dedication of two of the finest students this author has had the pleasure to employ, Mr. Sean Walmsley of McMaster University Department of Engineering Physics, and Mr. Stephen Wismayer of University of Waterloo Department of Engineering Physics. Mr. Walmsley worked almost exclusively on the interferometric sensors, and Mr. Wismayer worked exclusively on the attenuation sensors. Their work is greatly appreciated.

Prepared by:

R.J. Lewak
Engineer
Materials Chemistry Section

Recommended by:

R.W. Glass
Supervising Chemist
Materials Chemistry Section

Approved by:

D.J.R. Dodd
Manager
Chemical Research Department

8.0 REFERENCES

1. **Fiber Optic Sensors - An Introduction for Engineers and Scientists**, edited by Eric Udd, John Wiley & Sons, Inc., New York, 1991.

2. **Application of Optical Fiber Waveguides in Radiation Dosimetry**, W. Gaebler and D. Bräunig, Hahn-Meitner-Institut für Kernforschung Berlin Gmbh.

3. **Double Polarisation Interferometer for Digital Force Sensing by Fiber Tension Bending**, Norbert Fürstenau, Optics Letters, Vol.13, No.3, March 1988.

4. **Measurement of Small Phase Shifts Using a Single-Mode Optical-Fiber Interferometer**, D.A. Jackson, A Dandridge, and S.K. Sheem, Optics Letters, Vol.5, No.4, April, 1980.

5. **Fiber-Linked Interferometric Pressure Sensor**, G.Beheim, K. Fritsch and R.N. Poorman, Review of Scientific Instrumentation, Vol.58, No.9, Sept, 1987.

6. **Single-Mode Fibre-Optic Sensors: Conventional Interferometric, Polarimetric and Combined Devices**, J.D.C. Jones, P. Akhavan Leilabady, D.A. Jackson, M.Corke, and A.D. Kersey, Proceedings of the SPIE, Fibre Optics '85, Volume 522, pp.196 - 203, 1985.

7. **A Silicon-Based Fibre-Optic Temperature Sensor**, Isko Kajanto and Ari T. Friberg, J.Phys. E:Sci. Instrum., Vol 21, pp. 652 - 656, 1988.

8. **Sensor Heads Based On "All Fiber" Couplers**, Paolo Bassi and Maurizio Zoboli, Optics Communications, Volume 75, No.1, pp. 21-24, Feb., 1990.

9. **Fiber-Optic Sensing of Pressure and Temperature**, G.B. Hocker, Applied Optics, Vol.18, No.9, May, 1979.

10. **Fiber Optic Damage Detection in Composite Structures**, B. Hofer, ICAS Report ICAS-86-4.1.2, 1986.

11. **Use of Embedded Optical Fibre for Early Fatigue Damage Detection in Composite Materials**, S.R. Waite, Composites, Vol.21, No.2, March, 1990.

12. **All-Fiber Polarimetric Sensor**, Marc D. Mermelstein, Applied Optics, Vol.25, No.8, April 1986.

13. **Fibre Optic Two Polarization Interferometer with Unabiguous Digital Readout and Its Application as Remote Strain Sensor**, Norbert Fürstenau, Proceedings of SPIE, Fibre Optics '86, Vol. 630, pp 220-224, 1986.

14. **Fiber Optic Temperature and Strain Sensors**, G. Meltz, J.R. Dunphy, W.H. Glenn, J.D. Farina, and F.J. Leonberger, Proceedings of SPIE, Fiber Optic Sensors II, Vol. 798, pp 104-110, 1987.

15. **Fiber-Coil Deformation-Sensor Immune from Temperature Disturbances**, Y. Ohtsuka, M.Kamaishi, Y.Imai, International Journal of Optoelectronics, Vol.3, No.5, pp.371-380, 1988.

16. **Use of Optical Fiber for Damage and Strain Detection in Composite Materials**, S.R. Waite, R.P. Tatam, and A. Jackson, Composites, Vol.19, No.6, November, 1988.

17. **Prototype Polarimetric Based Fiber Optic Strain Gauge**, Brian W. Brennan, Review of Progress In Quantitative Nondestructive Evaluation, pp 547-552, 1988.

18. **Combined Michelson and Polarimetric Fibre-Optic Interferometric Sensor**, M. Corke, J.D.C. Jones, A.D. Kersey, and D.A. Jackson, Electronics Letters, Vol.21, pp.148-9, 1983.

19. **Monomode Fiber-Optic Strain gauge with Simultaneous Phaseand Polarization-State Detection**, P. Akhavan Leilabady, J.D.C. Jones, and D.A. Jackson, Optics Letters, Vol.10, No.11, November, 1985.

20. **High-Sensitivity Fibre-Optic Strain sensors for Measuring Structural Distortion**, C.K. Asawa, S.K. Yao, R.C. Stearns, N.L. Mota, and J.W. Downs, Electronics Letters, Vol.18, No.9, April, 1982.

21. **Fibre-Optic Strain Measurement for Structural Integrity Monitoring**, A.J.A. Bruinsma, P. van Zuylen, C.W. Lamberts, and A.J.T. de Krijger, Proceedings of SPIE, Volume 514, 1984.

22. **Wide-Range Fiber-Optic Sensor**, Dean C. Marvin and Neil A. Ives, Applied Optics, Vol.23, No.23, December, 1984.

23. **A Strain Sensor Using Twisted Optical Fibers**, Tetsuji Abe, Yutaka Mitsunaga, and Hiroaki Koga, IEEE Journal of Lightwave Technology, Vol.7, No.3, March 1989.

24. **Fiber-Optic Strain Gauge**, Jonathan D. Weiss, IEEE Journal of Lightwave Technology, Vol.7, No.9, Sept. 1989.

25. **Fiber Optics Strain Gauge**, C.D. Butter and G.B. Hocker, Applied Optics, Vol.17,No.18, September, 1978.

26. **The Dynamical Behavior of a Single-Mode Optical Fiber Strain Gage**, Mario Martinelli, IEEE Journal of Quantum Electronics, Vol.QE-18, No.4, April, 1982.

27. **Interferometric Optical Fibre Strain Measurement**, D. Uttam, B. Culshaw, J.D. Ward, and D. Carter, J.Phys. E:Sci.Instrum., Vol.18, pp 290-293, 1985.

28. **Interferometric Strain Measurement Using Optical Fibres**, P. Akhavan Leilabady, J.D.C. Jones, D.A. Jackson, Proceedings of SPIE, Fiber Optic Sensors, Vol.586, 1985.

29. **An Overview of Mach-Zehnder Interferometric Sensors**, S.F. Watanabe and R.F. Cahill, Proceedings of SPIE, Fiber Optic and Laser Sensors III, Vol.566, 1985.

30. **A Rugged Optical Fiber Interferometer for Strain Measurements Inside a Composite Material Laminate**, Kent Murphy and John C. Duke, Jr., ASTM Journal of Composites Technology and Research, pp 11- 15, 1988.

31. **Interferometric-Fiber-Optic Strain Sensor**, J.S. Sirkis and C.E. Taylor, Experimental Mechanics, Vol. 28, No.2, June, 1988.

32. **Direct Measurement of Strain in Optical Fibres During Tensile Tests on composite Optical Communications Conductor**, S.R.M. Robertson, Central Electricty Generating Board Report TPRD/L/2557/N83, London, UK, November, 1983.

33. **Nondestructive Testing of Composite Materials by OTDR in Imbedded Optical Fibers**, R.O. Claus, B.S. Jackson, and K.D. Bennett, Proceedings of SPIE, Fiber Optic and Laser Sensors III, Vol.566, 1985.

34. **Distributed Fiber-Optic Sensors: An Overview**, Stuart A. Kingsley, Proceedings of SPIE, Fiber Optic and Laser Sensors III, Vol.566, 1985.

35. **Novel Method to Pseudoheterodyne a Polarimetric Fiber Optic Sensor**, Mario Martinelli and Paolo Vavassori, Applied Optics, Vol. 28, No.12, June 1989.

36. **Homodyne Demodulation Scheme for Fiber Optic Sensors Using Phase Generated Carrier**, Anthony Dandridge, Alan B. Tveten, and Thomas G. Giallorenzi, IEEE Journal of Quantum Electronics, Vol QE-18, No.10, October, 1982.

37. **Synthetic-Heterodyne Interferometric Demodulation**, James H. Cole, Bruce A. Danver, Joseph A. Bucaro, IEEE Journal of Quantum Electronics, Vol.QE-18, No.4, April, 1982.

38. **Passive Demodulation of Optical Interfermometric Sensors**, Eugene L. Green and Peter G. Cable, IEEE JOurnal of Quantum Electronics, Vol QE-18, No. 10, October, 1982.

39. **Pseudoheterodyne Detection Scheme for Optical Interferometers**, D.A. Jackson, A.D. Kersey, M. Corke, J.D.C. Jones, Electronics Letters, Vol.18, No.25, December, 1982.

40. **Synchronous Phase Detection for Optical Fiber Interferometric Sensors**, I. Jeffrey Bush and Ronald L. Phillips, Applied Optics, Vol.22, No.15, August, 1983.

41. **Applications of Embedded Optical Fiber Sensors In Reinforced Conrete Buildings and Structures**, A. Méndez, T.F. Morse and F. Méndez, Proceedings of SPIE, Fiber Optic Smart Structures and Skins II, Vol.1170, 1989.

42. **Embedded Optical Fiber Sensors for Materials Evaluation**, R.O. Claus, K.D. Bennett, A.M. Vengsarkar, K.A. Murphy, Journal of Nondetructive Evaluation, Vol.8, No.2, 1989.

43. **Distributed Optical-Fibre Sensors for the Measurement of Pressure, Strainand Temperature**, A.J. Rogers, Journal of the Institution of Electronic and radio Engineers, Vol.58, No.5(Supplement), July/August, 1988.

44. **Optical Fibre Sensing Using Light Scattering Techniques**, Robert G.W. Brown, J.Phys.E: Sci.Instrum., Vol.20, pp.1312-1320, 1987.

45. **Multiplexed and Distributed Optical Fibre Sensor Systems**, J.P. Dakin, J.Phys.E: Sci.Instrum., Vol.20, pp.955-967, 1987.

46. **Sensors in Industrial Metrology**, Barry E. Jones, J.Phys.E: Sci. Instrum., Vol.20, pp.1113-1126, 1987.

47. **Optical Fiber Sensor Technology**, Thomas G. Giallorenzi, Joseph A. Bucaro, Anthony Dandridge, G.H. Sigel,Jr., James H. Cole, Scott C. Rashleigh, and Richard G. Priest, IEEE Journal of Quantum Electronics, Vol. QE-18, No.4, April, 1982.

48. **Fiber Optic Sensor Overview**, Ramon Perez De Paula and Emery Lightner Moore, Proceedings of SPIE, Fiber Optic and Laser Sensors III, Vol.566, 1985.

49. **Pickering NGS 1990 Vacuum Building Outage - Inspection of the Pressure Relief Duct Expansion/Contraction Joint Seals**, R.J. Lewak, Ontario Hydro Chemical Research Department Report 90-204-K, September, 1990.

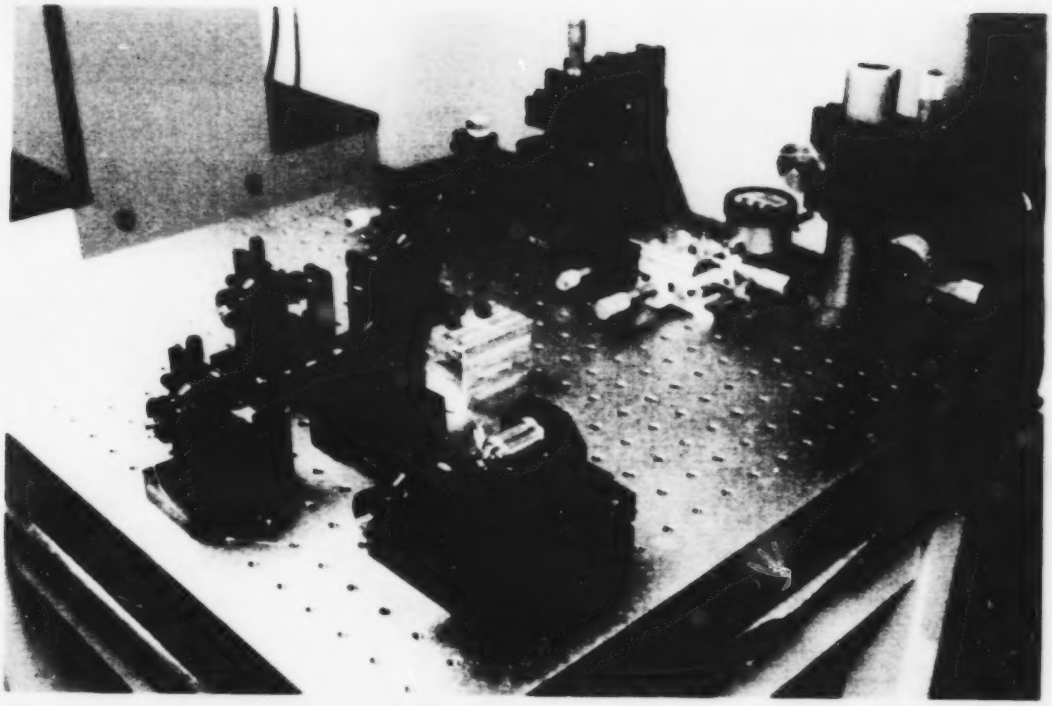

FIGURE 1. EQUIPMENT ARRANGEMENT ON OPTICAL TABLE FOR INTERFEROMETRIC SENSOR TRIALS - OBLIQUE VIEW

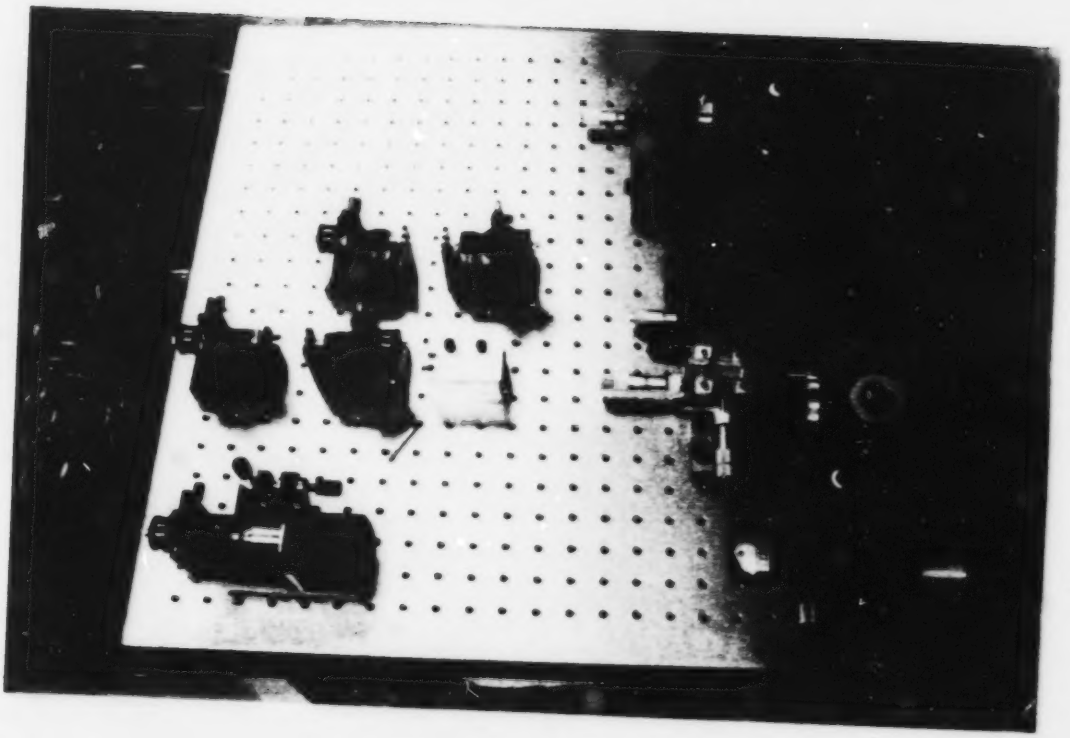

FIGURE 2. EQUIPMENT ARRANGEMENT ON OPTICAL TABLE FOR INTERFEROMETRIC SENSOR TRIALS - TOP VIEW

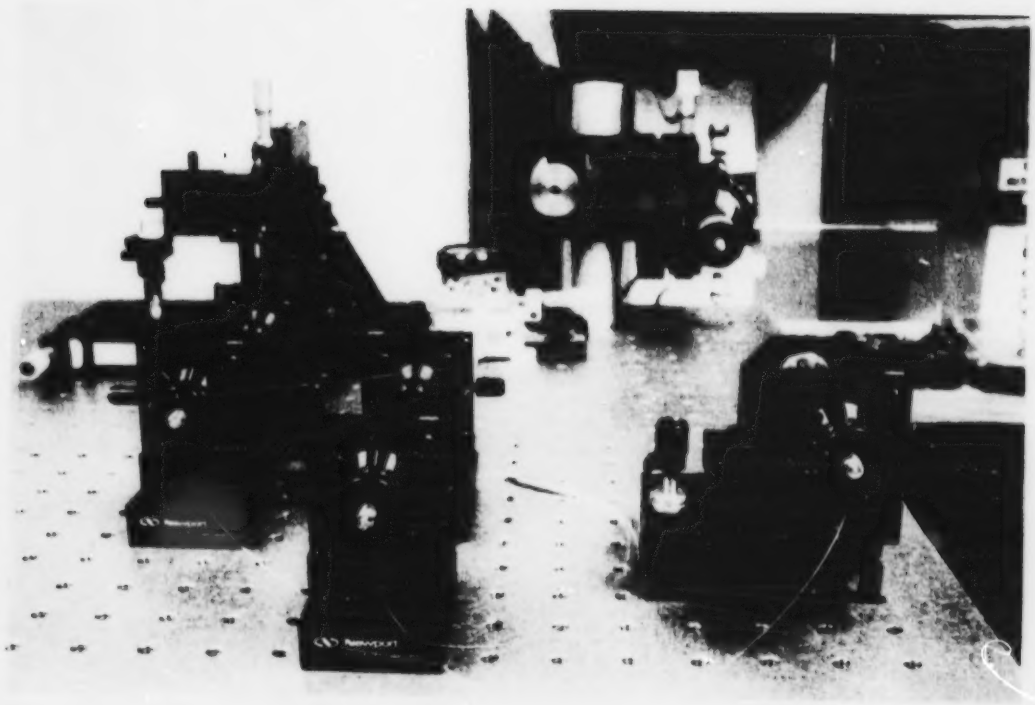

FIGURE 3. EQUIPMENT ARRANGEMENT ON OPTICAL TABLE FOR INTERFEROMETRIC SENSOR TRIALS - SIDE VIEW

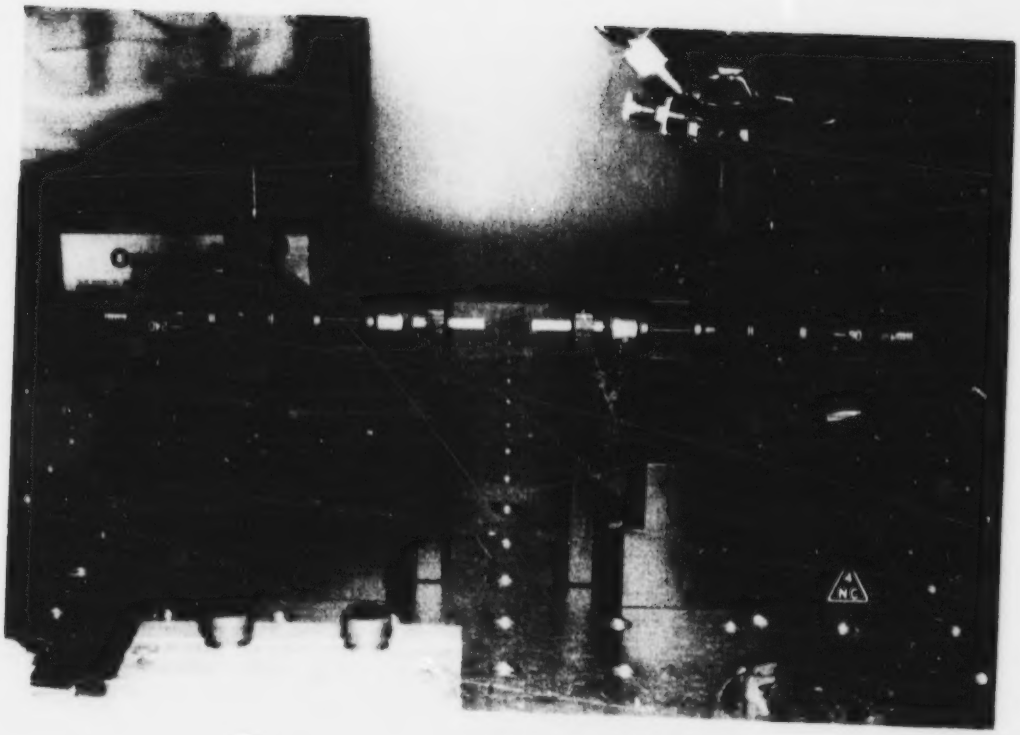

FIGURE 4. *GRIN* ROD LENSES IN *GRIN* ROD LENS HOLDERS USED TO COUPLE LIGHT FROM OPTICAL FIBER TO OPTICAL FIBER

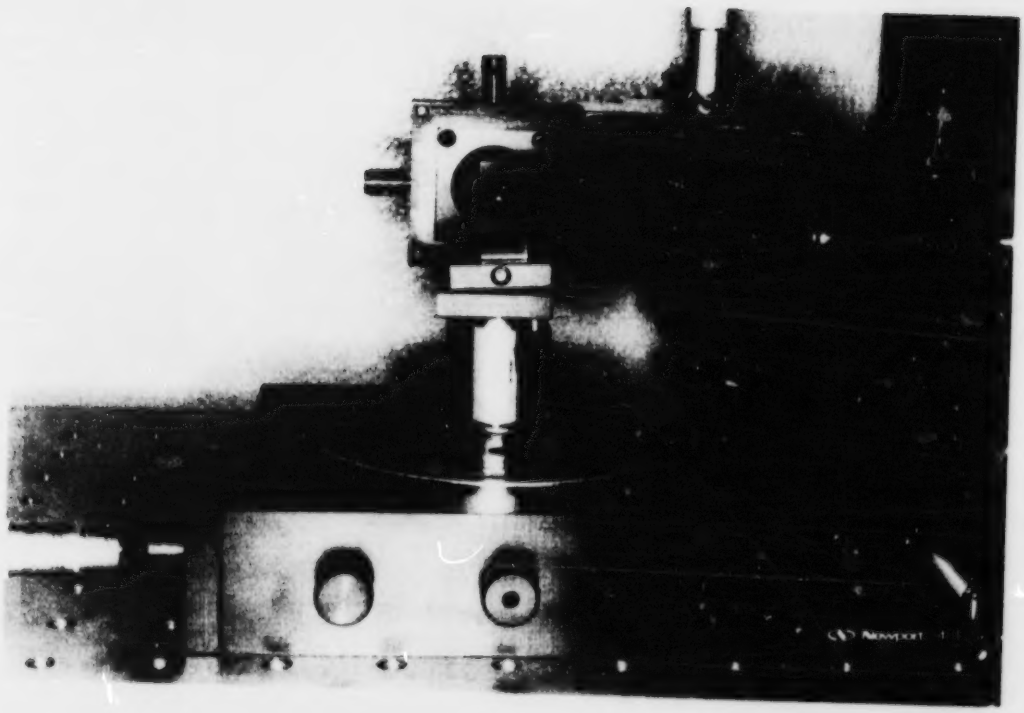

FIGURE 5. BEAM SPLITTER CUBED USED TO RECOMBINE BEAMS FROM BOTH ARMS OF INTERFEROMETRIC SENSOR

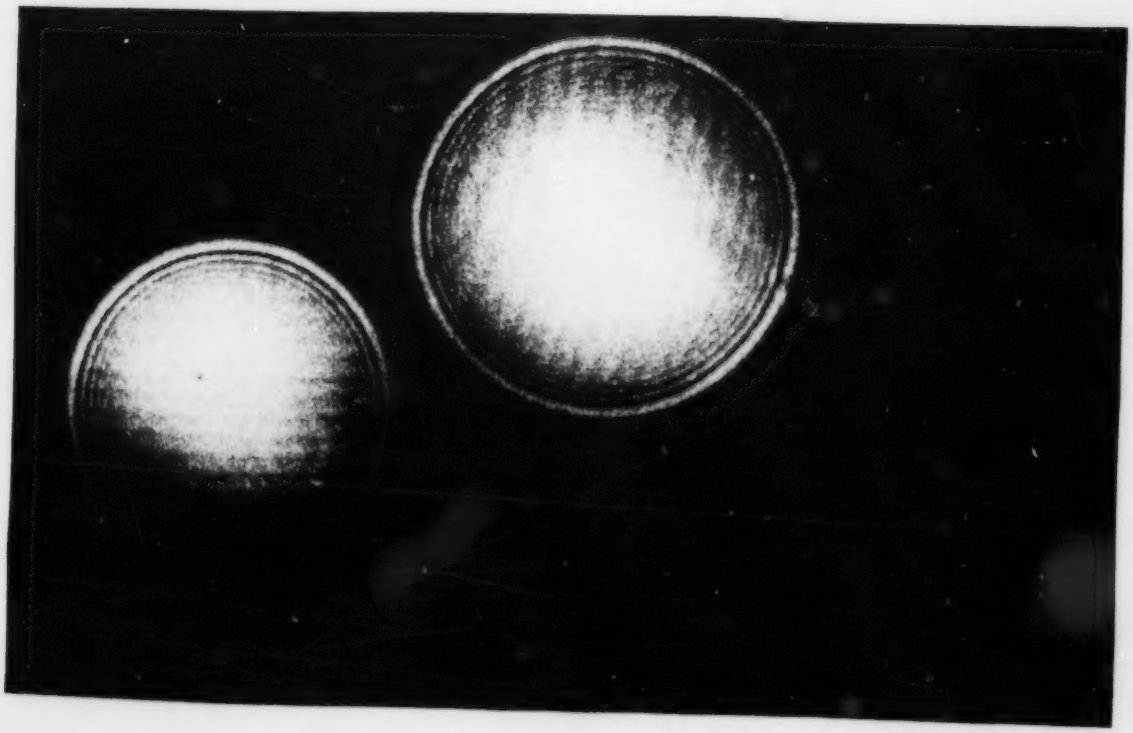

FIGURE 6. BEAMS FROM BOTH ARMS OF INTERFEROMETRIC SENSOR - SECONDARY FRINGES PRESENT

FIGURE 7. BEAMS FROM BOTH ARMS OF INTERFEROMETRIC SENSOR - SECONDARY FRINGES ABSENT

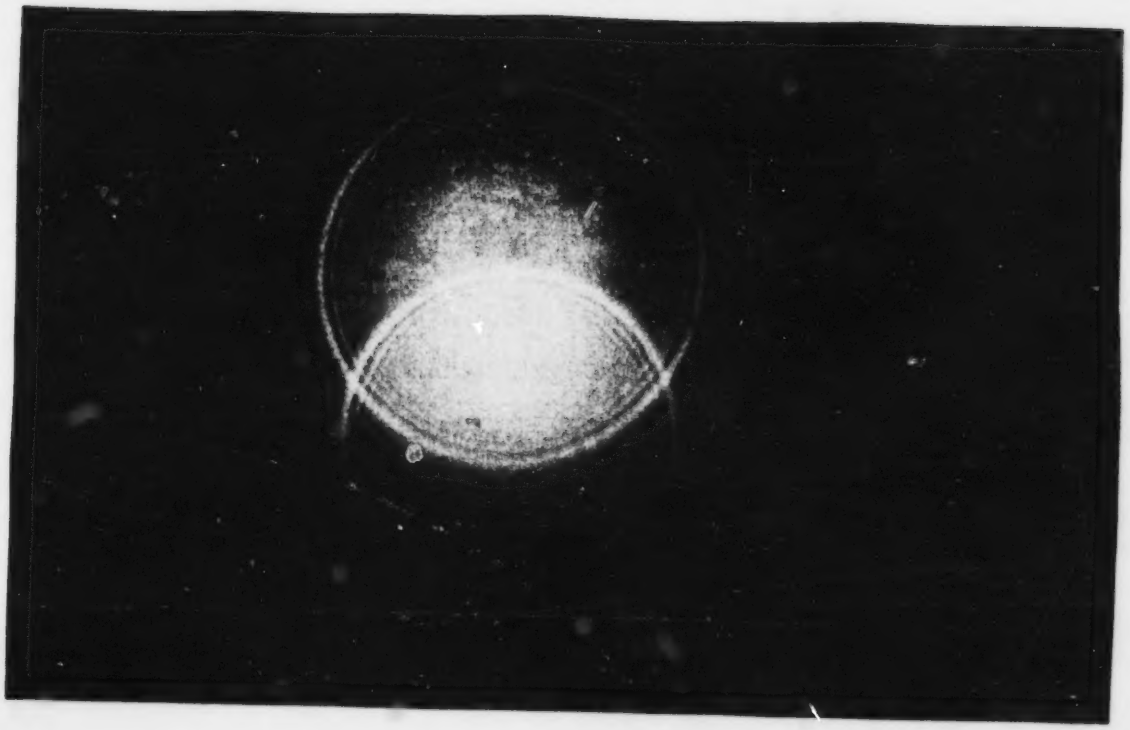

FIGURE 8. BRINGING TOGETHER BEAMS FROM BOTH ARMS OF MACH-ZEHNDER INTERFEROMETER

FIGURE 9. FRINGE PATTERN FORMED BY INTERFERENCE OF BEAMS FROM BOTH ARMS OF INTERFEROMETRIC SENSOR

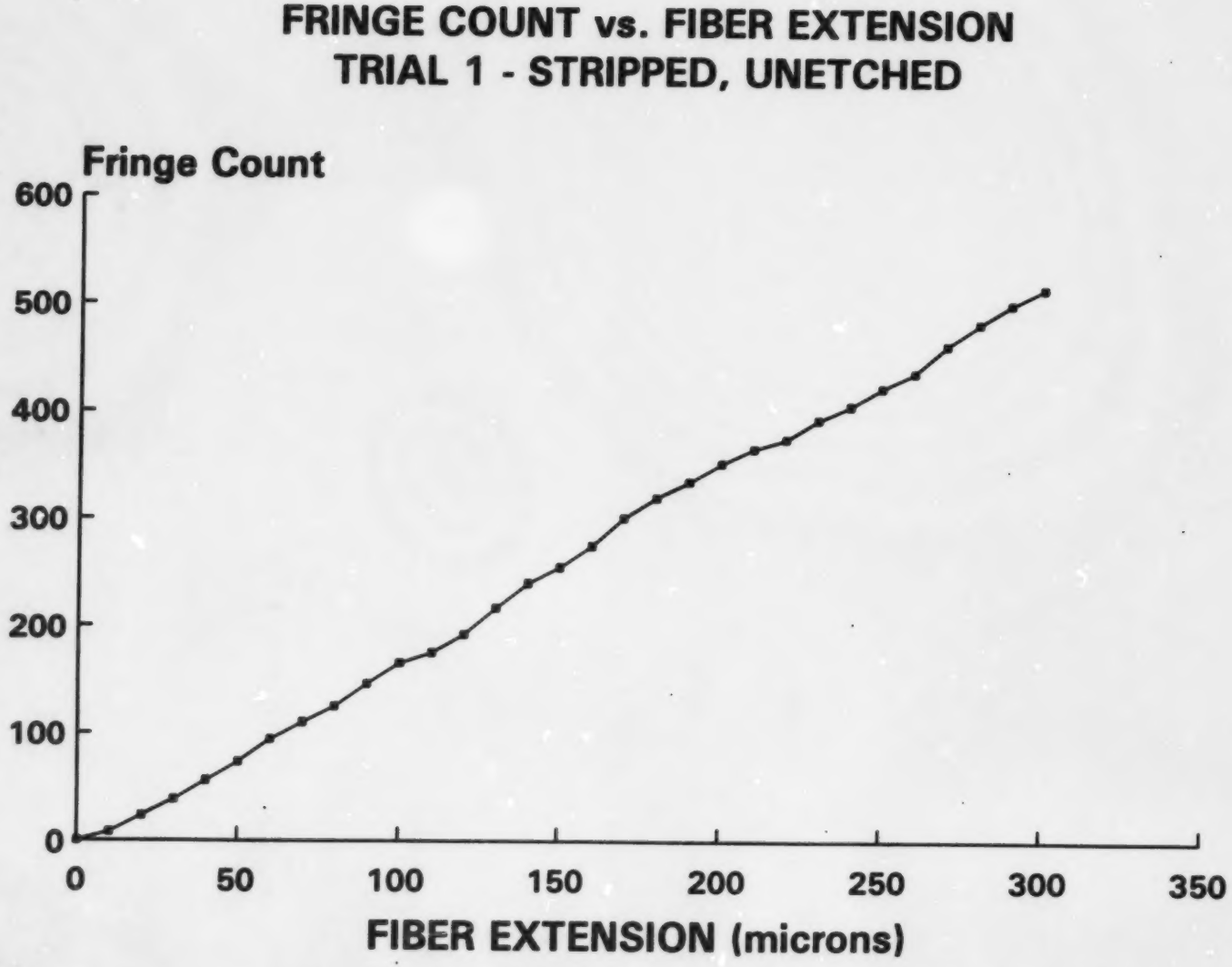

FIGURE 10. FRINGE COUNT VS. FIBER EXTENSION - TRIAL 1

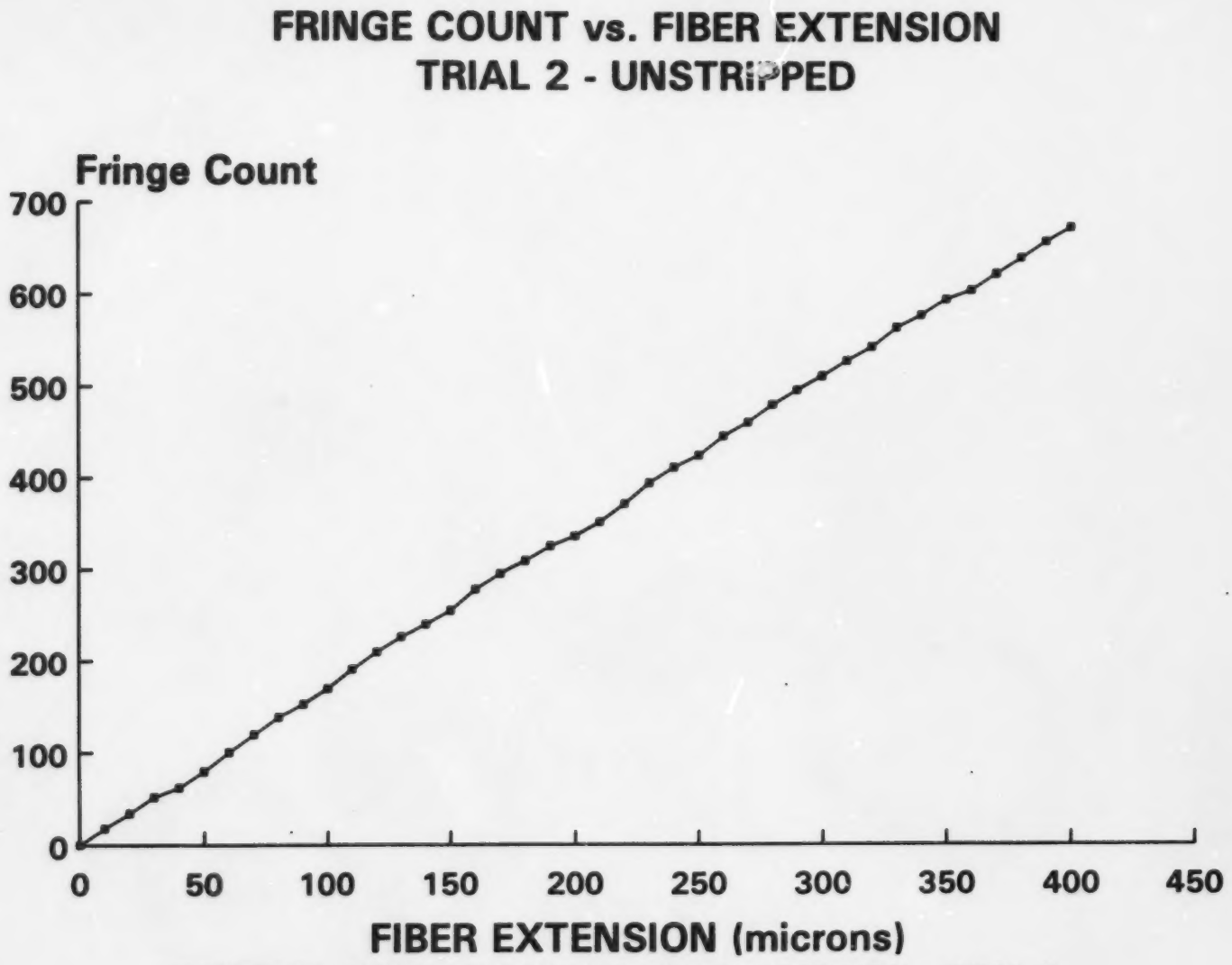

FIGURE 11 FRINGE COUNT VS. FIBER EXTENSION - TRIAL 2

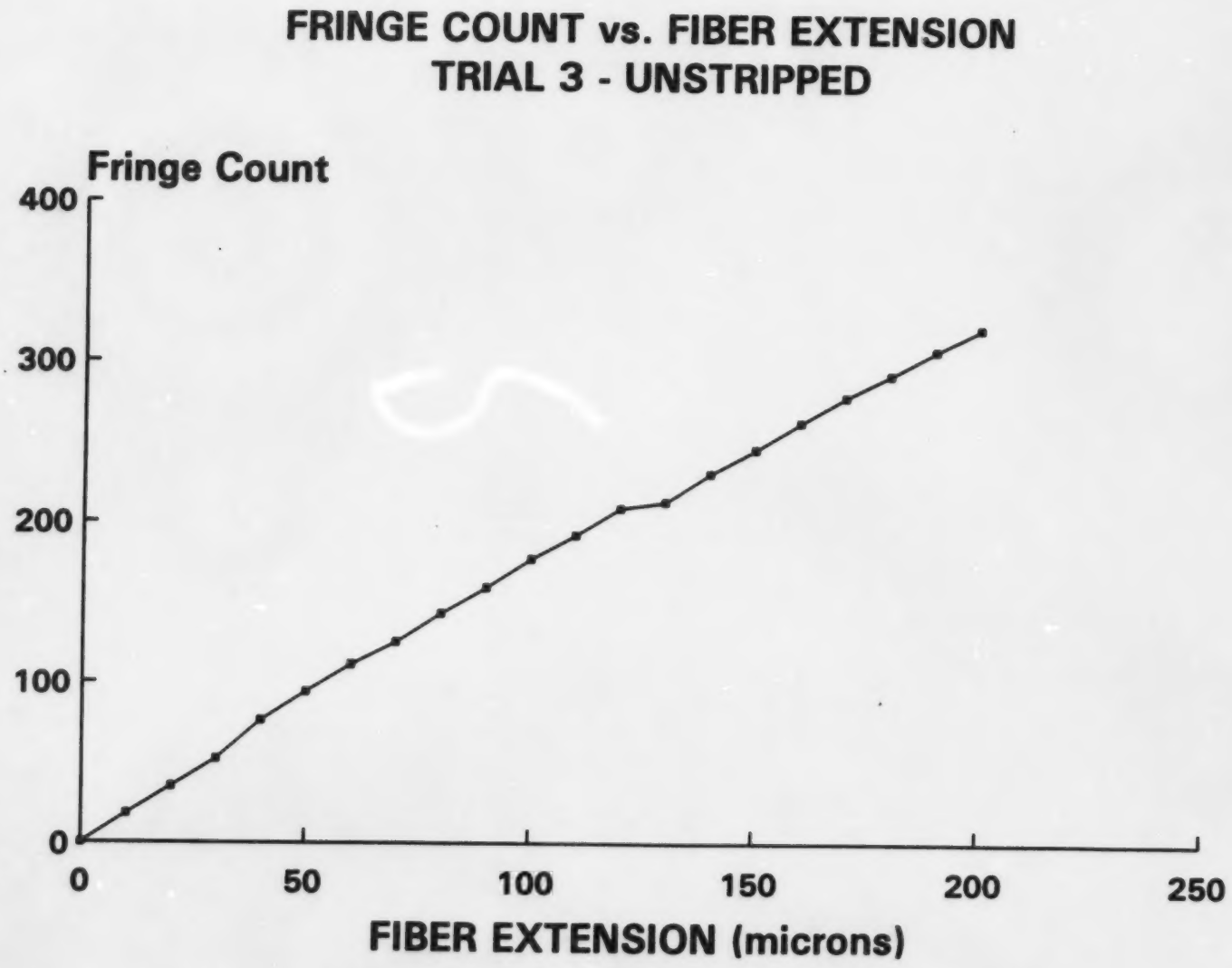

FIGURE 12. FRINGE COUNT VS. FIBER EXTENSION - TRIAL 3

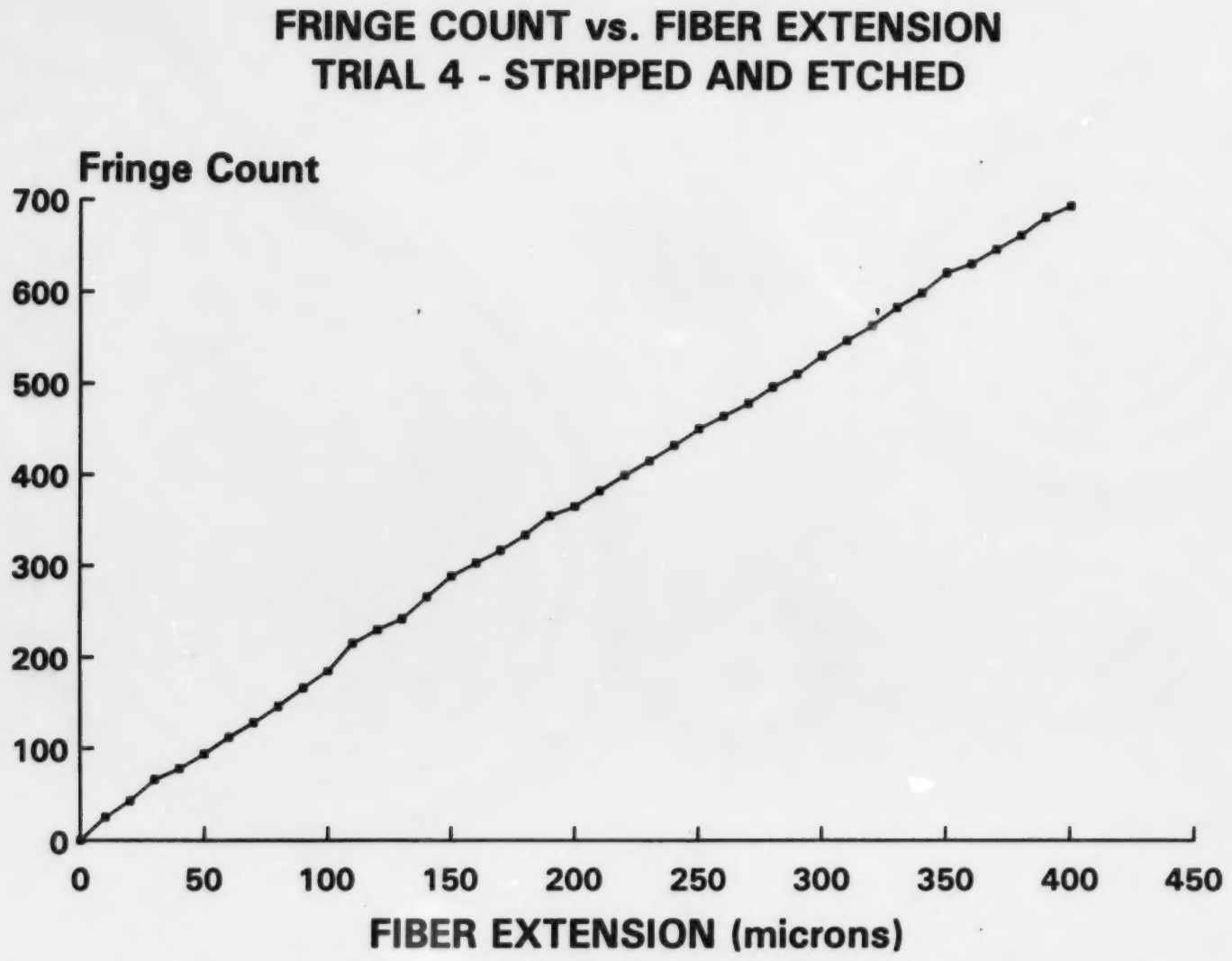

FIGURE 13. FRINGE COUNT VS. FIBER EXTENSION - TRIAL 4

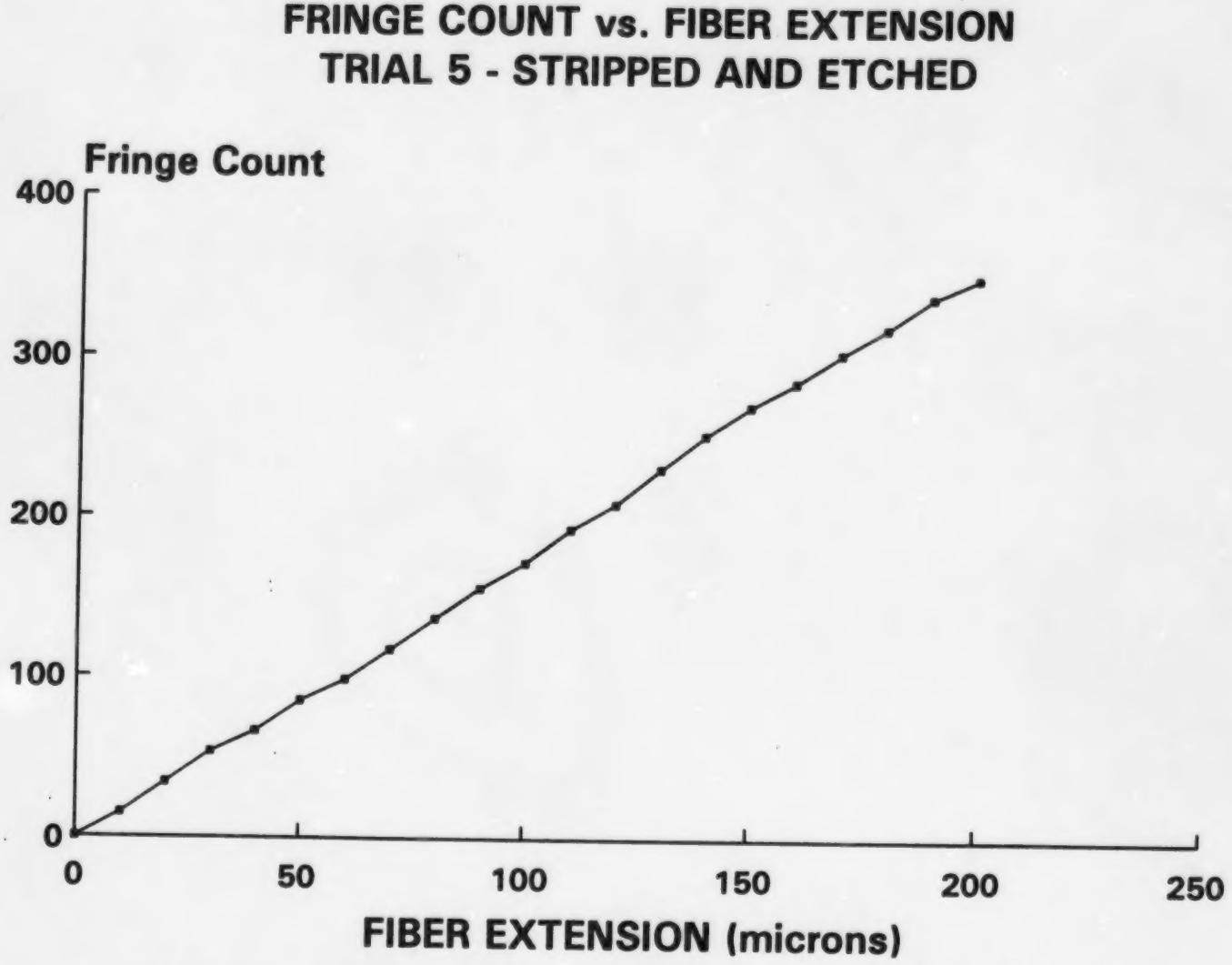

FIGURE 14. FRINGE COUNT VS. FIBER EXTENSION - TRIAL 5

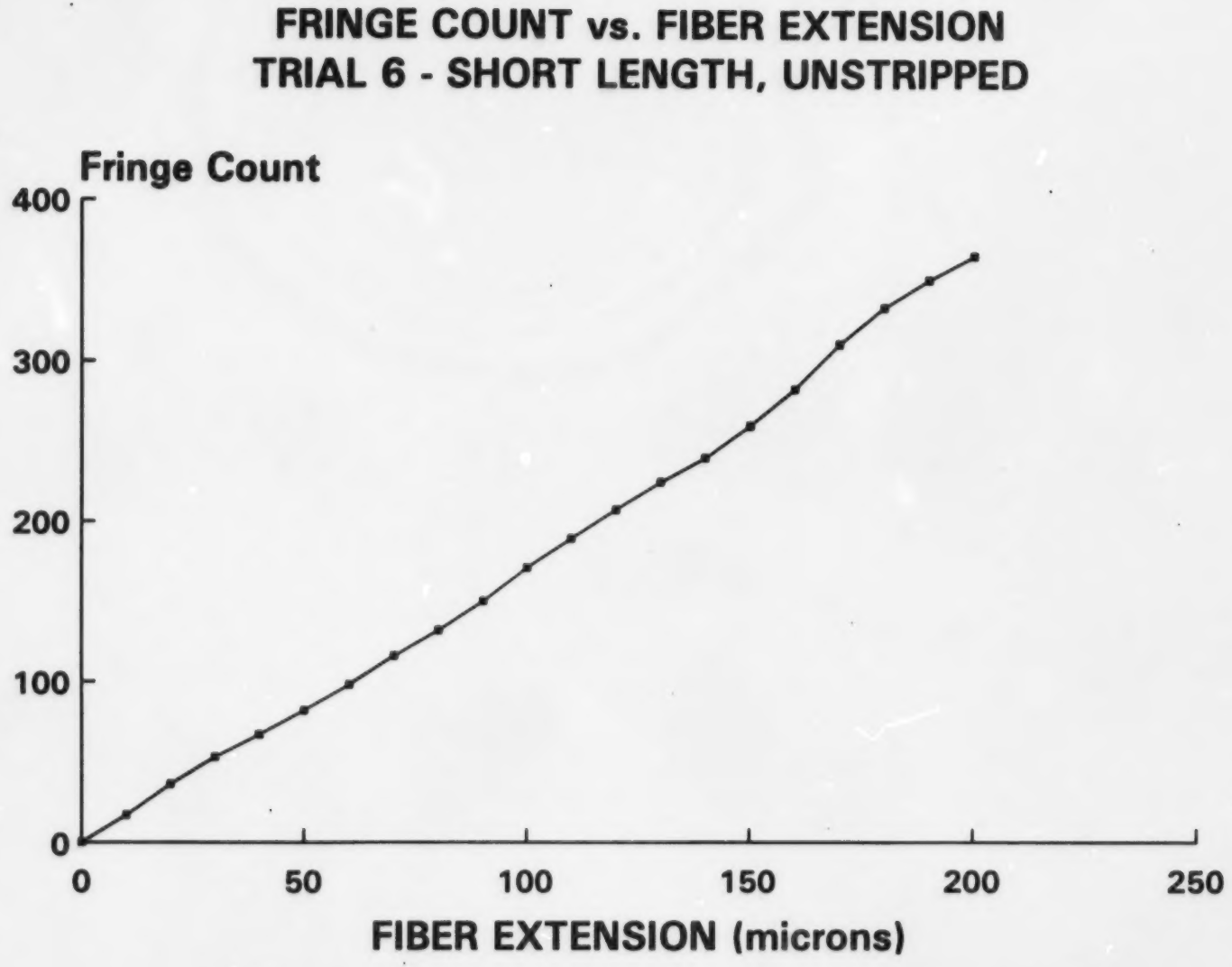

FIGURE 15. FRINGE COUNT VS. FIBER EXTENSION - TRIAL 6

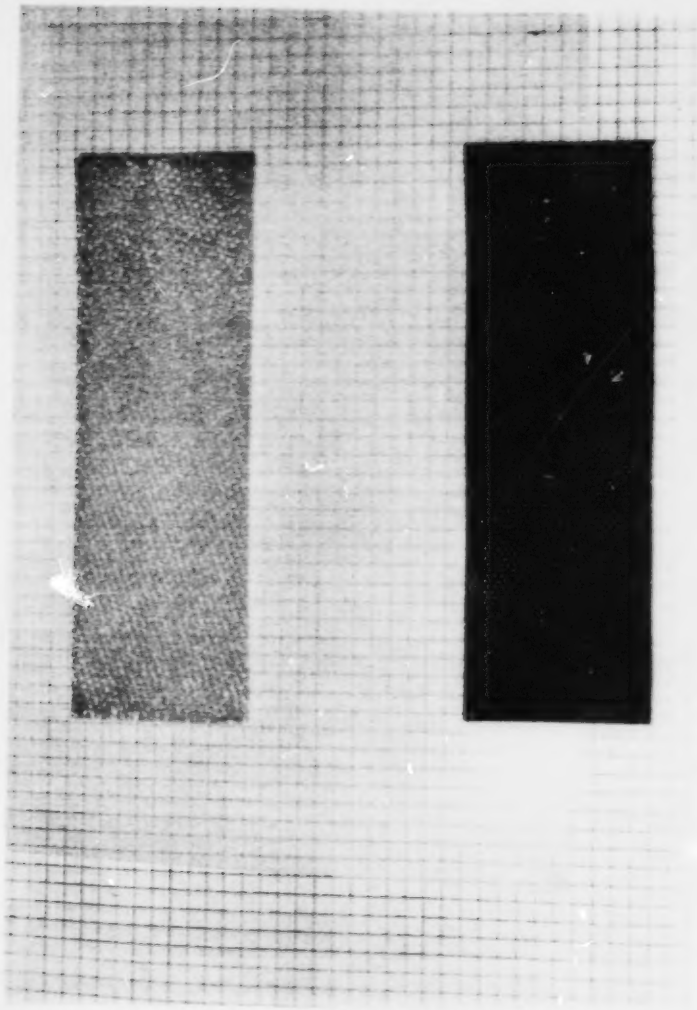

FIGURE 16. TWO LAYERS OF PREPREG FRP, EACH HAVING HALF THE PLIES OF THE FINAL SPECIMEN

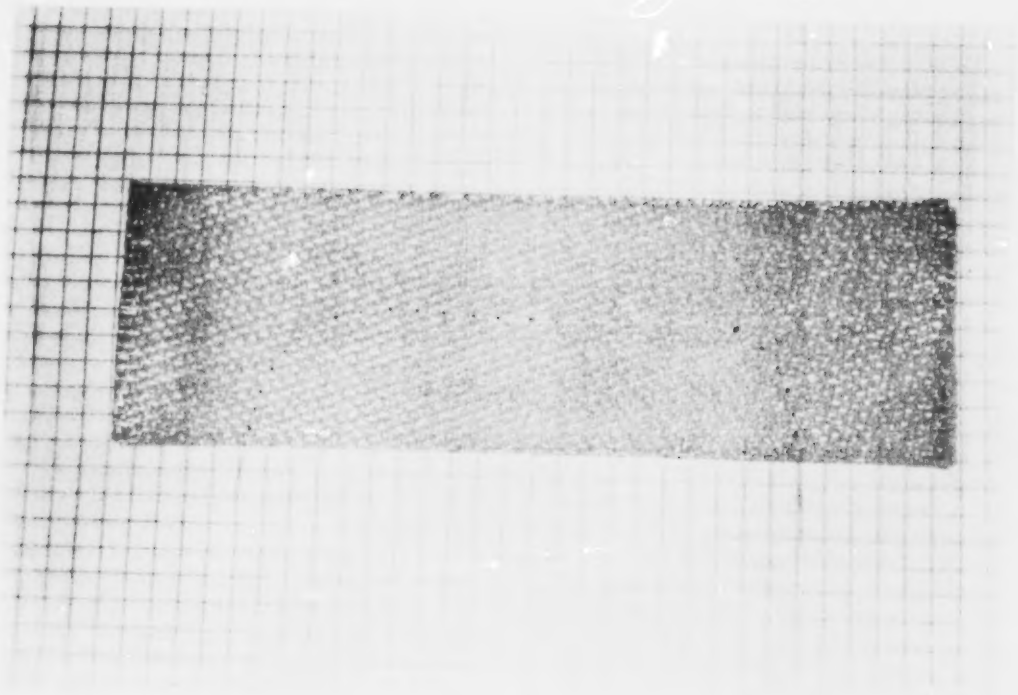

FIGURE 17. OPTICAL FIBER PLACED ONTO EPOXY SURFACE OF PREPREG LAYER

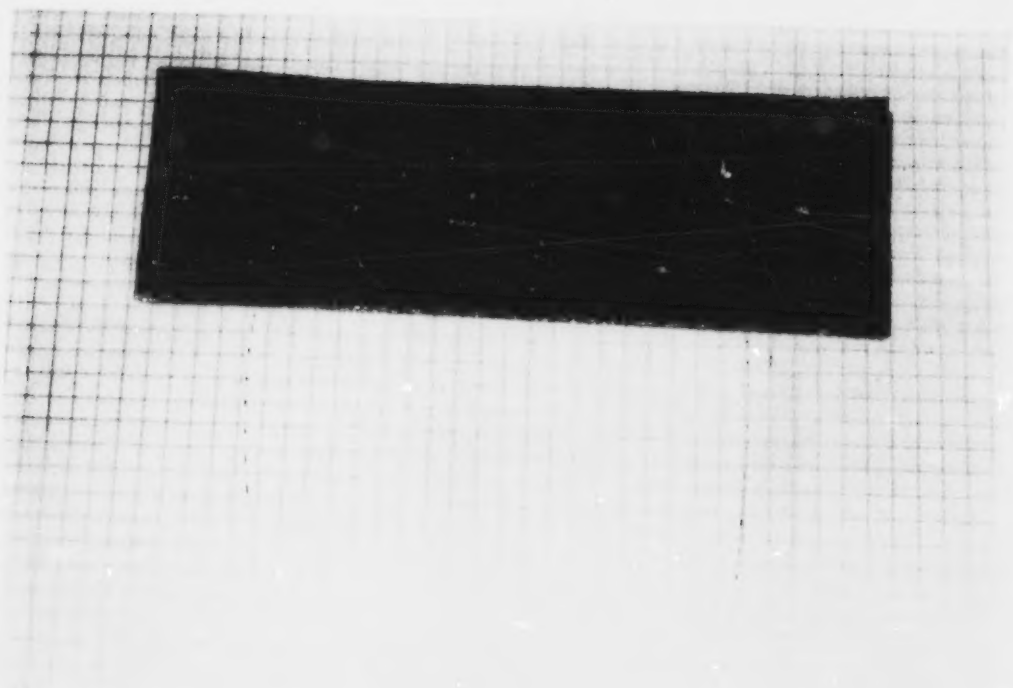

FIGURE 18. SECOND PREPREG LAYER PLACED OVER THE OPTICAL FIBER AND FIRST PREPREG LAYER

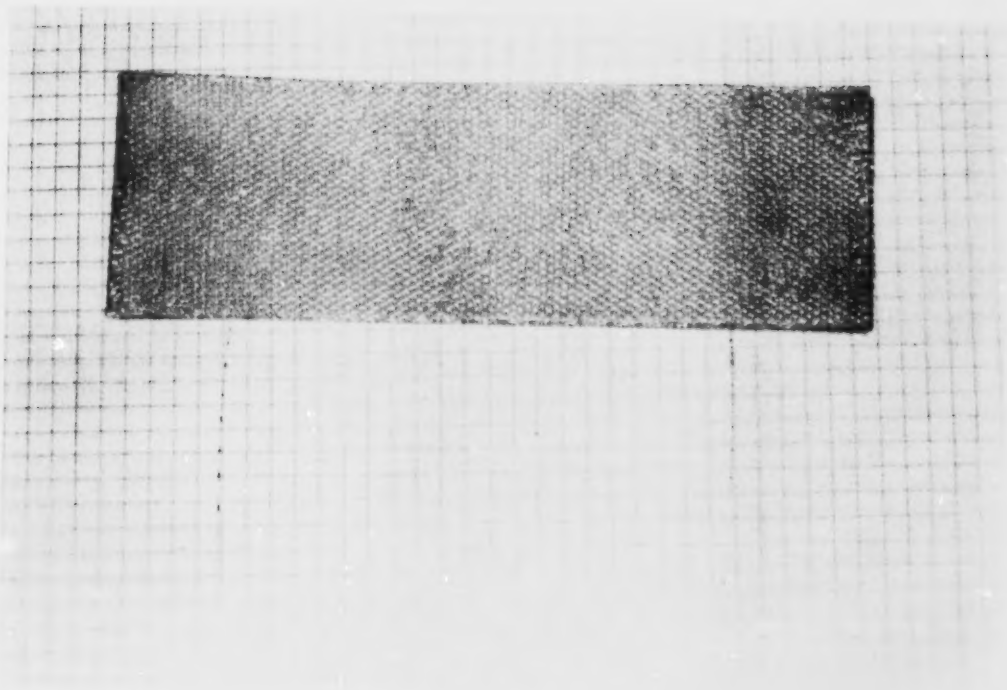

FIGURE 19. FRP SPECIMEN WITH OPTICAL FIBER SENSOR EMBEDDED IN CENTER BEFORE CURING

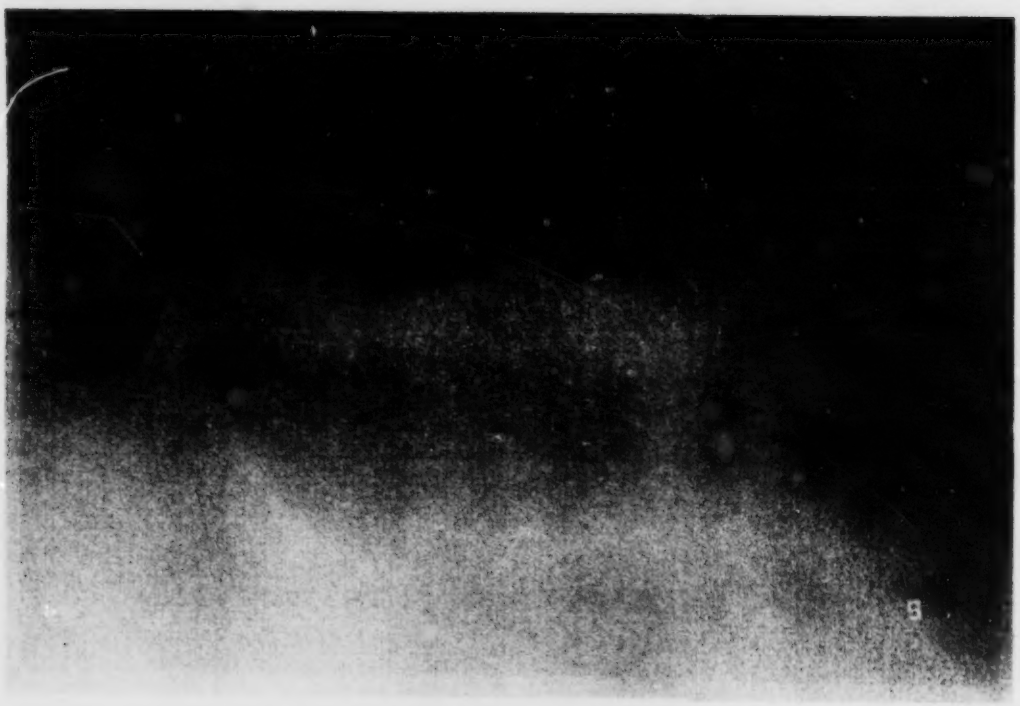

FIGURE 20. MYLAR FILM MASKED AT POSITIONS WHERE THE FIBER EXITS THE FRP SPECIMEN

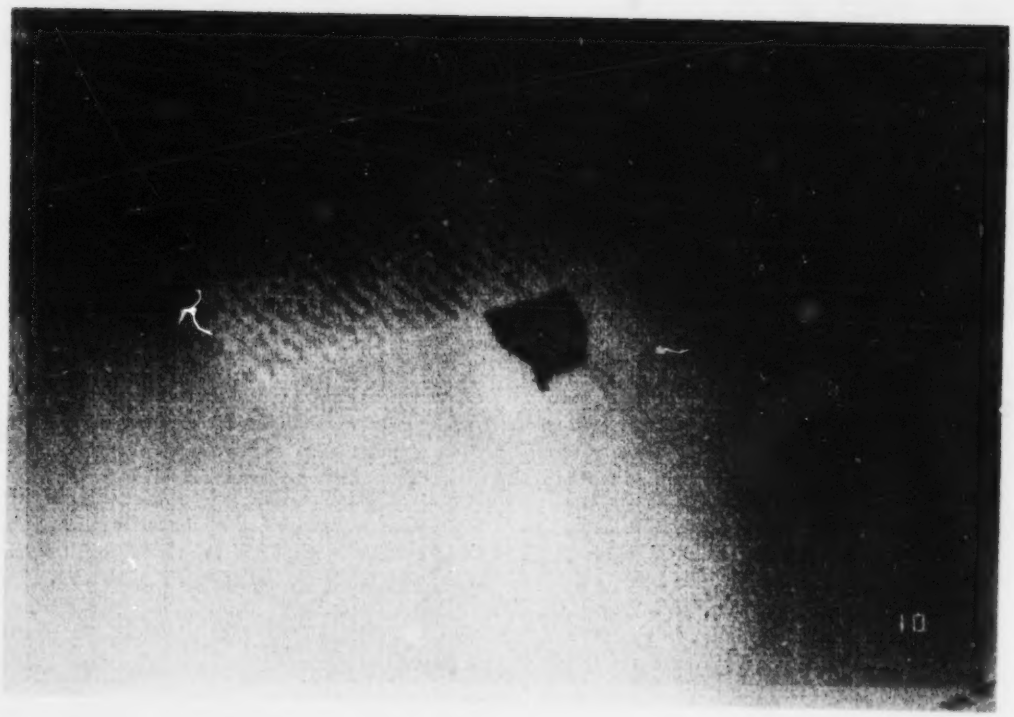

FIGURE 21. FIBER THREADED THROUGH HOLES AT MASKED AREA OF MYLAR FILM

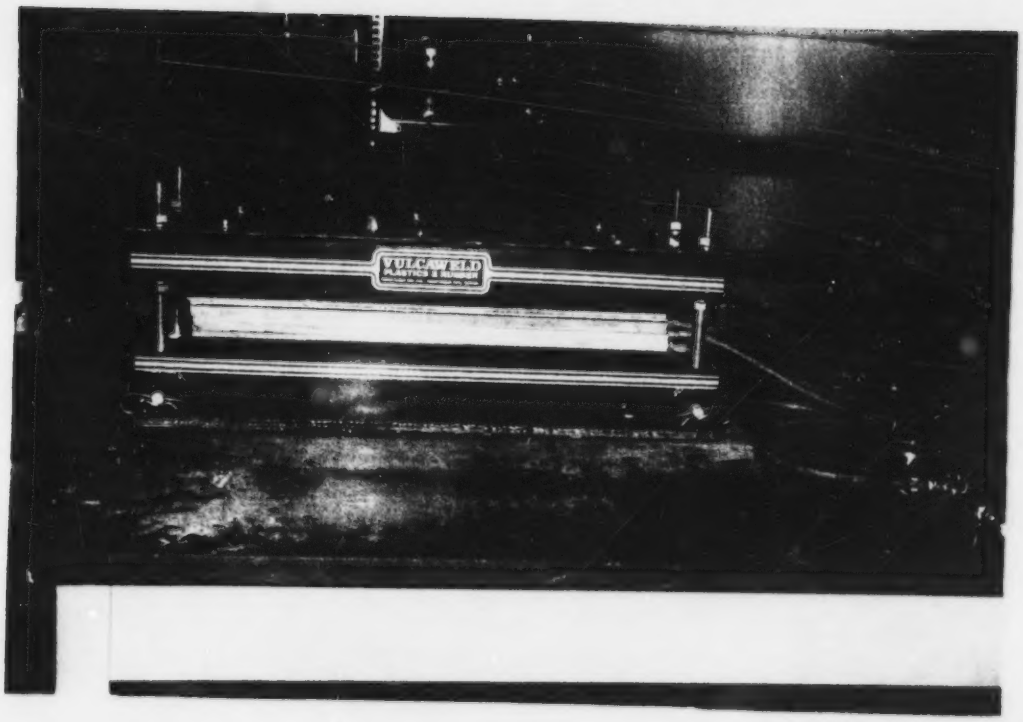

FIGURE 22. HEATED PRESS USED FOR CURING OF SPECIMENS

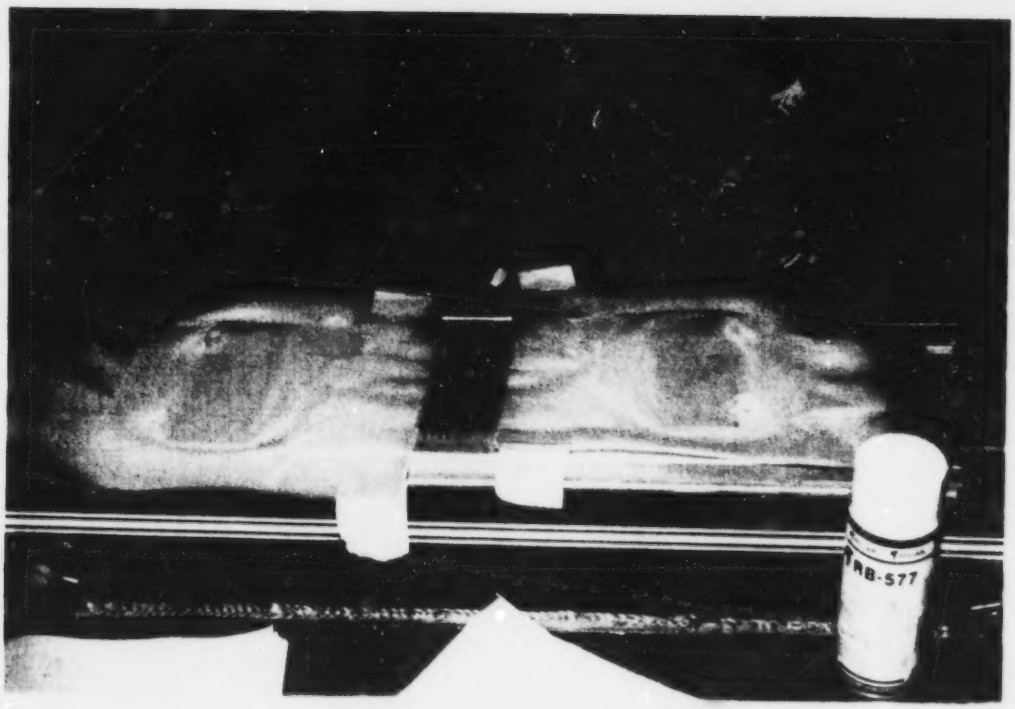

FIGURE 23. TWO SPECIMENS AFTER CURING IS COMPLETED

FIGURE 24. FINISHED FRP SPECIMEN CONTAINING EMBEDDED FIBER OPTIC SENSOR

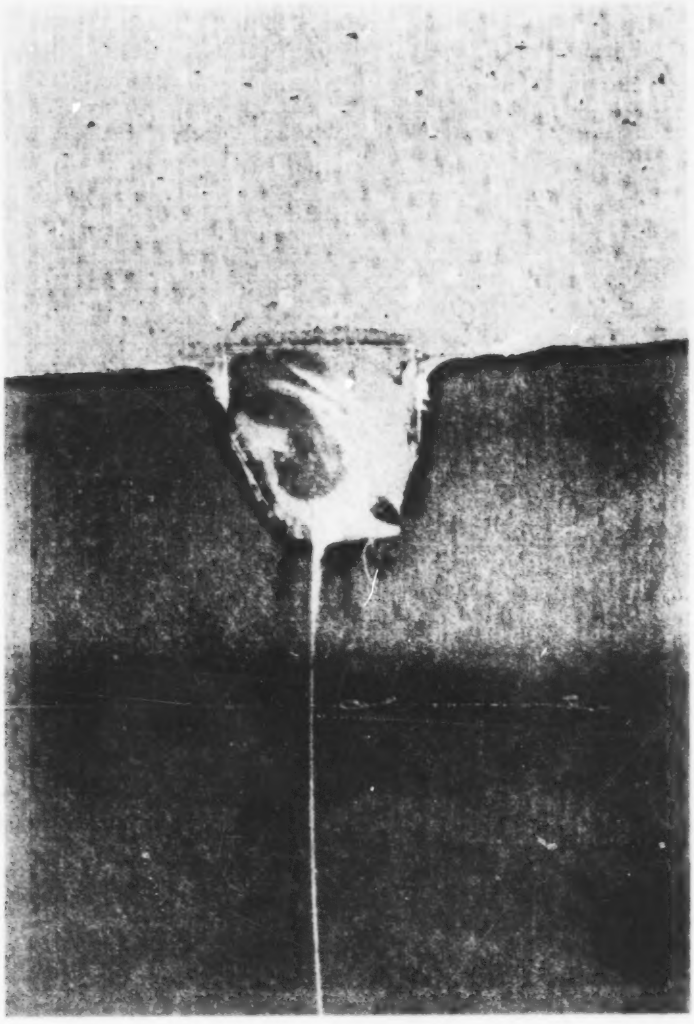

FIGURE 25. FRP/OPTICAL FIBER JUNCTION IN FINISHED FRP SPECIMEN

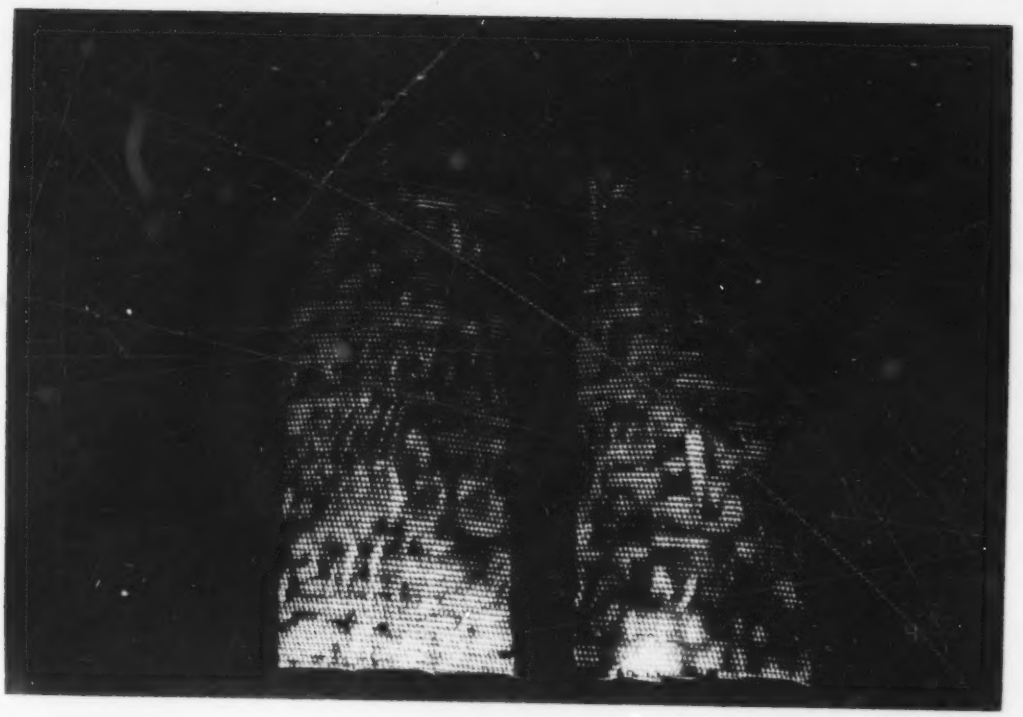

FIGURE 26. PIECES OF FABRIC REINFORCED SILICONE RUBBER WITH THE RUBBER REMOVED FROM ONE SIDE

FIGURE 27. CLOSE UP VIEW OF FABRIC REINFORCED SILICONE RUBBER WITH THE RUBBER REMOVED FROM ONE SIDE

FIGURE 28. BEAD OF RTV ON REINFORCED SILICONE RUBBER WITH RUBBER REMOVED FROM ONE SIDE

FIGURE 29. SPREADING BEAD OF RTV ON REINFORCED SILICONE RUBBER WITH RUBBER REMOVED FROM ONE SIDE

FIGURE 30. PIECES OF FABRIC REINFORCED SILICONE RUBBER WITH RUBBER REMOVED FROM ONE SIDE AND REPLACED WITH RTV

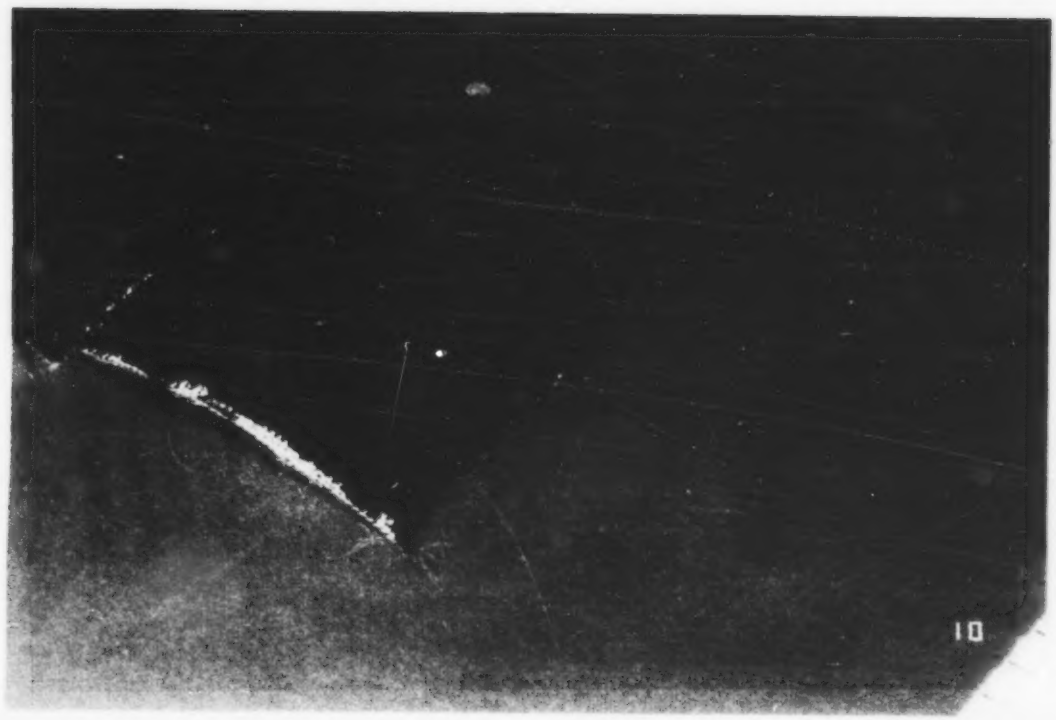

FIGURE 31. OPTICAL FIBER SENSOR EMBEDDED IN RTV

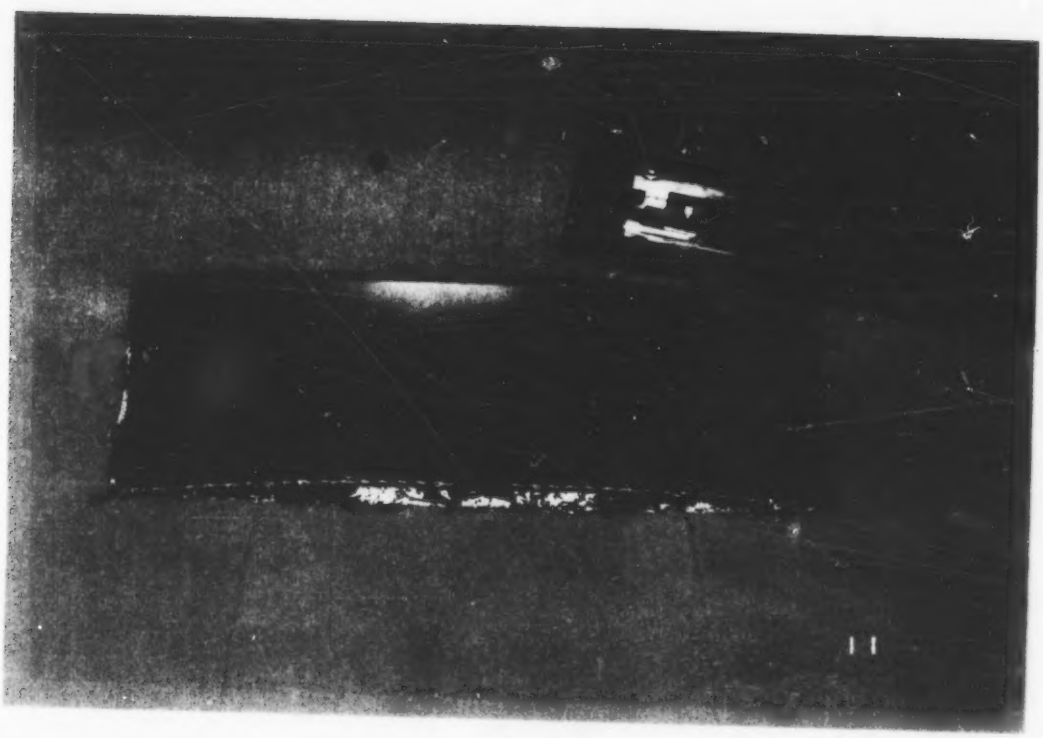

FIGURE 32. TWO PIECES OF REINFORCED SILICONE RUBBER WITH EMBEDDED OPTICAL SENSOR IN BETWEEN

FIGURE 33. COMPLETED POLYESTER FABRIC REINFORCED SILICONE RUBBER SPECIMEN WITH EMBEDDED OPTICAL SENSOR

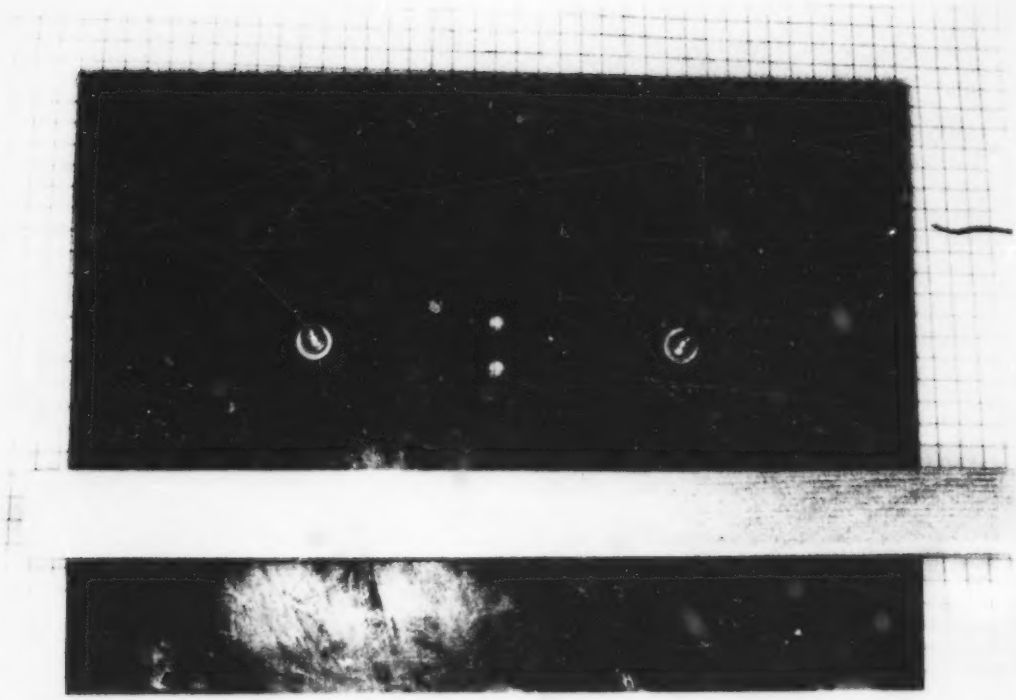

FIGURE 34. PHOTODIODES MOUNTED IN PHENOLIC RESIN ASSEMBLY

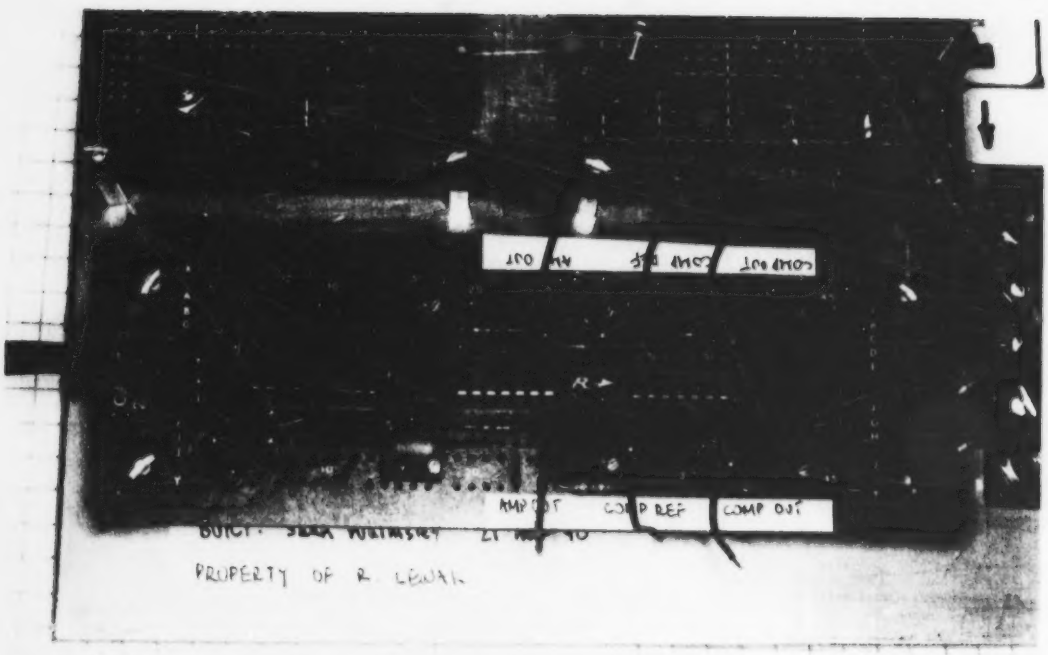

FIGURE 35. AMPLIFIER CIRCUIT

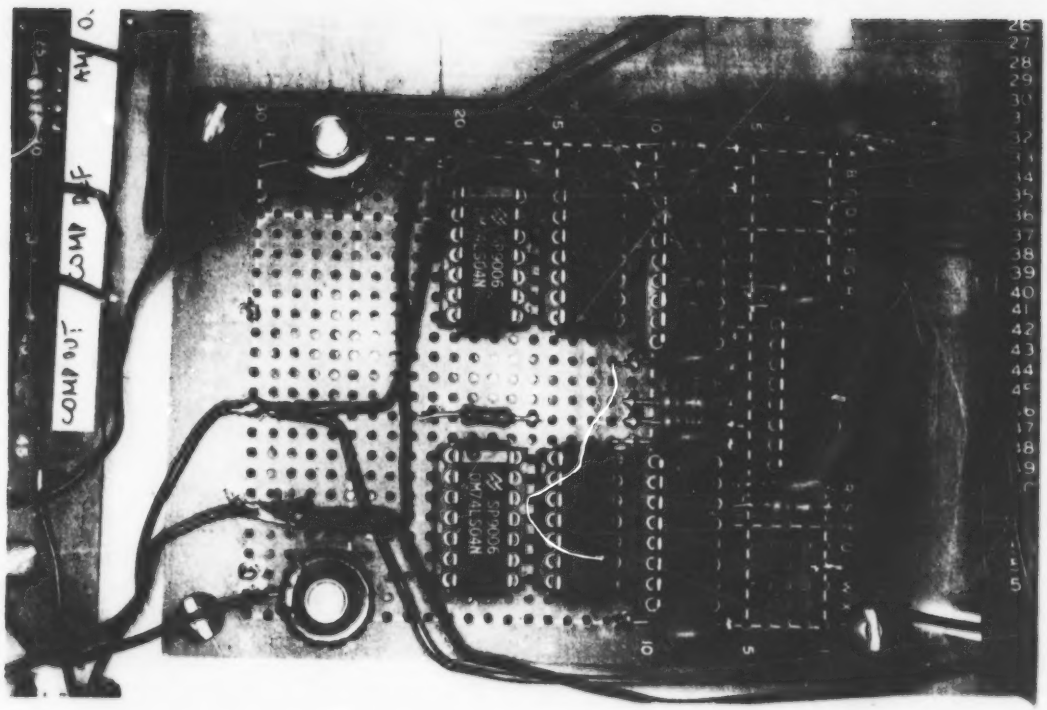

FIGURE 36. DIRECTION DISCRIMINATOR

DIRECTION DISCRIMINATOR – LOGIC DIAGRAM

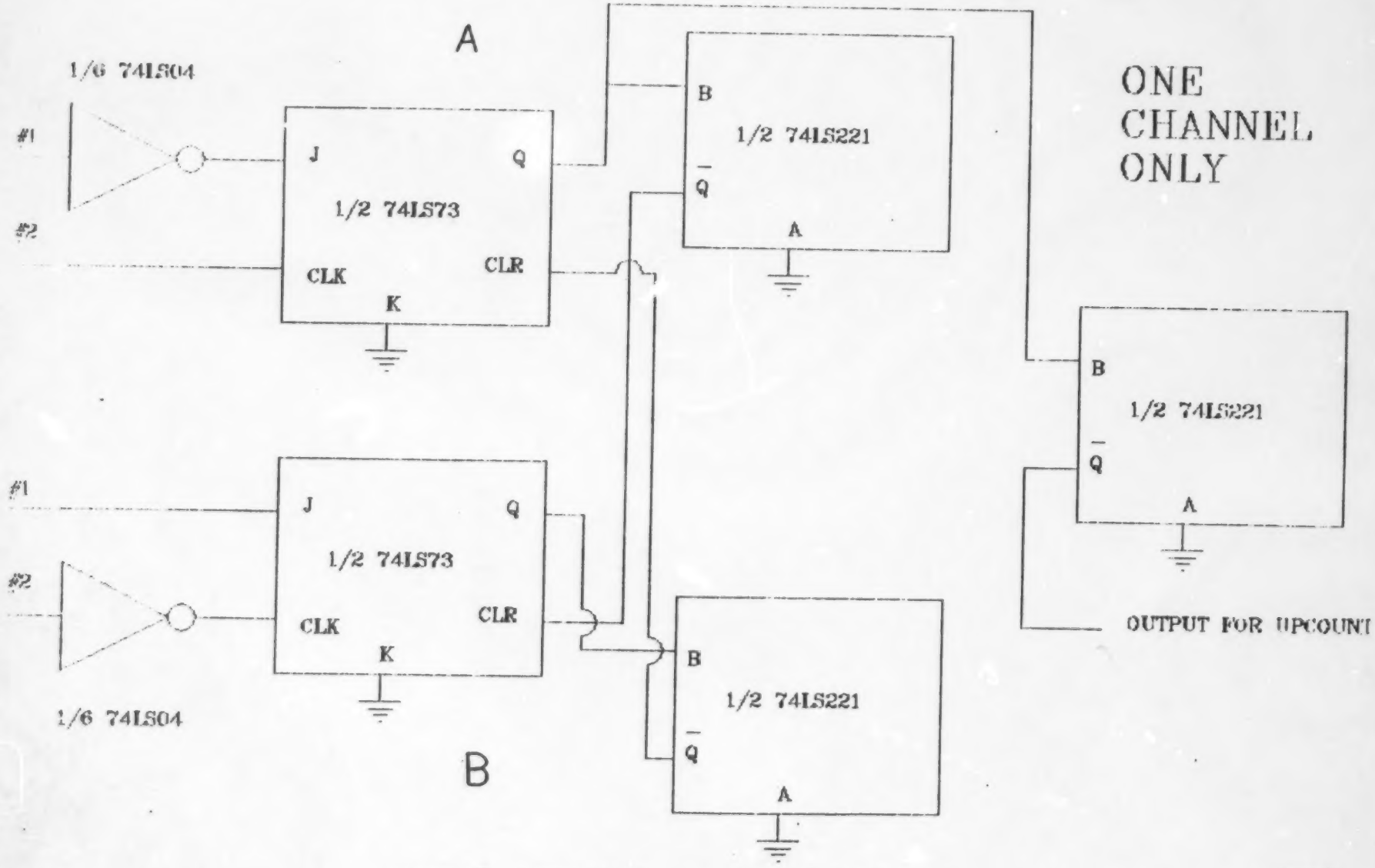

FIGURE 38. LOGIC DIAGRAM - DIRECTION DISCRIMINATOR

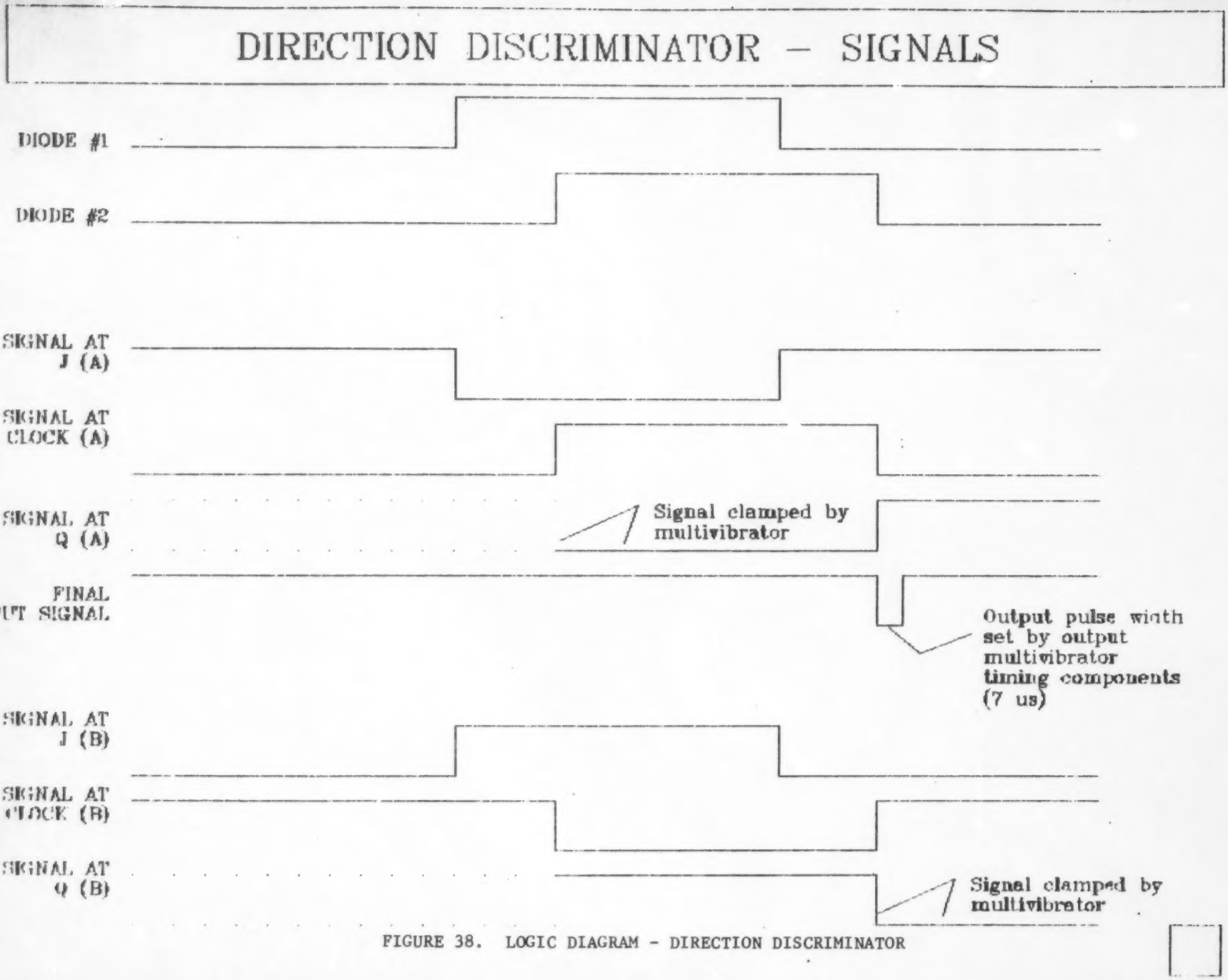

FIGURE 38. LOGIC DIAGRAM - DIRECTION DISCRIMINATOR

DIRECTION DISCRIMINATOR – SCHEMATIC DIAGRAM

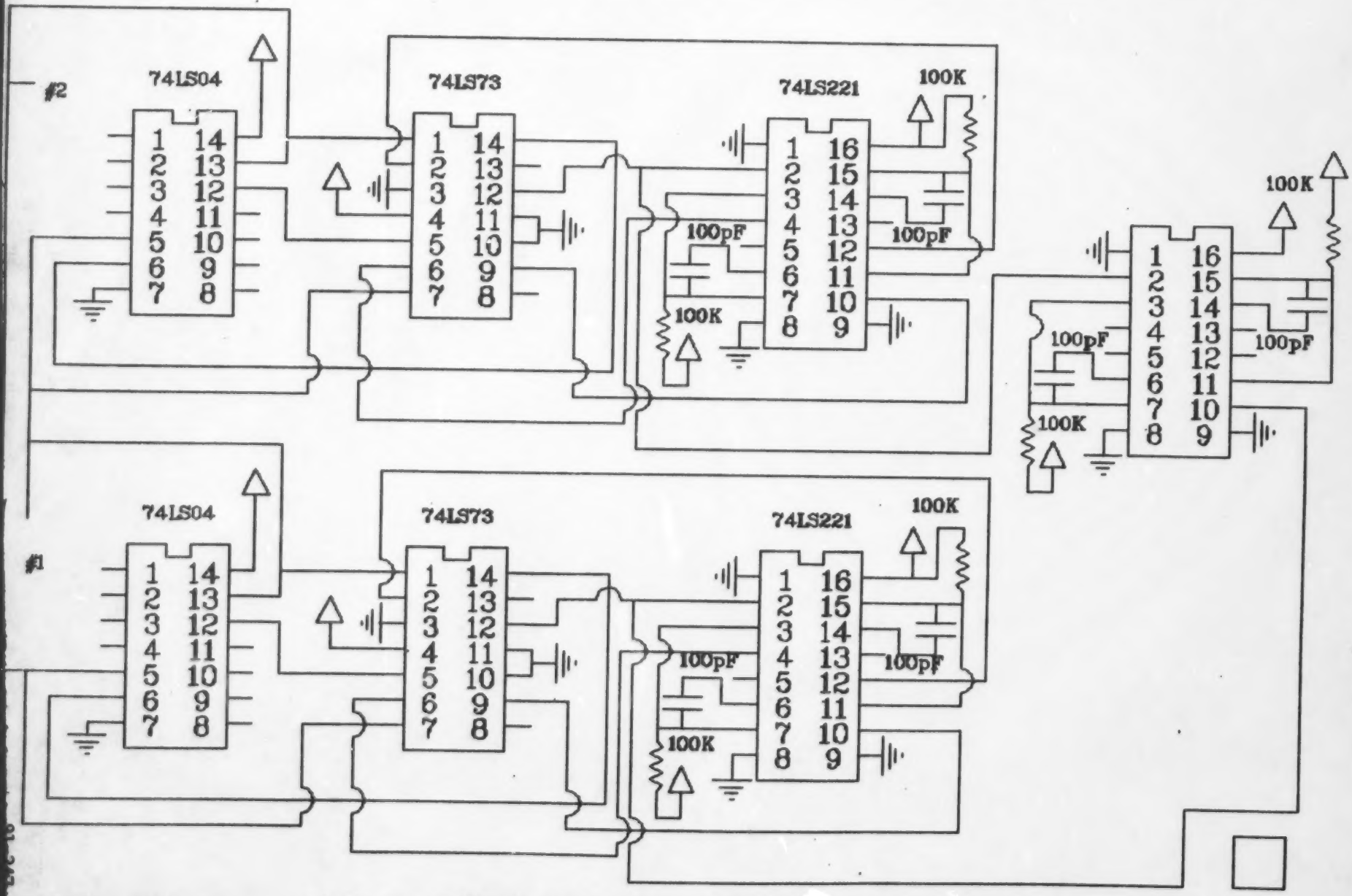

FIGURE 39. DIRECTION DISCRIMINATOR - SCHEMATIC

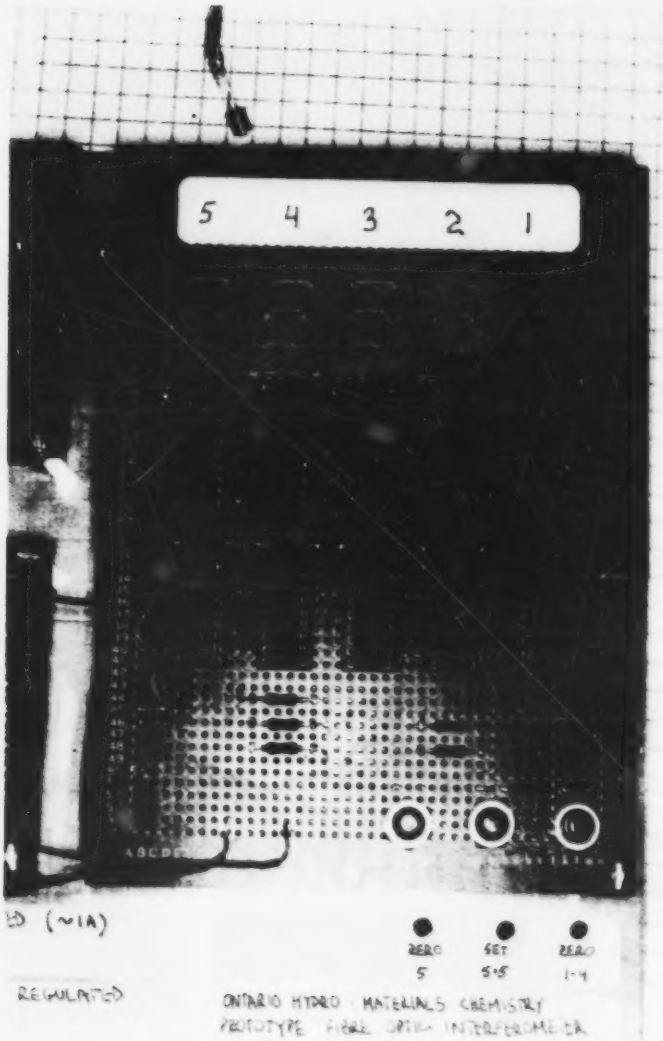

FIGURE 40. COUNTER/DISPLAY CIRCUIT

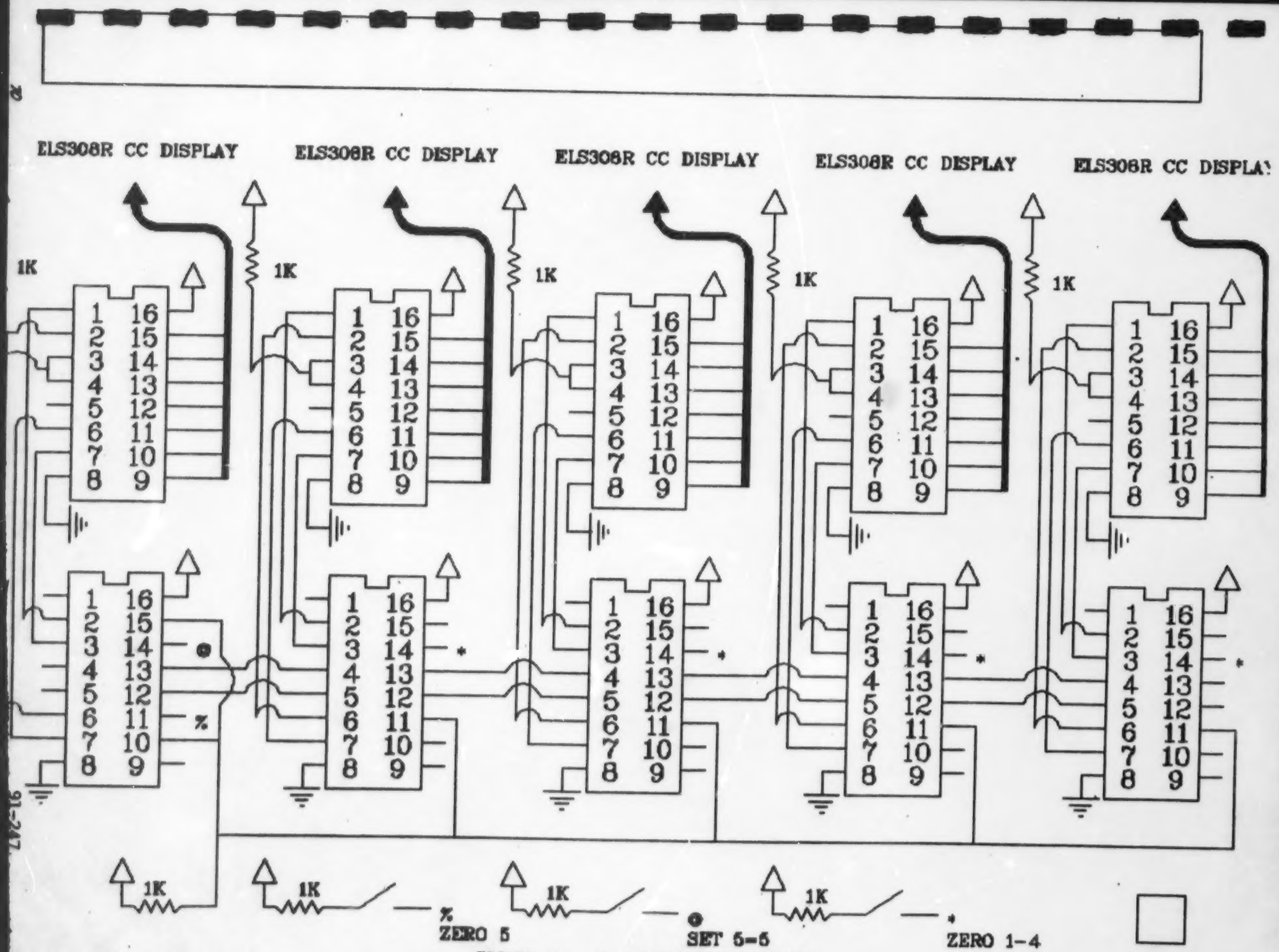

FIGURE 41. COUNTER/DISPLAY CIRCUIT

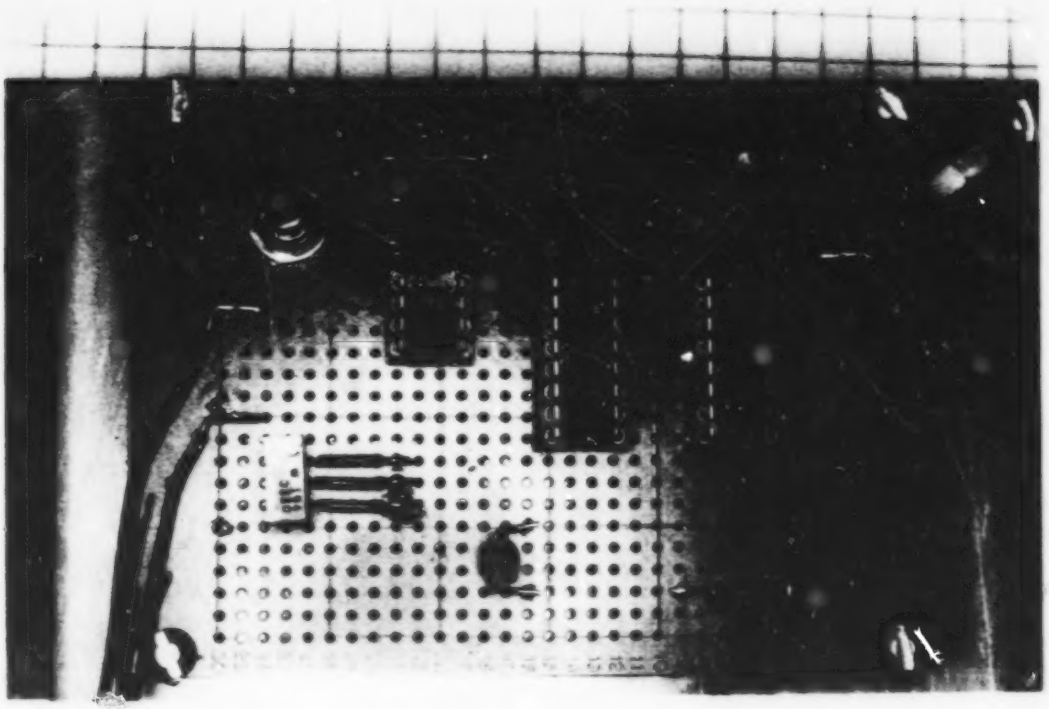

FIGURE 42. SIGNAL GENERATOR

SIGNAL GENERATOR CIRCUIT

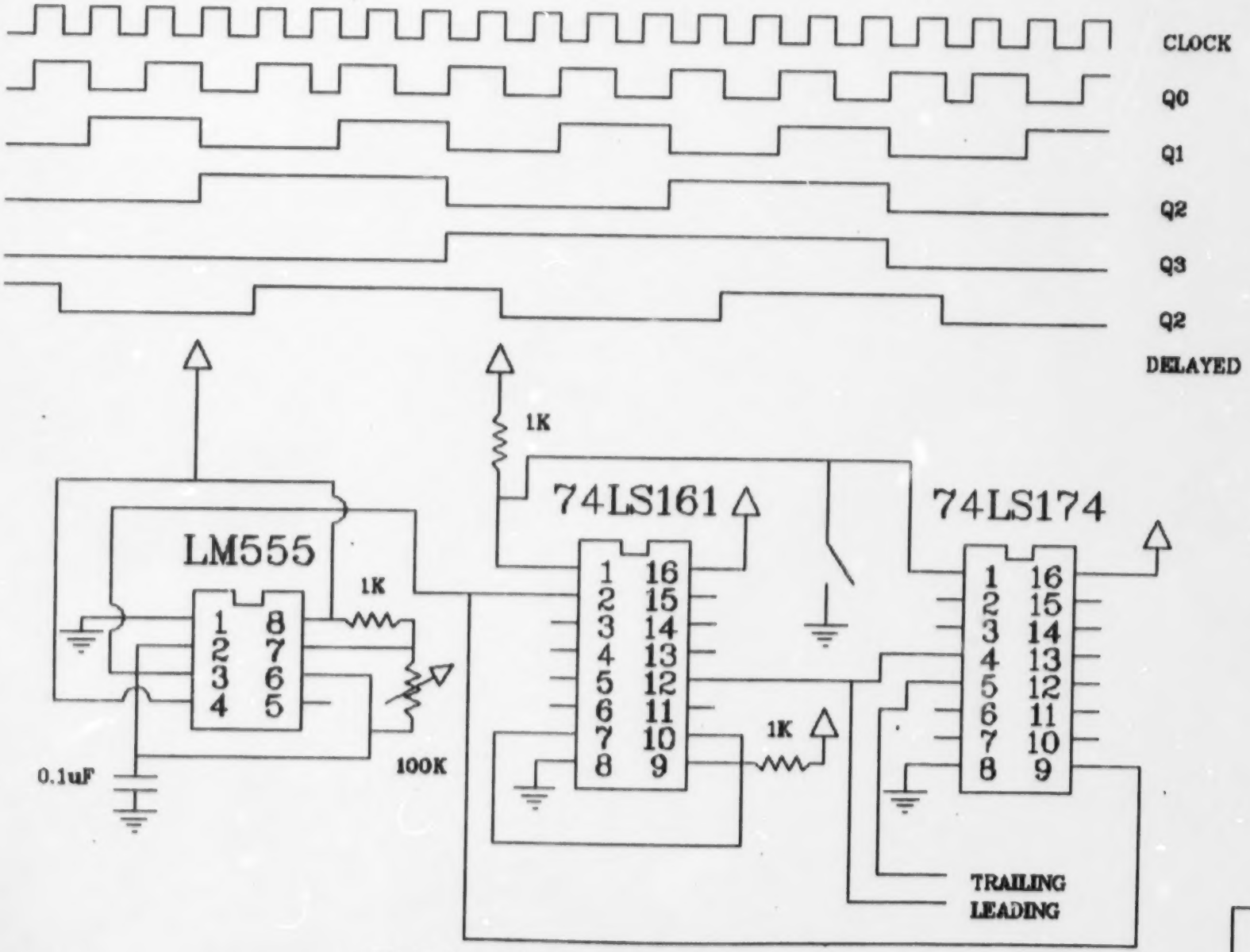

FIGURE 43. SIGNAL GENERATOR CIRCUIT

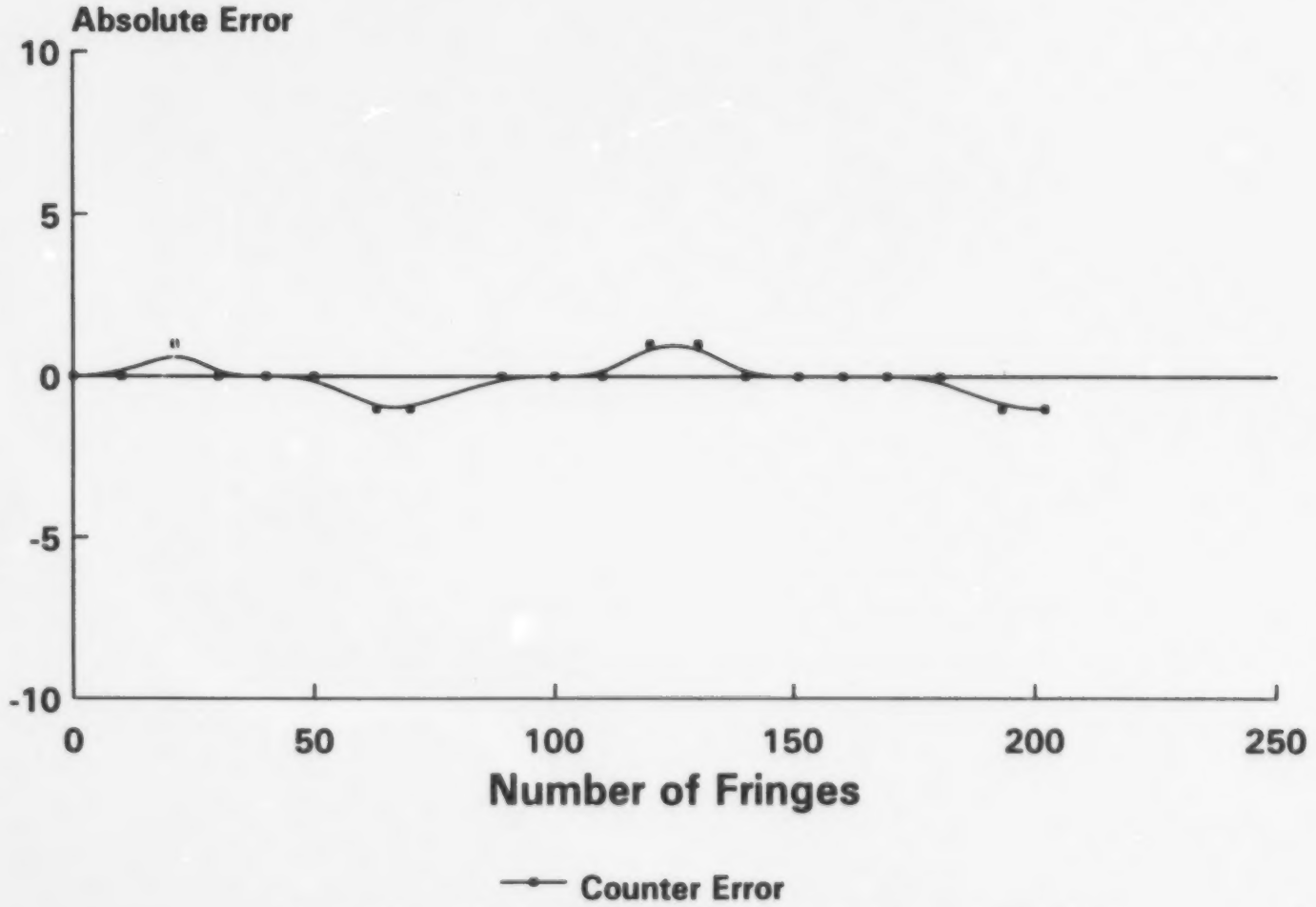

FIGURE 44. COUNTER ERROR vs. NUMBER OF FRINGES
COUNTER ERROR = MANUAL COUNT - FRINGE COUNTER COUNT

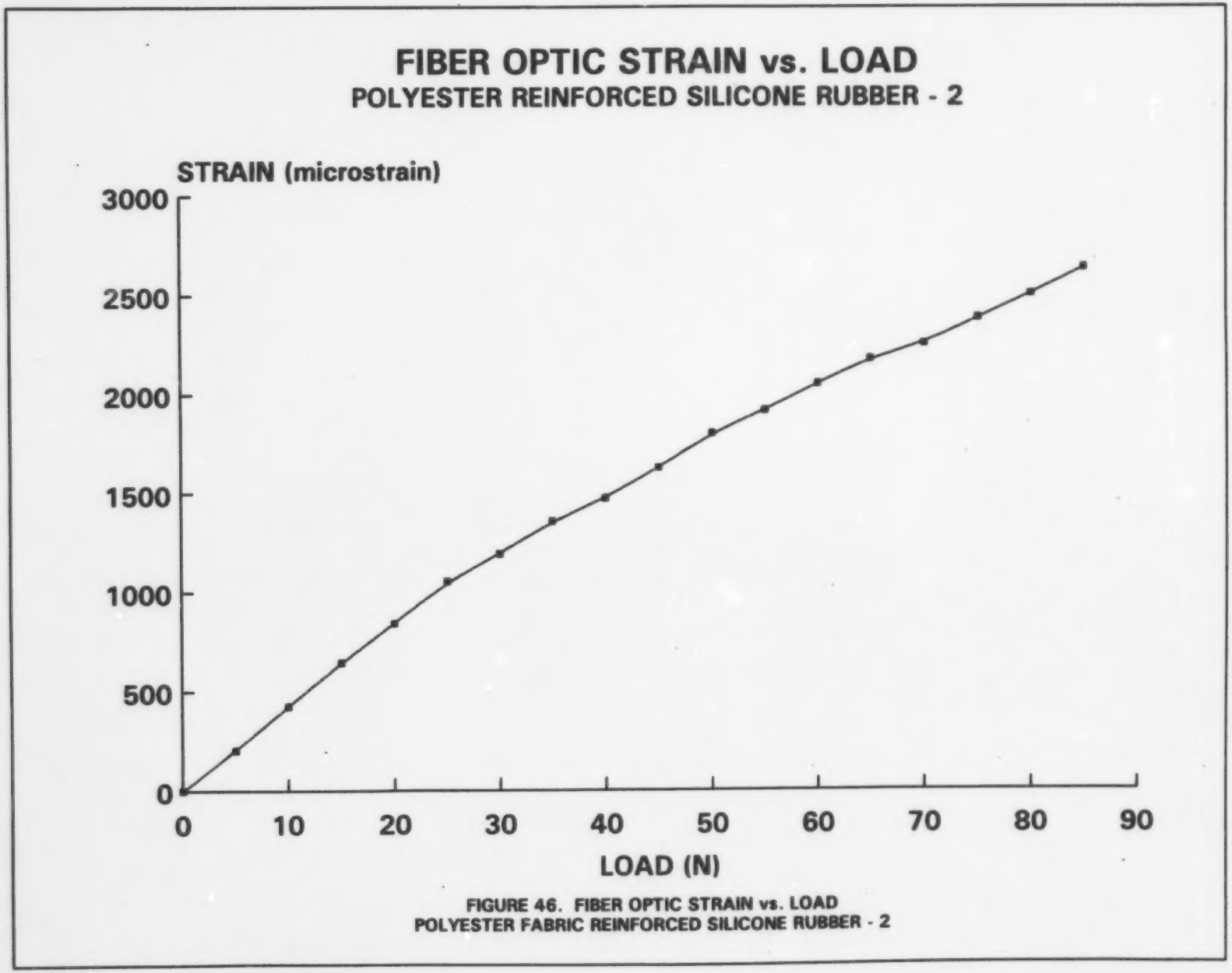

FIGURE 46. FIBER OPTIC STRAIN vs. LOAD
POLYESTER FABRIC REINFORCED SILICONE RUBBER - 2

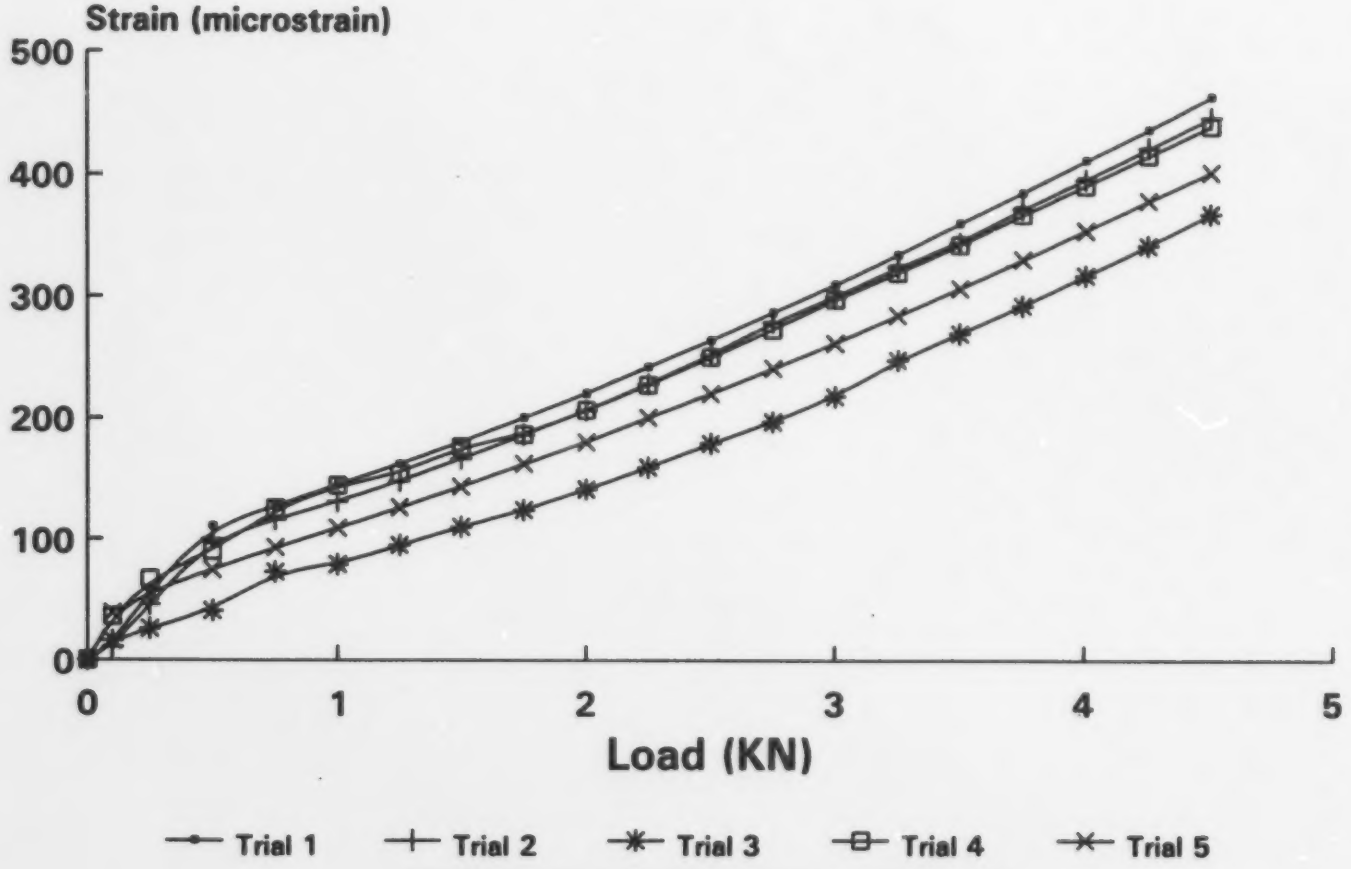

FIGURE 47. STRAIN GAUGE READING vs. TENSILE LOAD
FRP - FIVE TRIALS

AVERAGE STRAIN GAUGE READING vs. TENSILE LOAD - FRP

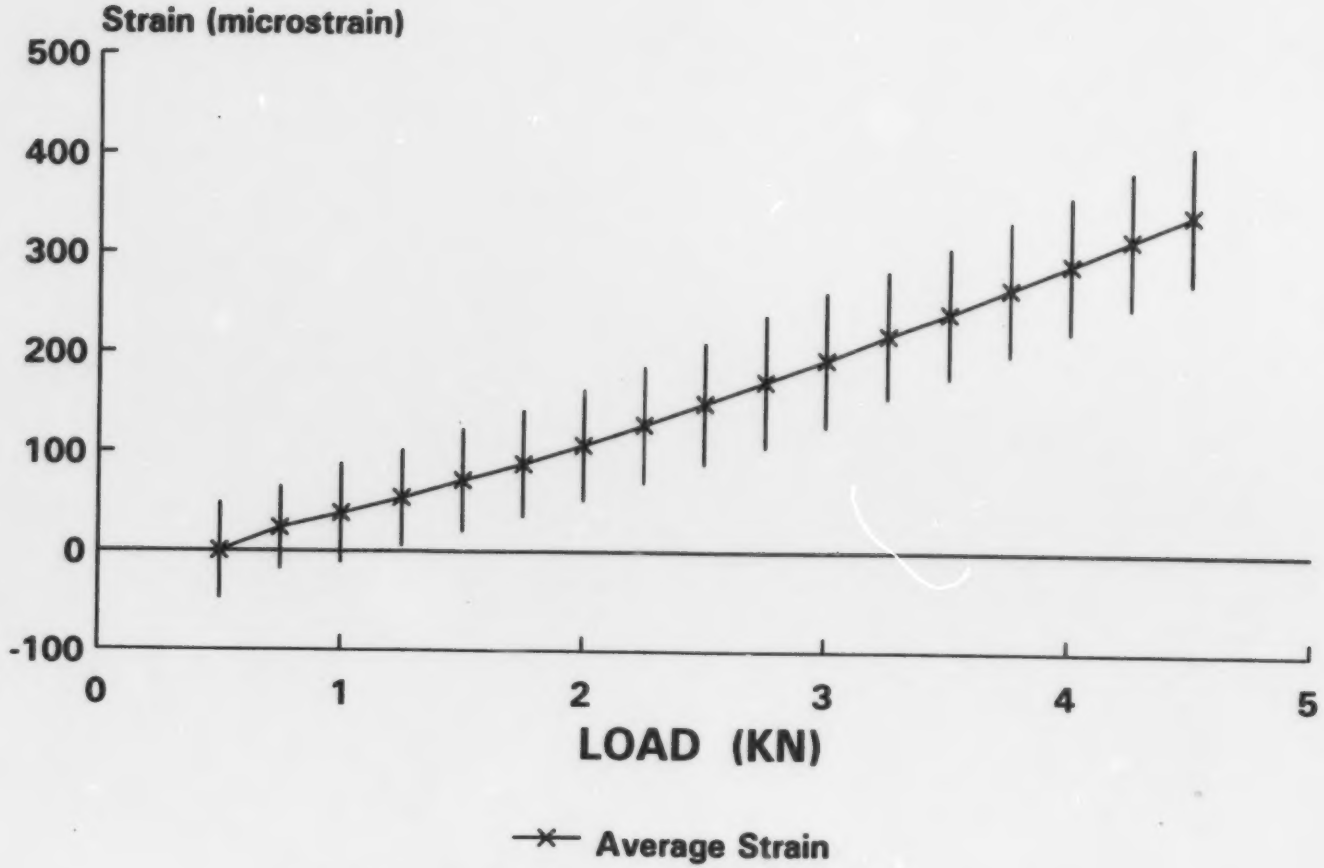

FIGURE 48. AVERAGE STRAIN GAUGE READING vs. TENSILE LOAD
FRP - ERROR BAND = 2 STANDARD DEVIATIONS

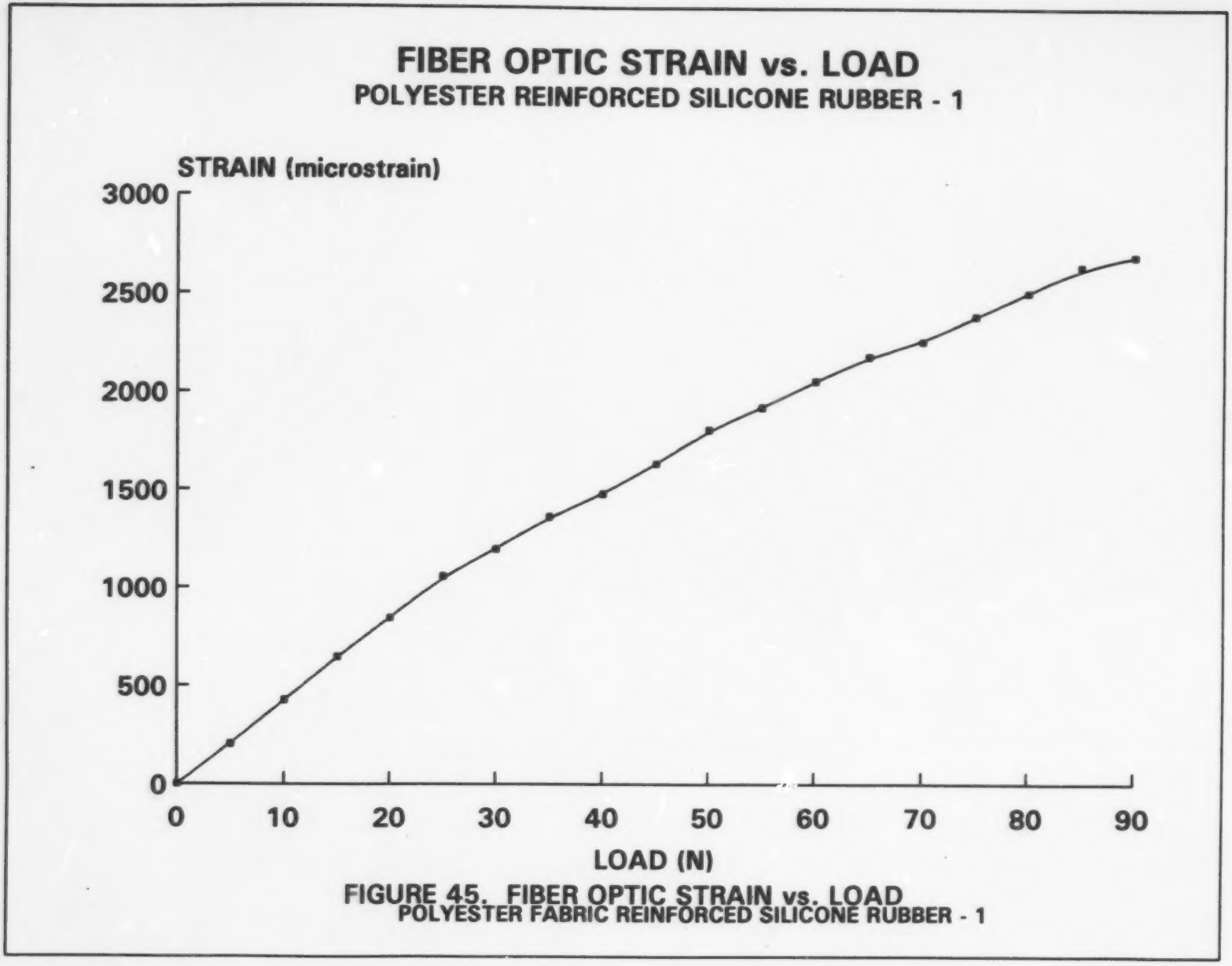

FIGURE 45. FIBER OPTIC STRAIN vs. LOAD
POLYESTER FABRIC REINFORCED SILICONE RUBBER - 1

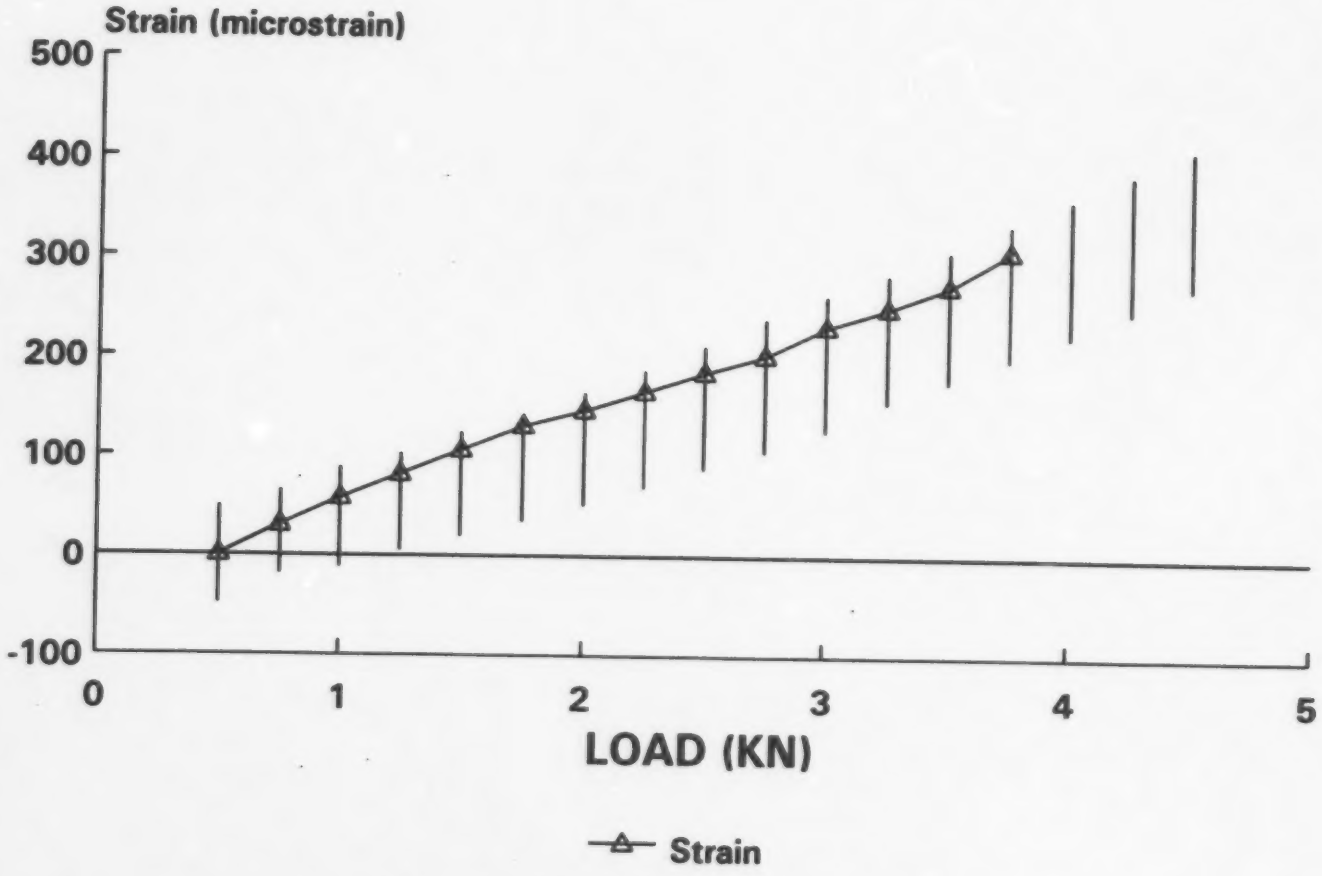

FIGURE 49. FIBER OPTIC STRAIN vs. LOAD - FRP 1
ERROR BAND FROM STRAIN GAUGE READINGS

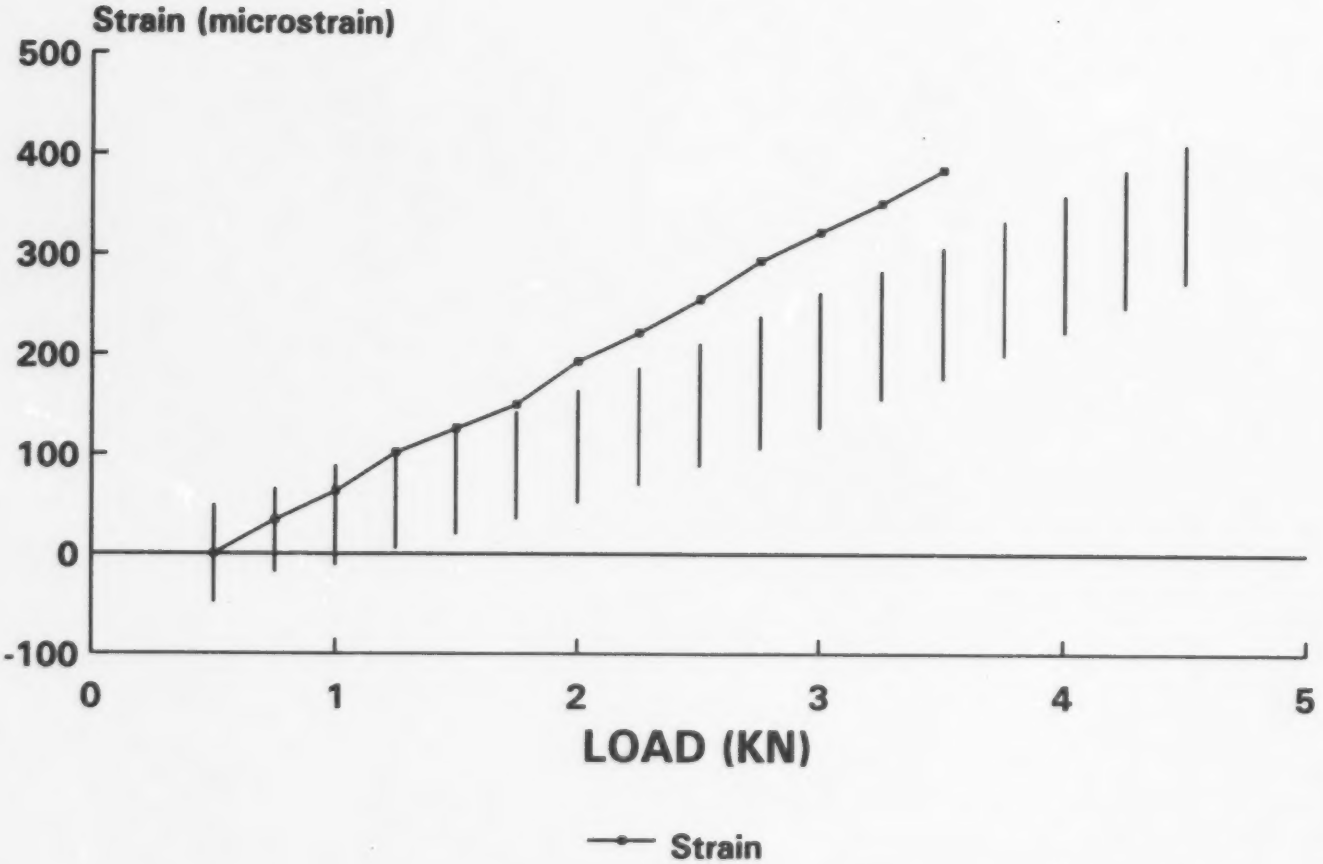

FIGURE 50. FIBER OPTIC STRAIN vs. LOAD - FRP 2
ERROR BAND FROM STRAIN GAUGE READINGS

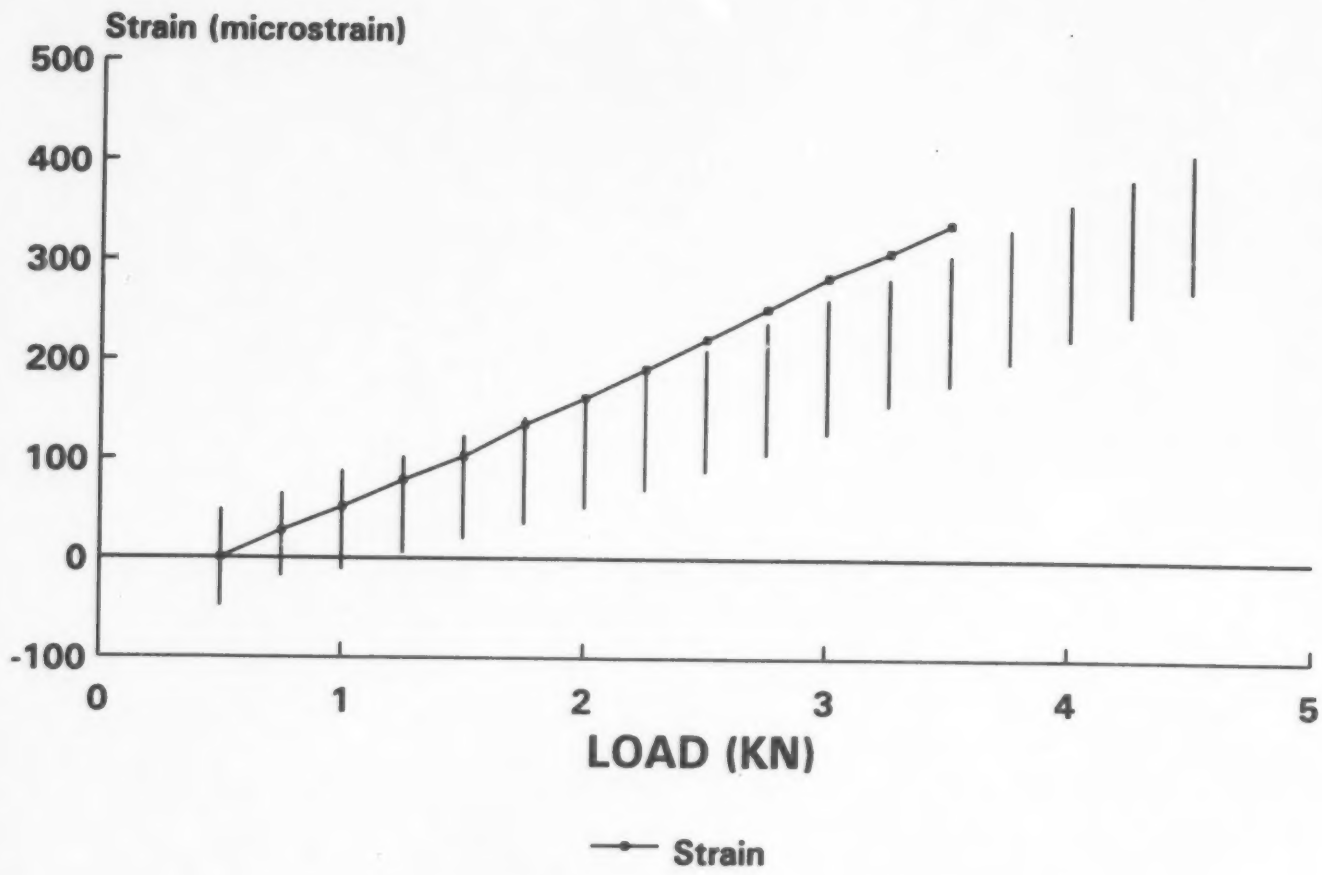

FIGURE 51. FIBER OPTIC STRAIN vs. LOAD - FRP 3
ERROR BAND FROM STRAIN GAUGE READINGS

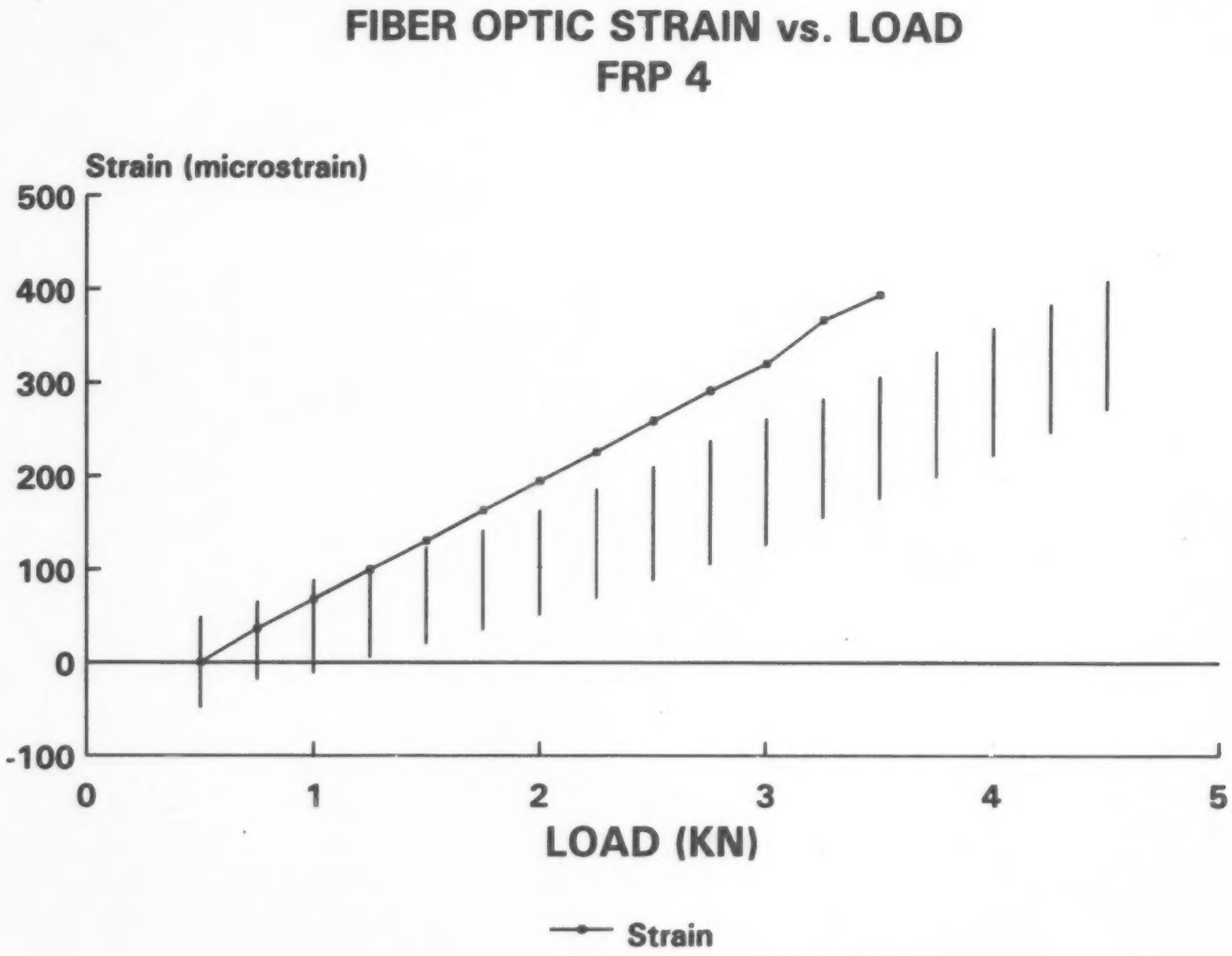

FIGURE 52. FIBER OPTIC STRAIN vs. LOAD - FRP 4
ERROR BAND FROM STRAIN GAUGE READINGS

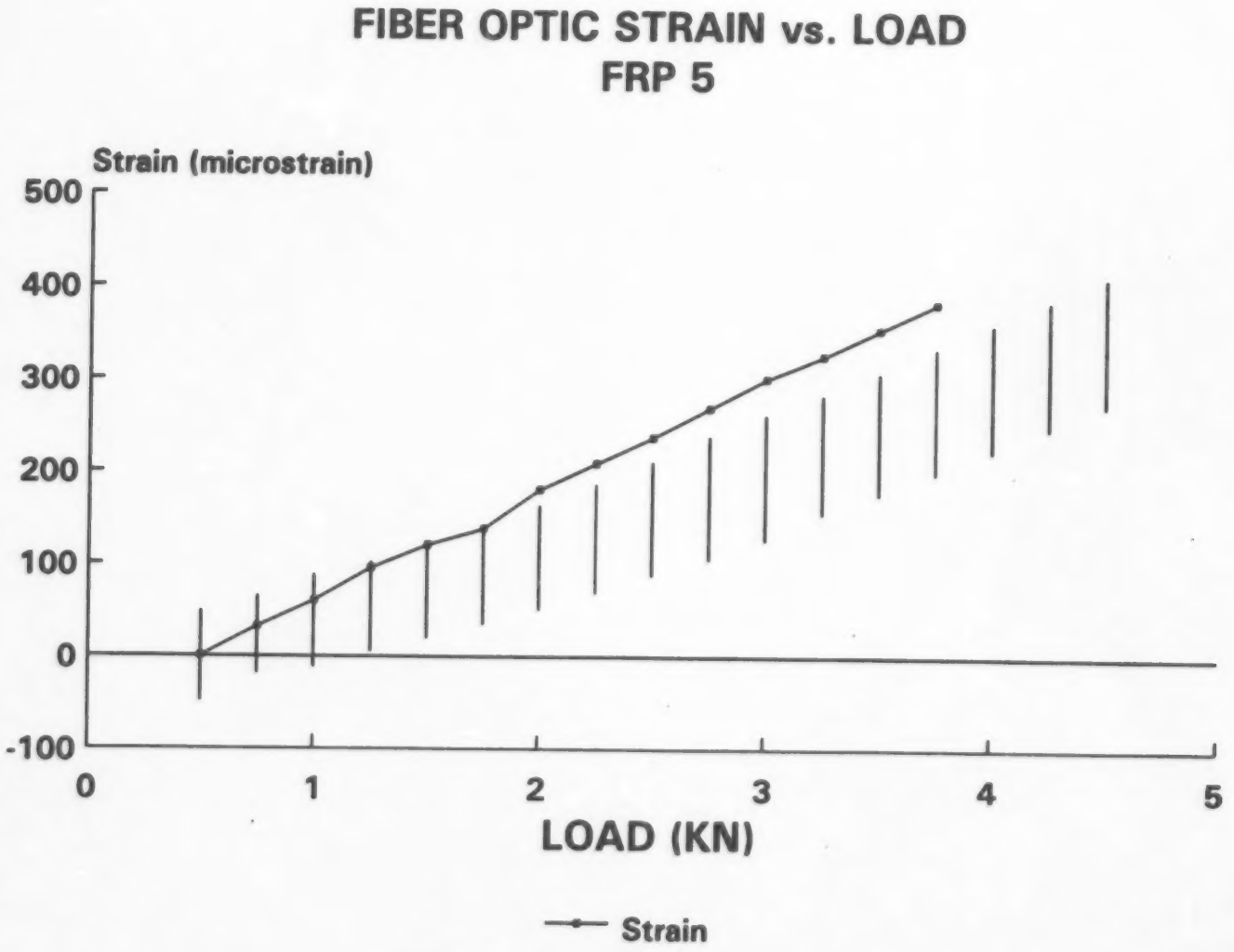

FIGURE 53. FIBER OPTIC STRAIN vs. LOAD - FRP 5
ERROR BAND FROM STRIAN GAUGE READINGS

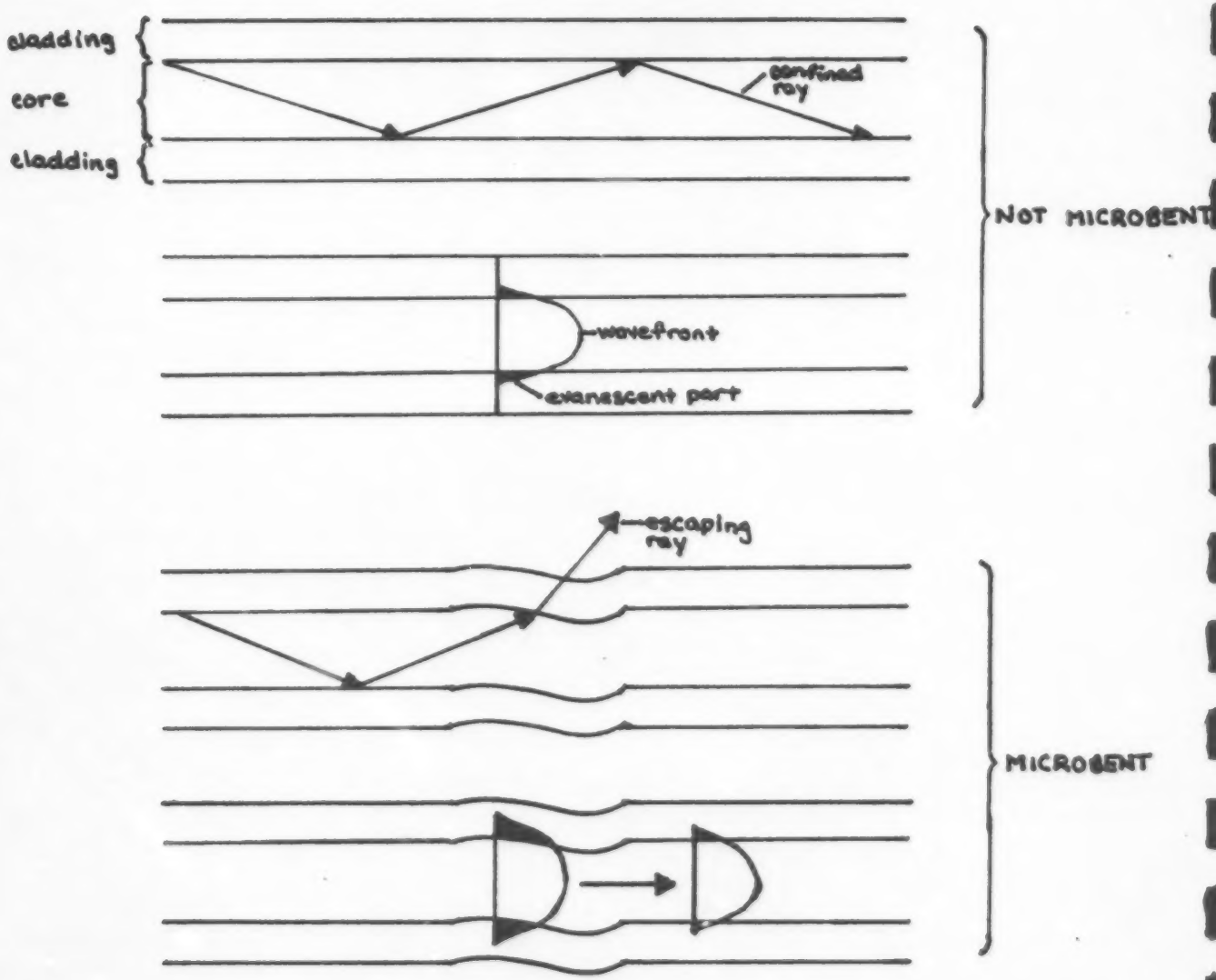

FIGURE 54. MICROBENDING OF OPTICAL FIBERS

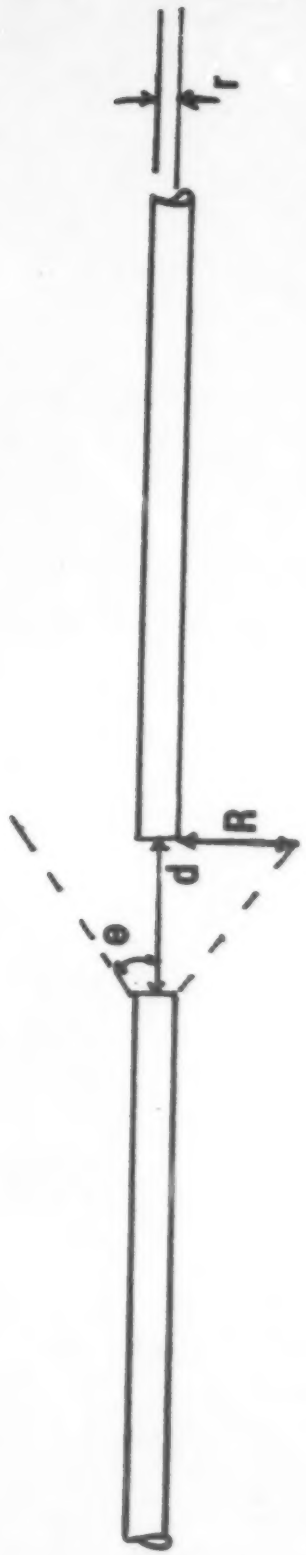

FIGURE 55. TWO OPTICAL FIBERS TO FORM MISALIGNMENT SENSOR

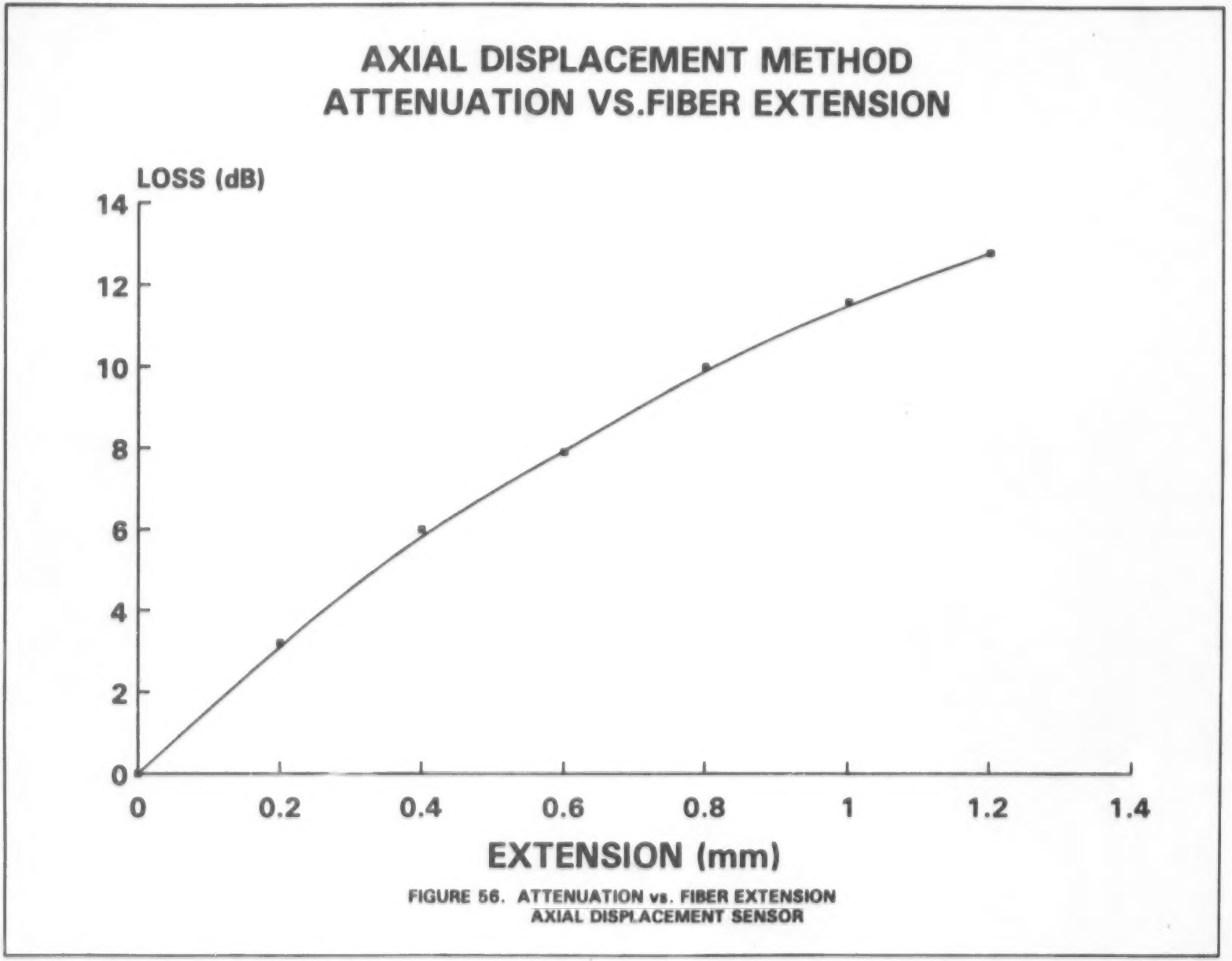

FIGURE 56. ATTENUATION vs. FIBER EXTENSION
AXIAL DISPLACEMENT SENSOR

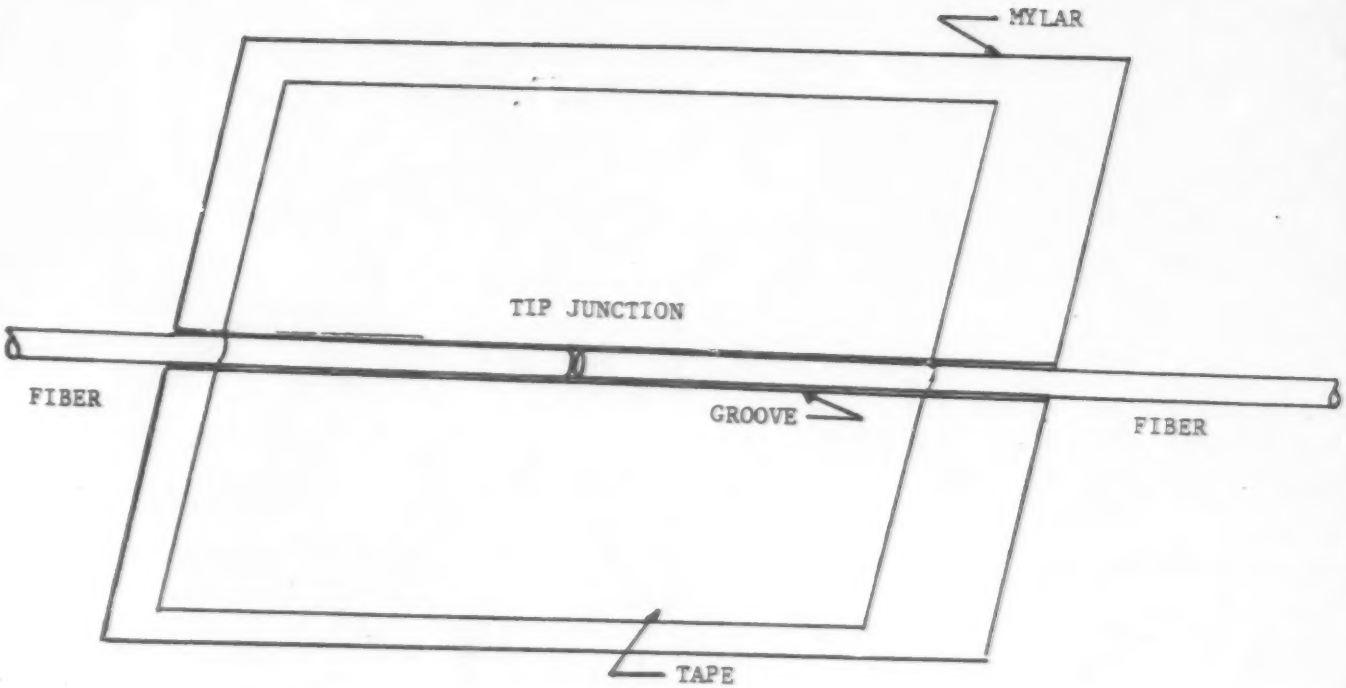

FIGURE 57. AXIAL DISPLACEMENT ATTENUATION SENSOR

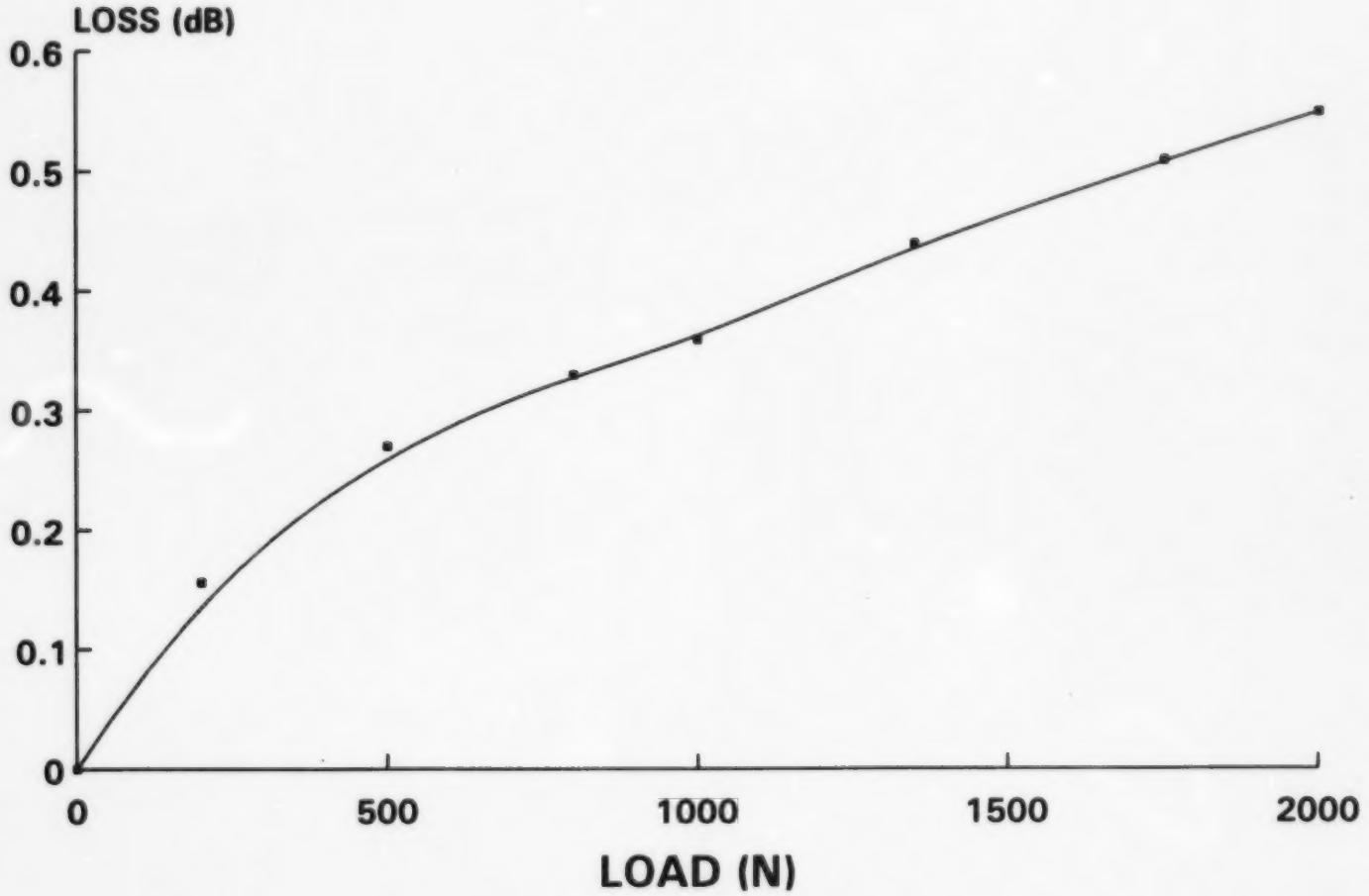

FIGURE 58. ATTENUATION vs. LOAD
FRP 1 - AXIAL DISPLACEMENT SENSOR

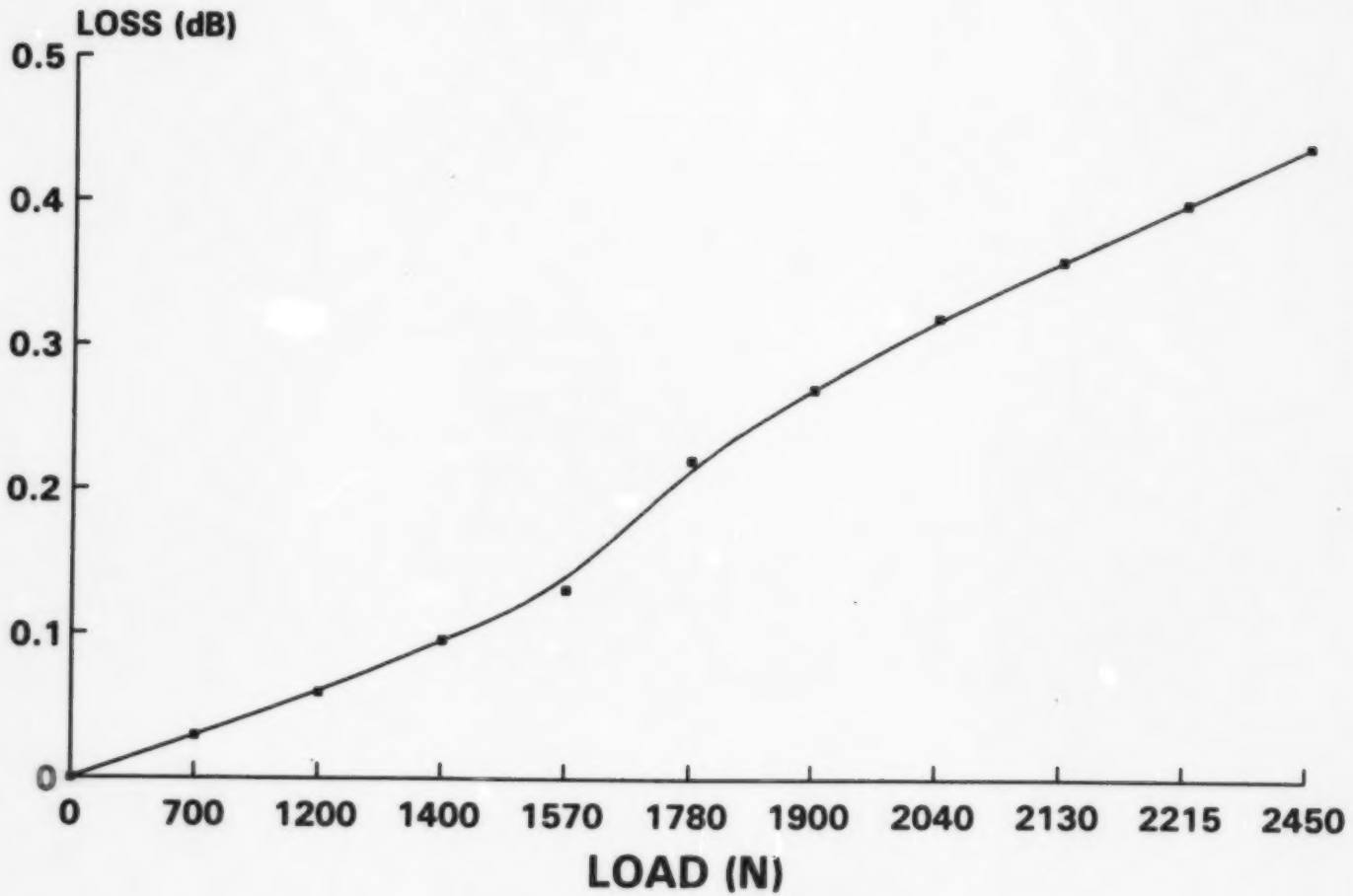

FIGURE 59. ATTENUATION vs. LOAD
FRP 2 - AXIAL DISPLACEMENT SENSOR

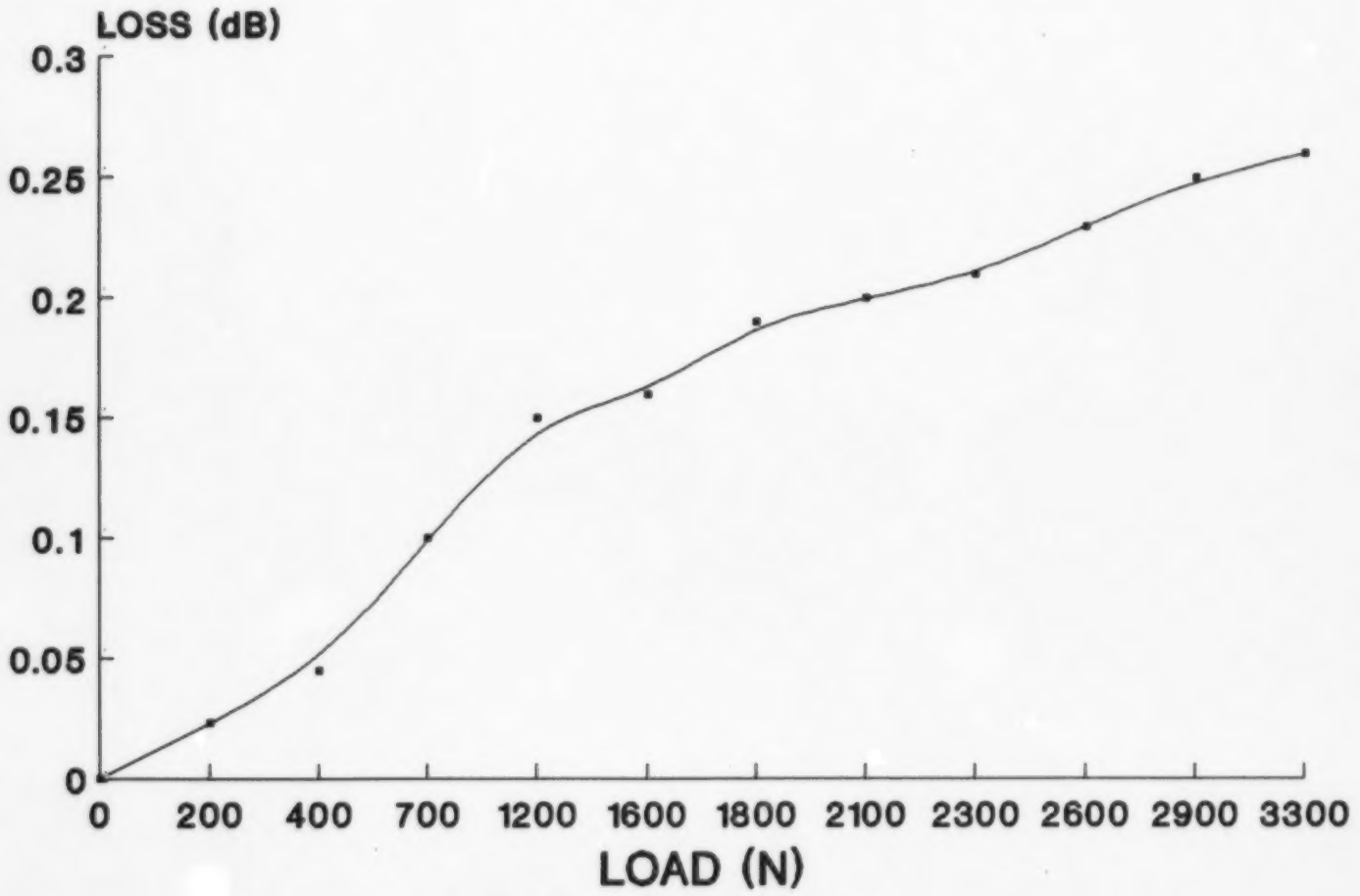

FIGURE 60. ATTENUATION vs. LOAD
FRP 3 - AXIAL DISPLACEMENT SENSOR

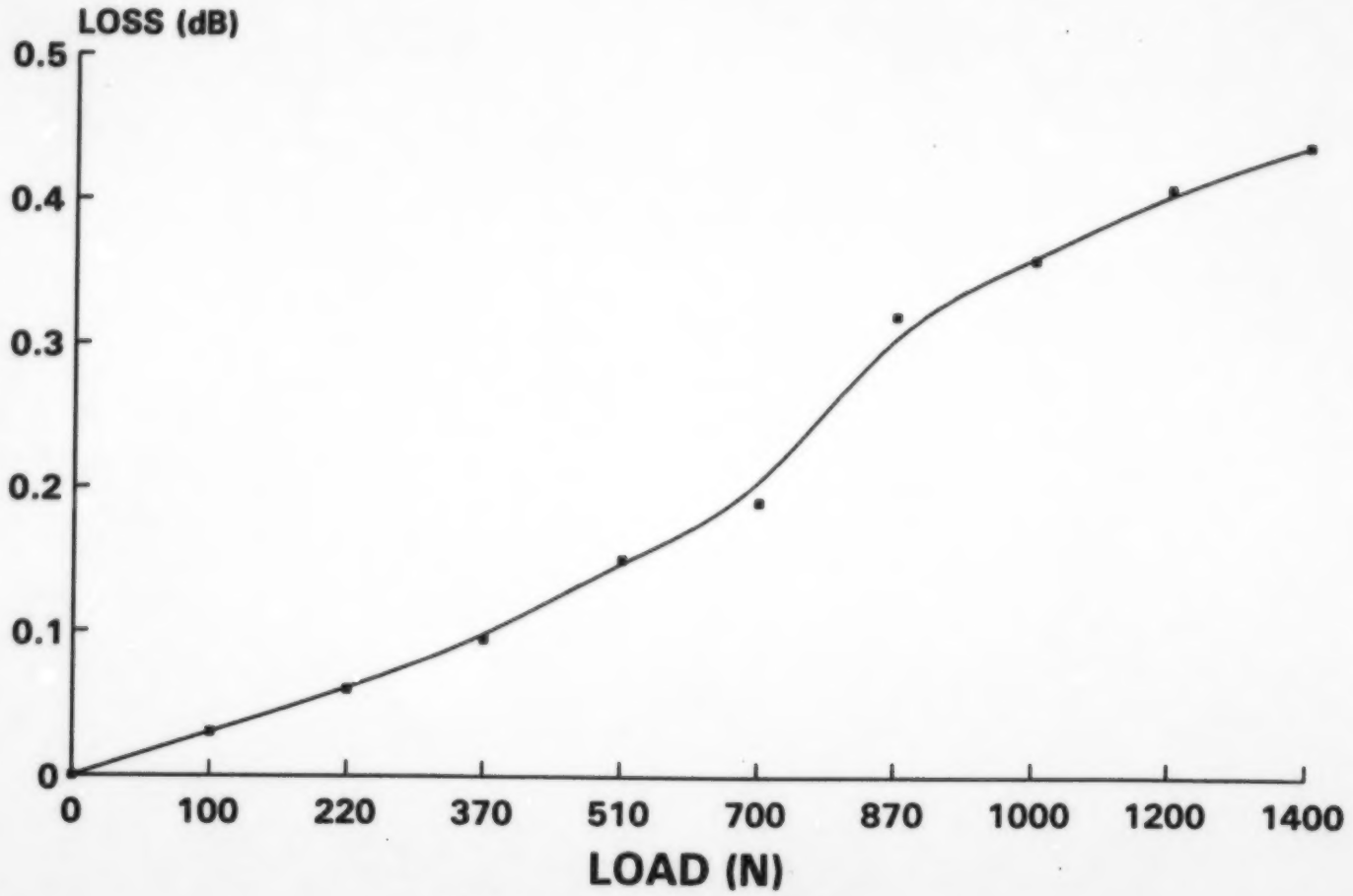

FIGURE 61. ATTENUATION vs. LOAD
FRP 4 - AXIAL DISPLACEMENT SENSOR

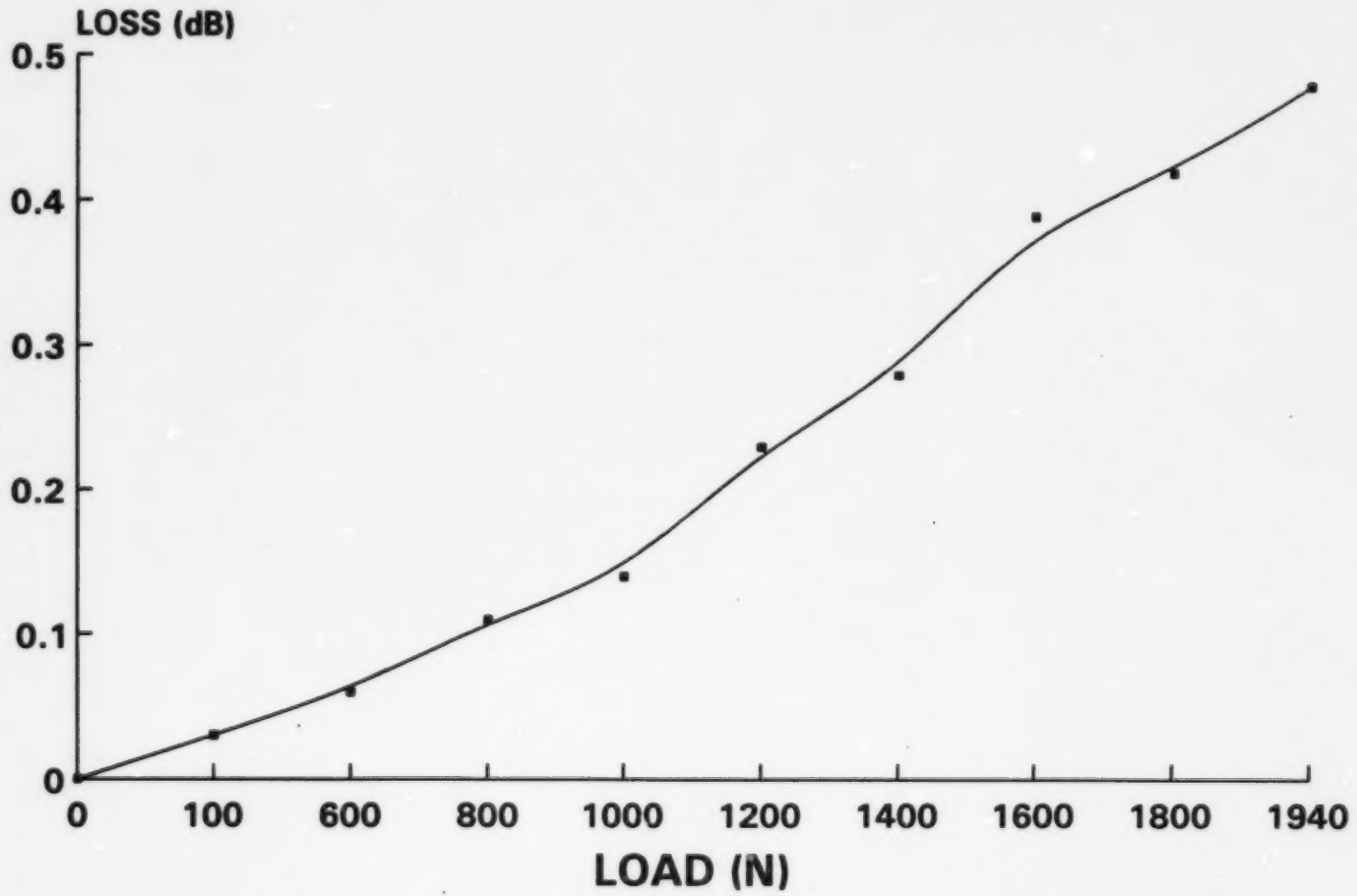

FIGURE 62. ATTENUATION vs. LOAD
FRP 5 - AXIAL DISPLACEMENT SENSOR

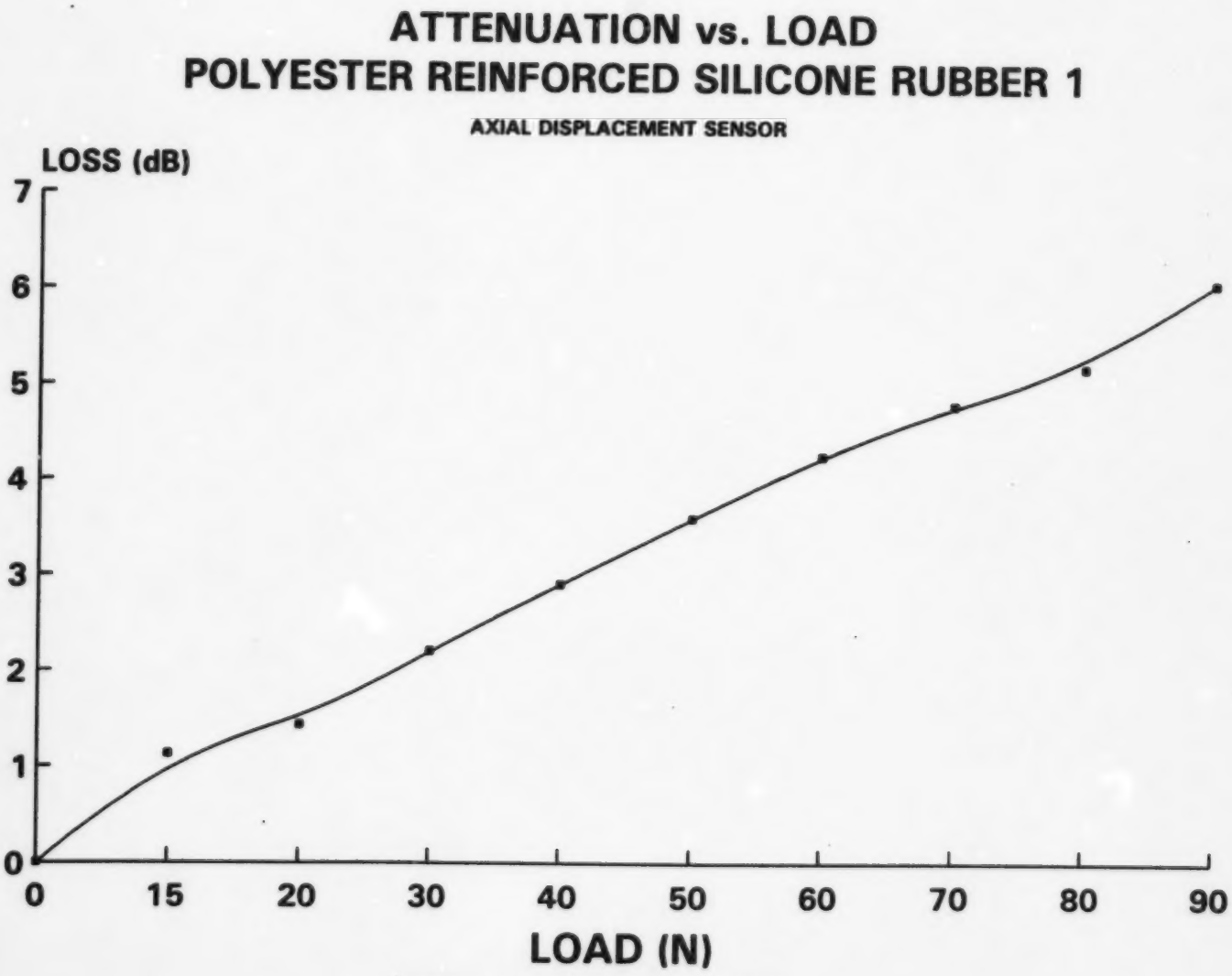

FIGURE 63. ATTENUATION vs. LOAD
RUBBER 1 - AXIAL DISPLACEMENT SENSOR

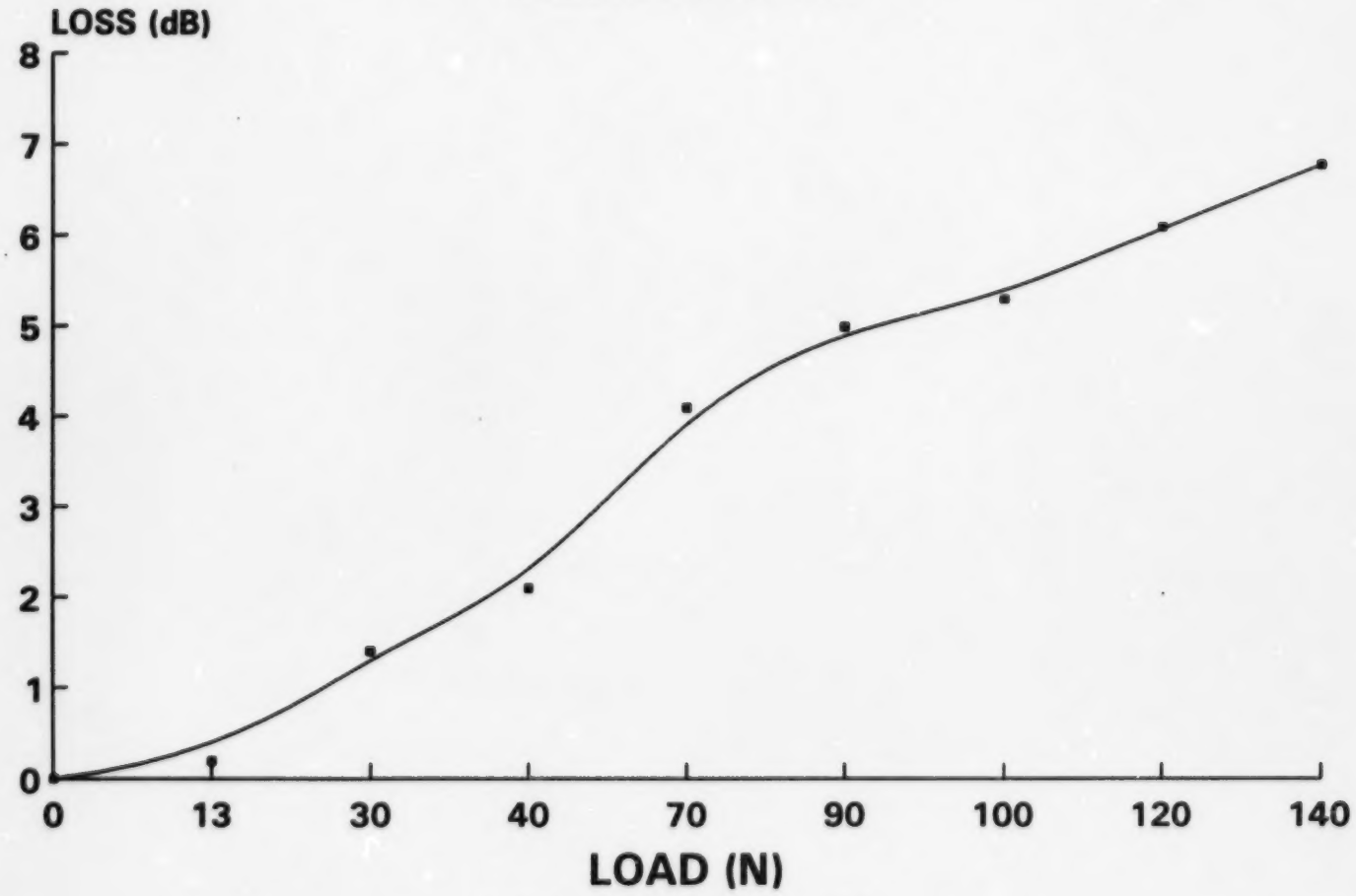

FIGURE 64. ATTENUATION vs. LOAD
RUBBER 2 - AXIAL DISPLACEMENT SENSOR

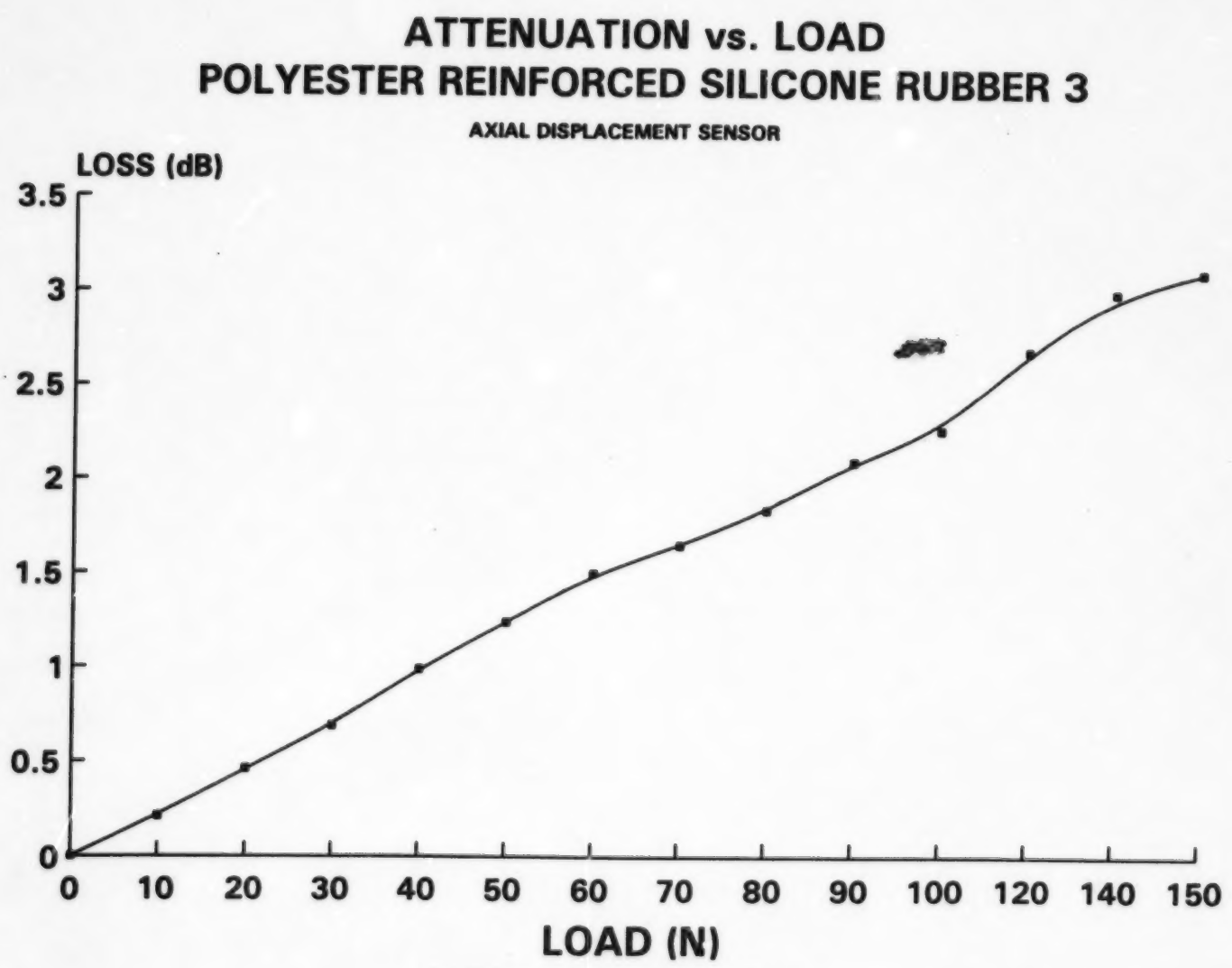

FIGURE 65. ATTENUATION vs. LOAD
RUBBER 3 - AXIAL DISPLACEMENT SENSOR

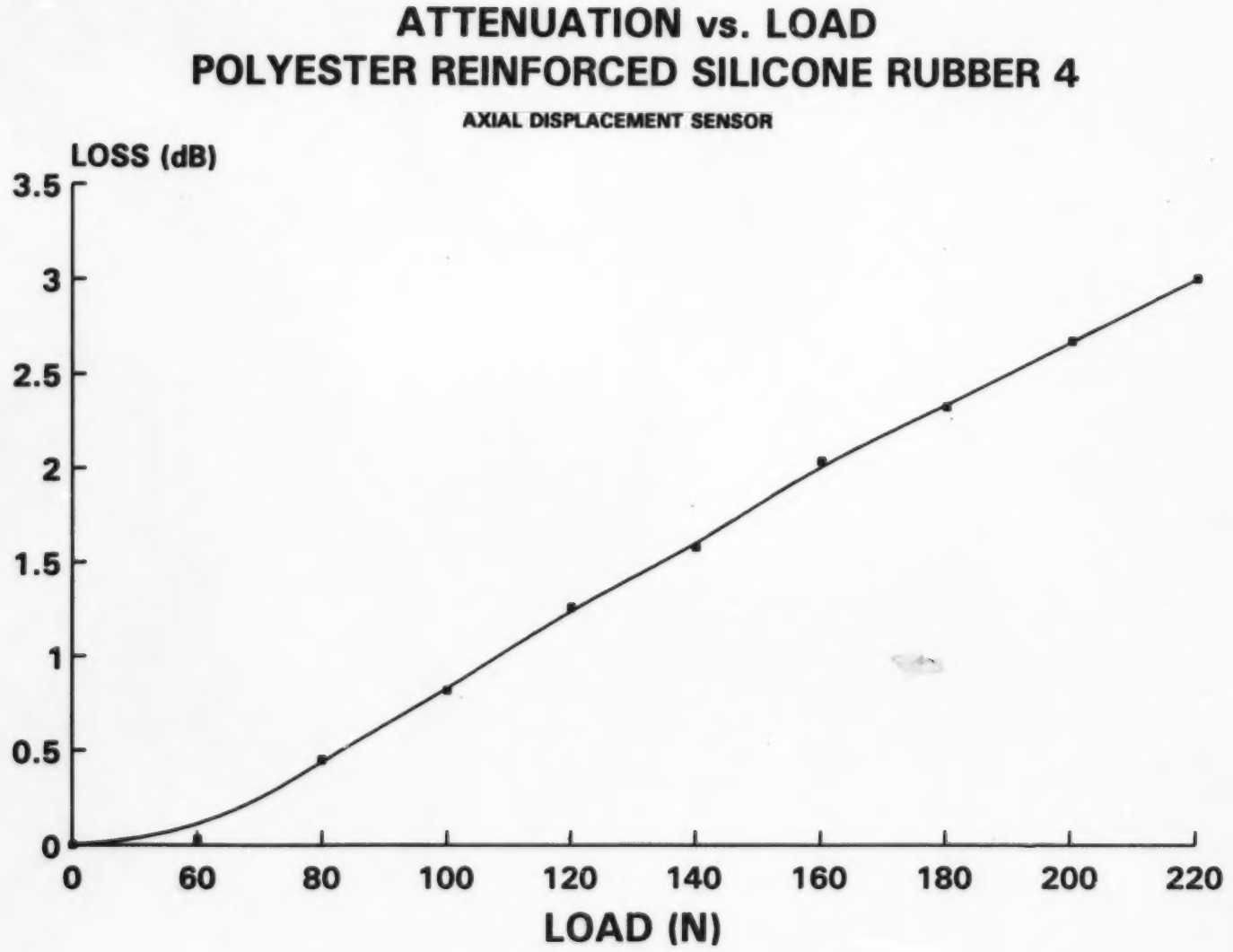

FIGURE 66. ATTENUATION vs. LOAD
RUBBER 4 - AXIAL DISPLACEMENT SENSOR